FFIE/678/115

Approved
Kjeller, 13 June 1997

Paul Narum
Chief Scientist

A REVIEW OF THEORY AND MATERIALS FOR OPTICAL PARAMETRIC OSCILLATORS IN THE INFRARED

ARISHOLM Gunnar, RUSTAD Gunnar

FFI/RAPPORT-97/02589

FORSVARETS FORSKNINGSINSTITUTT
Norwegian Defence Research Establishment
P O Box 25, N-2007 Kjeller, Norway

NORWEGIAN DEFENCE RESEARCH ESTABLISHMENT (NDRE)
FORSVARETS FORSKNINGSINSTITUTT (FFI)

POST OFFICE BOX 25
N-2007 KJELLER, NORWAY

UNCLASSIFIED

SECURITY CLASSIFICATION OF THIS PAGE
(when data entered)

REPORT DOCUMENTATION PAGE

1) PUBL/REPORT NUMBER	2) SECURITY CLASSIFICATION	3) NUMBER OF PAGES
FFI/RAPPORT-97/02589	UNCLASSIFIED	117
1a) PROJECT REFERENCE	2a) DECLASSIFICATION/DOWNGRADING SCHEDULE	
FFIE/678/115		

4) TITLE

A REVIEW OF THEORY AND MATERIALS FOR OPTICAL PARAMETRIC OSCILLATORS IN THE INFRARED

5) NAMES OF AUTHOR(S) IN FULL (surname first)

ARISHOLM Gunnar, RUSTAD Gunnar

6) DISTRIBUTION STATEMENT

Approved for public release. Distribution unlimited.
(Offentlig tilgjengelig)

7) INDEXING TERMS IN ENGLISH:	IN NORWEGIAN:
a) Optical parametric oscillators	a) Optiske parametriske oscillatorer
b) Optical materials	b) Optiske materialer
c) Optical frequency conversion	c) Optisk frekvenskonvertering
d) Infrared sources	d) Infrarøde kilder
e) Nonlinear optics	e) Ulineær optikk

THESAURUS REFERENCE: INSPEC 1995

8) ABSTRACT

The theory of optical parametric oscillators is presented, with emphasis on the details of phase matching and acceptance intervals. Materials suitable for generation in the 3-5 μm and 8-12 μm bands are reviewed and compared, and we try to point out the most promising materials for each wavelength range. The materials we review are KTP, KTA, RTP, RTA, CTA, $LiNbO_3$, $LiIO_3$, $KNbO_3$, $AgGaS_2$, $AgGaSe_2$, $ZnGeP_2$, CdSe, $CdGeAs_2$, GaSe and GaAs.The final chapter discusses some issues in practical OPO design.

9) DATE	AUTHORIZED BY	POSITION
13 June 1997	This page only Paul Narum *P Narum*	Director of Research

ISBN 82-464-0171-8

UNCLASSIFIED

SECURITY CLASSIFICATION OF THIS PAGE
(when data entered)

CONTENTS

		Page
1	INTRODUCTION	5
	References	6
2	THEORY	7
2.1	Nonlinear polarization and susceptibility	7
2.2	Nomenclature	10
2.3	Coupled amplitude equations for plane waves	11
2.4	Phase matching and tuning	17
2.5	Coupled amplitude equations with transverse effects	24
2.6	Signal bandwidth	25
2.7	Noise initiation of parametric oscillation	25
	References	26
3	MATERIALS FOR SECOND ORDER PROCESSES	28
3.1	Material parameters	28
	References	31
3.2	The KTP isomorphs	32
	References	32
3.3	KTP ($KTiOPO_4$)	33
	References	38
3.4	KTA ($KTiOAsO_4$)	41
	References	43
3.5	RTP ($RbTiOPO_4$)	45
	References	46
3.6	RTA ($RbTiOAsO_4$)	48
	References	50
3.7	CTA ($CsTiOAsO_4$)	51
	References	52
3.8	$LiNbO_3$ (LNO)	54
	References	58
3.9	$LiIO_3$ (LIO)	60
	References	62
3.10	$KNbO_3$ (KNO)	64
	References	67
3.11	$LiTaO_3$ (LTA) and other related materials	69
	References	69
3.12	$AgGaS_2$ (AGS)	70

	References	73
3.13	$AgGaSe_2$ (AGSe)	75
	References	78
3.14	$ZnGeP_2$ (ZGP)	80
	References	83
3.15	CdSe	85
	References	88
3.16	$CdGeAs_2$ (CGA)	90
	References	92
3.17	GaSe	94
	References	97
3.18	GaAs with domain inversion	98
	References	100
3.19	Materials for 1-5 μm generation - Summary	102
	References	103
3.20	Materials for 8-12 μm generation - Summary	104
4	OPO DESIGN	106
4.1	OPOs versus parametric generators	106
4.2	Resonant signals in OPOs	107
4.3	Resonators and mode matching	109
4.4	Coatings and mirrors	110
4.5	Walk-off compensation	110
4.6	Pump beam quality	110
4.7	OPO threshold	110
4.8	Composite OPO systems	111
	References	111
APPENDIX		
A	NONLINEAR INTERACTION IN A BIREFRINGENT MEDIUM	113
	Distribution list	117

A REVIEW OF THEORY AND MATERIALS FOR OPTICAL PARAMETRIC OSCILLATORS IN THE INFRARED

1 INTRODUCTION

The $3-5\,\mu$m and $8-12\,\mu$m transmission windows in the atmosphere are utilized in many military applications, such as laser radar, infrared imaging systems, and missile seekers. Efficient laser sources in these wavelength regions are therefore strongly desired in electro-optic countermeasures applications. Except for the 9.2–10.8 μm CO_2 laser and some $3\,\mu$m laser systems, practical laser systems that emit in these wavelength regions do not exist. However, laser radiation in these wavelength regions can be generated by the use of various nonlinear wavelength shifting devices, in particular optical parametric oscillators (OPOs).

In an OPO a strong pump laser beam is down converted in frequency by the nonlinear process. The principle behind this is that a pump photon of frequency ω_3 is annihilated and two photons with frequencies ω_1 and ω_2 are created by the interaction between the pump photon and the nonlinear optical medium. The generated photons obey energy conservation, i.e.

$$\omega_3 = \omega_1 + \omega_2 \tag{1.1}$$

By a careful selection of nonlinear material and external parameters, it is possible to obtain efficient frequency conversion from available laser pump sources (e.g. a Nd:YAG laser at $1.06\,\mu$m) to the desired wavelengths. Another important quality of OPOs is that, in theory, any given pair of (ω_1, ω_2) that obey (1.1) can be generated. The set that is actually generated is determined by the working conditions for the OPO. A change in these conditions (usually a change in the orientation of the nonlinear material) may cause another set to be generated. The result is that the output from an OPO is tunable over a wide frequency range, and this is very useful in many applications, such as electro-optic countermeasures and remote sensing.

The most important consideration in the design of an efficient OPO is the choice of the nonlinear material. To date, OPO operation has been demonstrated in a large number of materials, and several of these may be chosen for the intended application. Experimental trial-and-error measurements for different materials is a time consuming and costly procedure. It is therefore important to establish a reliable numerical tool with which the performance of different materials can be predicted and compared, and the proper material choice can be made. These simulations requires detailed knowledge of a number of the material parameters, such as the transparency range, the birefringence, the nonlinearity, and the damage threshold.

In Chapter 2 we introduce the theory of OPOs and second order nonlinear interactions in general. The basic theory of OPOs is well covered in textbooks [1, 2]. There is no need to repeat this theory here, so we have only summarized it briefly to establish our notation. A large part of Chapter 2 is devoted to details about phase matching and acceptance angles. These details are not covered in textbooks, but they are very important in practical OPO design. The equations describing second order nonlinear interactions exist in many different forms in the literature. Confusion can easily arise

when equations from different sources are compared or combined, so for ease of reference we have included the basic equations in many different forms.

In Chapter 3 we summarize the properties of some relevant nonlinear materials. For some of the materials, we briefly describe some published experimental results with devices using them. A large number of references have been included, but nevertheless many interesting references have been omitted. During the work with this report, we built reference databases which should be useful if more references or more detailed notes on a reference is required.

Chapter 4 covers some additional topics related to OPO design, like choice of resonators and resonant wavelengths.

For the convenience of the reader, we have listed the references after each section (each material) in Chapter 3. In the other chapters, the references are listed at the end of the chapter.

References

[1] R.W. Boyd. *Nonlinear optics.* Academic Press, 1992.
[2] Y. R. Shen. *The principles of nonlinear optics.* Wiley, 1984.

2 THEORY

In this chapter, we review the basic mechanisms that underlay optical parametric amplification and oscillation. We first introduce the nonlinear polarization and its properties. Then there is a section on choice of coordinate axes and nomenclature for second order interactions. The equations for three plane waves interacting via the second order susceptibility exist in various forms corresponding to different representations of the fields. There are also different equations for degenerate and non-degenerate processes. (A non-degenerate process is one with 3 distinct interacting waves, while a degenerate process involves only 2 waves, of frequencies ω and 2ω respectively). We present the equations for both cases in many varieties. By collecting all these equations in one place, and clearly stating the relations between them, we hope to sort out the possible confusion once and for all as far as future work in our group is concerned. After discussing solutions of the plane wave coupled amplitude equations, we consider phase matching and the related topics of tuning and acceptance intervals. The problems with birefringent phase matching, walk-off and small acceptance intervals, are pointed out, and quasi phase matching is discussed as a possible solution. Since transverse effects turn out to be important in nonlinear devices, we briefly discuss the coupled amplitude equations with diffraction and walk-off. The next section discusses the effects of pump and signal bandwidths in OPOs. Finally there is a section on noise initiation of OPOs.

2.1 Nonlinear polarization and susceptibility

2.1.1 Representation of the fields

Two different representations of the real electric field and polarization are often used in the literature. They are

$$\tilde{\mathbf{E}} = \int_{-\infty}^{\infty} d\omega \mathbf{E}(\omega) \exp(-i\omega t) \qquad \tilde{\mathbf{P}} = \int_{-\infty}^{\infty} d\omega \mathbf{P}(\omega) \exp(-i\omega t) \tag{2.1}$$

or

$$\tilde{\mathbf{E}} = \frac{1}{2}\int_{-\infty}^{\infty} d\omega \mathbf{E}'(\omega) \exp(-i\omega t) \qquad \tilde{\mathbf{P}} = \frac{1}{2}\int_{-\infty}^{\infty} d\omega \mathbf{P}'(\omega) \exp(-i\omega t) \tag{2.2}$$

where tilde indicates real, rapidly oscillating quantities, and boldface is used to denote vector quantities. Because the fields are real, $\mathbf{E}(-\omega) = \mathbf{E}(\omega)^*$ and $\mathbf{P}(-\omega) = \mathbf{P}(\omega)^*$, where superscript * denotes complex conjugation. We shall follow the convention in Equation (2.1), but we sometimes state results corresponding to Equation (2.2) for comparison.

2.1.2 Nonlinear polarization

In general, the spectrum of the polarization can be written

$$\mathbf{P}(\omega) = \epsilon_0 \left(\chi^{(1)}(\omega) : \mathbf{E}(\omega) + \int_{-\infty}^{\infty} d\omega' \chi^{(2)}(\omega, \omega', \omega - \omega') : \mathbf{E}(\omega')\mathbf{E}(\omega - \omega') + \right.$$
$$\left. \int\int_{-\infty}^{\infty} d\omega' d\omega'' \chi^{(3)}(\omega, \omega', \omega'', \omega - \omega' - \omega'') : \mathbf{E}(\omega')\mathbf{E}(\omega'')\mathbf{E}(\omega - \omega' - \omega'') \cdots \right) \tag{2.3}$$

where ':' denotes tensor product and $\chi^{(n)}$ are the susceptibility tensors. Note that Equation (2.3) represents one of the two conventions for nonlinear susceptibilities used in the SI system: In the other convention, the factor ϵ_0 is included in $\chi^{(n)}$, for $n > 1$, leading to different values for these. See [1, Appendix A]. If we had written the fields as in Equation (2.2), Equation (2.3) would have had a factor 1/2 in the second order term, 1/4 in the third order term, etc.

$\chi^{(n)}$ is a tensor of rank $(n+1)$. $\chi^{(1)}$ is the linear susceptibility leading to linear absorption and refractive index. $\chi^{(2)}$ is the second order susceptibility responsible for sum and difference frequency generation (SFG and DFG). These effects include second harmonic generation (SHG) and optical parametric amplification (OPA). The third order susceptibility $\chi^{(3)}$ is responsible for nonlinear refractive index and 4-wave mixing. In general, $\chi^{(n+1)} \ll \chi^{(n)}$, so unless the intensity is extremely high, the lower order polarizations are more important than the higher order. We concentrate on the second order susceptibility. Third order polarization can usually be ignored in devices based on second order polarization. For simplicity, we often omit the superscript in $\chi^{(2)}$ and write just χ, unless this can cause confusion.

Being a third rank tensor, $\chi^{(2)}$ has 27 elements. In practice, many elements are zero or equal to each other because of symmetries of the material. These symmetries are determined by the point group. The form of $\chi^{(2)}$ for different point groups is shown in [1, Section 1.5]. The $\chi^{(2)}$-tensor is also simplified by symmetries related to the frequency arguments. The reality of the fields imply that $\chi(-\omega_3, -\omega_2, -\omega_1) = \chi(\omega_3, \omega_2, \omega_1)^*$. Intrinsic permutation symmetry, which is a consequence of the notation, implies that $\chi_{ijk}(\omega_3, \omega_1, \omega_2) = \chi_{ikj}(\omega_3, \omega_2, \omega_1)$. If the absorption is negligible, χ is real and we also have full permutation symmetry, which means that all indices can be permuted as long as the frequency arguments are permuted in the same way. If the frequencies involved are far from any resonance in the nonlinear medium, χ is essentially independent of frequency. In that case, all the indices can be permuted. This is called Kleinman symmetry.

When only a few discrete frequencies are present, we can represent their amplitudes individually instead of using the continuous spectrum as in Equation (2.3). For instance, two input signals of frequencies ω_a and ω_b are represented by $\mathbf{E}_a = \mathbf{E}(\omega_a)$, $\mathbf{E}_b = \mathbf{E}(\omega_b)$, and their negative frequency counterparts $\mathbf{E}_a^* = \mathbf{E}(-\omega_a)$ and $\mathbf{E}_b^* = \mathbf{E}(-\omega_b)$. We usually write equations only for the positive frequency components. The two input frequencies give rise to polarization components at $(\omega_a + \omega_b)$ and $|\omega_a - \omega_b|$. These polarizations can drive new waves, and the new waves can interact with each other, and with the original waves, to produce even more new frequencies and make the representation very complicated. In practical devices, only one particular interaction is phase matched. Phase matching is explained in Section 2.4. All the signals that are generated by non-phase matched processes are very small. Thus we can usually restrict our attention to three interacting waves for a non-degenerate process or two waves for a degenerate one. When there are three interacting waves, it is customary to denote the frequencies ω_1, ω_2, and ω_3 with $\omega_3 = \omega_1 + \omega_2$ and $\omega_2 \geq \omega_1$.

We first consider the non-degenerate case and then the degenerate. The equation for

the second order polarization $\mathbf{P}^{(2)}$ in a non-degenerate process can be written

$$\begin{aligned}\mathbf{P}_1^{(2)} &= 2\epsilon_0\chi(\omega_1,\omega_3,\omega_2):\mathbf{E}_3\mathbf{E}_2^* \\ \mathbf{P}_2^{(2)} &= 2\epsilon_0\chi(\omega_2,\omega_3,\omega_1):\mathbf{E}_3\mathbf{E}_1^* \\ \mathbf{P}_3^{(2)} &= 2\epsilon_0\chi(\omega_3,\omega_1,\omega_2):\mathbf{E}_1\mathbf{E}_2\end{aligned} \tag{2.4}$$

The factor 2 comes from the intrinsic permutation symmetry. If we had used the conventions in Equation (2.2), this factor would be cancelled by the factor $1/2$ in the second order polarization term, so the constant in Equation (2.4) would be just $\epsilon_0\chi$. On component form, we have, (taking wave 3 as an example)

$$P_{3i}^{(2)} = 2\epsilon_0\chi_{ijk}(\omega_3,\omega_2,\omega_1)E_{2j}E_{1k} \tag{2.5}$$

where summation over repeated indices is implied. The equations for the other waves are similar. In a practical device with phase matching, each wave has a fixed linear polarization, so in a plane wave model we can write $\mathbf{E}_m = E_m\mathbf{e}_m$ where $\mathbf{e}_m$ is a unit vector in the direction of the field. The wave E_m is coupled to the nonlinear polarization through the scalar product of the polarization vector $\mathbf{P}_m^{(2)}$ and the unit field vector $\mathbf{e}_m$, so we can define an effective nonlinear polarization and an effective susceptibility χ_{eff} by, (again taking wave 3 as an example)

$$P_{3,\text{eff}}^{(2)} = 2\epsilon_0\chi_{ijk}(\omega_3,\omega_2,\omega_1)e_{3i}e_{2j}e_{1k}E_1E_2 = 2\epsilon_0\chi_{\text{eff}}E_1E_2 \tag{2.6}$$

In Section 2.3 on the equations for the interacting waves, we use this effective susceptibility.

The term degenerate is sometimes used about any process with only two frequencies, ω and 2ω, involved. We use a more restrictive definition and classify a process as non-degenerate whenever there are three distinct interacting waves, even if $\omega_1 = \omega_2$. This is possible because in practice second order interactions take place in birefringent crystals. At frequency ω there are two eigenmodes with different wave vectors, so there may be two distinct waves. Let them have amplitudes E_{1a} and E_{1b} and polarization unit vectors $\mathbf{e}_{1a}$ and $\mathbf{e}_{1b}$. Then the general equation for the polarization $\mathbf{P}_2$ at 2ω, valid for both degenerate and non-degenerate processes, is

$$\begin{aligned}\mathbf{P}_2 &= \epsilon_0\chi(2\omega,\omega,\omega):(E_{1a}\mathbf{e}_{1a}+E_{1b}\mathbf{e}_{1b})^2 \\ &= \epsilon_0(\chi:\mathbf{e}_{1a}\mathbf{e}_{1a}E_{1a}^2+\chi:\mathbf{e}_{1b}\mathbf{e}_{1b}E_{1b}^2+2\,\chi:\mathbf{e}_{1a}\mathbf{e}_{1b}E_{1a}E_{1b})\end{aligned} \tag{2.7}$$

It is possible that $\chi^{(2)}$ has a form such that all terms on the right hand side are nonzero, but only one of them will be phase matched and contribute efficiently. If this term is E_{1a}^2 or E_{1b}^2, the process is degenerate, and if it is $E_{1a}E_{1b}$ the process in non-degenerate. Note that the factor 2 from the permutation symmetry appears only in the non-degenerate case.

In a degenerate process, only one of the fields E_{1a} and E_{1b} contributes. Writing just E_1 for this field, the degenerate versions of Equation (2.4) are

$$\mathbf{P}_1 = 2\epsilon_0\chi(\omega,2\omega,\omega):\mathbf{E}_2\mathbf{E}_1^* \tag{2.8}$$

$$\mathbf{P}_2 = \epsilon_0\chi(2\omega,\omega,\omega):\mathbf{E}_1^2 \tag{2.9}$$

The same difference applies to the degenerate versions of Equations (2.5) and (2.6).

2.1.3 Miller's rule

As indicated by the notation, the susceptibility tensors depend on the frequencies. The dispersion can be approximated using Miller's delta [2, Section 2.8], which is defined by

$$\Delta_{ijk} = \frac{\chi^{(2)}_{ijk}(\omega_3, \omega_2, \omega_1)}{\chi^{(1)}_{ii}(\omega_3)\chi^{(1)}_{jj}(\omega_2)\chi^{(1)}_{kk}(\omega_1)} \tag{2.10}$$

This coefficient has small dispersion and it is almost constant for many crystals. It can be used for estimating the value of $\chi^{(2)}$ at frequencies other than those at which it was measured. Note that the correction factors introduced by Miller's rule do not possess Kleinman symmetry. This is consistent, because if Kleinman symmetry were valid, χ would not depend on frequency.

2.1.4 Contracted notation for nonlinear coefficients

The nonlinear susceptibility is often represented by the tensor $d = \chi^{(2)}/2$. Similarly, $d_{\text{eff}} = \chi_{\text{eff}}/2$. When Kleinman symmetry is valid (or when $\omega_1 = \omega_2$), $d_{ijk} = d_{ikj}$. In these cases, it is common to simplify notation by writing d as a 3 by 6 matrix defined by $d_{ip} = d_{ijk}$, where p corresponds to jk in the following manner: 1 = 11, 2 = 22, 3 = 33, 4 = 23 (or 32), 5 = 13 (or 31), and 6 = 12 (or 21). In OPOs we usually have $\omega_1 \neq \omega_2$, and often at least one of the interacting frequencies is close to an absorption edge. Therefore, we cannot assume Kleinman symmetry, and the matrix notation is not always appropriate in the context of OPOs.

Data on nonlinear susceptibilities are usually reported as elements of the d-matrix, measured at a particular set of wavelengths. If the measurement is done with second harmonic generation (SHG), which is often the case, use of the contracted notation is justified. Unfortunately, the contracted notation is also used in most work on OPOs, even when one of the wavelengths is near the edge of the transmission spectrum. Even though the contracted notation is used, it is usually possible to infer from the description of the experiment which element of the d-tensor was actually used in the process. Note that this problem only affects the elements d_{ip} with $p > 3$, because these correspond to two tensor elements that may be different. The other elements of the d-matrix correspond to unique tensor elements.

2.2 Nomenclature

There is a lack of consistent nomenclature in reports of properties of nonlinear crystals. The main problem is that different axes are used for reporting tensor properties like χ_{ijk}. The refractive indices are reported in the frame of the principal dielectric axes, xyz. The nonlinear coefficients are reported in a system of axes XYZ. The latter set of axes is unequivocal, because it is defined in terms of crystal structure. The principal axes xyz, on the other hand, may change due to dispersion in monoclinic and triclinic crystals. Roberts [3] has discussed the problems and the relevant IEEE/ANSI standard. For some crystals, there is a de facto standard that differs from the IEEE/ANSI

standard, and Roberts suggested a modification to the standard. Unfortunately, neither the standard nor the modifications have been generally accepted, so we follow the conventions of the literature for ease of reference. To avoid confusion, we describe the axes used for each biaxial material we discuss, and indicate when the system we use differs from the standard.

In uniaxial crystals, we choose the principal dielectric axes such that z is the optic axis, i.e. n_z is the extraordinary index. The crystal is called negative uniaxial if $n_z < n_x = n_y$ and positive otherwise. In biaxial crystals, it is conventional to choose the principal axes so that $n_x < n_y < n_z$. Then the optic axes lie in the xz-plane, making an angle Ω with the z-axis. The crystal is called positive biaxial if $\Omega < 45°$ and negative otherwise.

Propagation directions are specified by spherical coordinates in the XYZ axes, with θ being the angle between the Z-axis and the propagation vector, and ϕ being the angle between the X-axis and the projection of the propagation vector on the XY-plane.

The two waves generated in an OPO are often called signal and idler. The term signal may be used for the wave that is resonant (if only one is resonant), the highest frequency, or the wave of interest (if the other is discarded). To avoid confusion, and to emphasize the equal status of the two waves, we use the term signal for both.

2.3 Coupled amplitude equations for plane waves

In this section, we derive coupled amplitude equations for a non-degenerate second order interaction. We follow the convention of Equation (2.1). After deriving the equations, we present the results using the convention of Equation (2.2) and two other representations of the field. We also present the equations for degenerate interactions.

2.3.1 Derivation of the equations

We consider linearly polarized plane waves propagating in the z-direction. In other words, we assume that the amplitudes of Equation (2.1) have the form

$$\mathbf{E}_m = \mathbf{e}_m e_m(z,t) \exp(ik_m z)$$

where $\mathbf{e}_m$ is a unit vector in the polarization direction, $k_m = \omega_m n(\omega_m)/c$, n is the refractive index, and c is the speed of light in vacuum. We make the slowly varying envelope assumption, i.e. we assume that $e_m(z,t)$ changes slowly with z and t compared to the optical period. We also assume that the medium is lossless, implying that χ_{eff} is real and that it is the same for all the three waves. We denote χ_{eff} just by χ.

From Maxwell's equations, we can derive the wave equation

$$\nabla^2 \tilde{\mathbf{E}} - \nabla \cdot (\nabla \tilde{\mathbf{E}}) = \mu_0 \epsilon_0 \epsilon \ddot{\tilde{\mathbf{E}}} + \mu_0 \ddot{\tilde{\mathbf{P}}}^{(2)} \tag{2.11}$$

where $\epsilon = 1 + \chi^{(1)}$ is the dielectric tensor and $\tilde{\mathbf{P}}^{(2)}$ is the 2. order part of the nonlinear polarization. Note that the first term on the right hand side includes the linear

polarization. The term $\nabla \cdot (\nabla \tilde{\mathrm{E}})$ can be ignored if we assume that $\mathbf{e}_m$ is normal to the propagation direction. This restriction is lifted in the more detailed treatment in Appendix A. Inserting the expressions for the fields and polarizations, we can find the equation for e_m by multiplying both sides of Eq. (2.11) with $\exp(-ik_m z)$ and equating terms at ω_m. For example, for e_3 we have:

$$-k_3^2 e_3 + 2ik_3 \frac{\partial e_3}{\partial z} = -\frac{\omega_3^2 n_3^2}{c^2} e_3 - i\frac{\omega_3 n_3^2}{c^2}\frac{\partial e_3}{\partial t} - \frac{\omega_3^2}{c^2} 2\chi e_1 e_2 \exp(-i\Delta k z) \tag{2.12}$$

where $\Delta k = k_3 - k_2 - k_1$ is called the phase mismatch. Second derivatives of e_3 were ignored because of the slowly varying envelope approximation. By definition of k_3, the first terms on both sides of the equation cancel. If we assume steady state, the second term on the right hand side vanishes. Alternatively, this term can be removed by going to a moving frame with $t' = t - nz/c$ and neglecting the difference in group velocity between the 3 waves. This approximation is appropriate for pulse lengths down to a few ps. In any of these cases, the equation becomes

$$2ik_3 \frac{\partial e_3}{\partial z} = -\frac{\omega_3^2}{c^2} 2\chi e_1 e_2 \exp(-i\Delta k z) \tag{2.13}$$

or

$$\frac{\partial e_3}{\partial z} = i\frac{\omega_3}{n_3 c}\chi e_1 e_2 \exp(-i\Delta k z) \tag{2.14}$$

The equations for the other fields are similar:

$$\frac{\partial e_1}{\partial z} = i\frac{\omega_1}{n_1 c}\chi e_3 e_2^* \exp(i\Delta k z) \tag{2.15}$$

$$\frac{\partial e_2}{\partial z} = i\frac{\omega_2}{n_2 c}\chi e_3 e_1^* \exp(i\Delta k z) \tag{2.16}$$

If we use the convention of Equation (2.2), a factor of $1/2$ appears in the driving terms on the right hand sides of these equations.

It is sometimes useful to represent the fields by transformed amplitudes a such that the intensity is $I = |a|^2$. In the SI system, intensity and amplitude are related by

$$I = \frac{n}{Z_0}\langle \tilde{\mathrm{E}}^2 \rangle = \frac{2n}{Z_0}|e|^2 = \frac{n}{2Z_0}|e'|^2 \tag{2.17}$$

where angle brackets denote time average, $Z_0 = \sqrt{\mu_0/\epsilon_0} = \mu_0 c$ is the vacuum impedance, and e and e' are the slowly varying field amplitudes using the conventions of Equations (2.1) or (2.2) respectively. Equating this expression for the intensity to $|a|^2$, we find

$$a = e\sqrt{\frac{2n}{Z_0}} = e'\sqrt{\frac{n}{2Z_0}} \tag{2.18}$$

The equations for a become

$$\frac{\partial a_1}{\partial z} = i\omega_1 \gamma a_3 a_2^* \exp(i\Delta k z) \tag{2.19}$$

$$\frac{\partial a_2}{\partial z} = i\omega_2 \gamma a_3 a_1^* \exp(i\Delta k z) \tag{2.20}$$

$$\frac{\partial a_3}{\partial z} = i\omega_3 \gamma a_1 a_2 \exp(-i\Delta k z) \tag{2.21}$$

$$\text{where } \gamma = \chi\sqrt{\frac{1}{2n_1 n_2 n_3 c^3 \epsilon_0}} \tag{2.22}$$

Note that we get the same result regardless of whether we start with the amplitudes e or e'.

Another useful representation of the fields is the amplitudes b such that $N = |b|^2$ is the number of photons per unit time and area. From the equation $N = I/(\hbar\omega) = |a|^2/(\hbar\omega)$ we find $b = a/\sqrt{\hbar\omega}$ and

$$\frac{\partial b_1}{\partial z} = i\eta b_3 b_2^* \exp(i\Delta k z) \tag{2.23}$$

$$\frac{\partial b_2}{\partial z} = i\eta b_3 b_1^* \exp(i\Delta k z) \tag{2.24}$$

$$\frac{\partial b_3}{\partial z} = i\eta b_1 b_2 \exp(-i\Delta k z) \tag{2.25}$$

$$\text{where } \eta = \chi\sqrt{\frac{\hbar\omega_1\omega_2\omega_3}{2n_1n_2n_3c^3\epsilon_0}} \tag{2.26}$$

Note that in this representation, all the equations have the same coupling coefficient η, with dimension $s^{1/2}$. A dimensionless from of the equations may also be useful. Let L be the length of the OPA, $\zeta = z/L$, and $q_i = \eta L b_i$. The equations become

$$\frac{\partial q_1}{\partial \zeta} = iq_3 q_2^* \exp(i(\Delta k L)\zeta) \tag{2.27}$$

$$\frac{\partial q_2}{\partial \zeta} = iq_3 q_1^* \exp(i(\Delta k L)\zeta) \tag{2.28}$$

$$\frac{\partial q_3}{\partial \zeta} = iq_1 q_2 \exp(-i(\Delta k L)\zeta) \tag{2.29}$$

and the length of the OPA is 1.

In the equations presented so far, the relative phase of the slowly varying amplitudes differ from the relative phase of physical fields because of the phase mismatch. The relative phase of the the physical fields is

$$\Delta\Phi = \arg(E_3) - \arg(E_2) - \arg(E_1) = \arg(e_3) - \arg(e_2) - \arg(e_1) + \Delta k z \tag{2.30}$$

This is reflected in the factor $\exp(\pm i\Delta k z)$ that is included in the driving terms. When doing computations, it is important to keep track of the relative phases. It is possible to transform the equations such that the slowly varying amplitudes reflect the relative phase directly. By making the transformation $a_1' = a_1 \exp(-i\Delta k z)$ we can write the equations as

$$\partial a_1'/\partial z = i\omega_1\gamma a_3 a_2^* - i\Delta k a_1' \tag{2.31}$$

$$\partial a_2/\partial z = i\omega_2\gamma a_3 a_1'^* \tag{2.32}$$

$$\partial a_3/\partial z = i\omega_3\gamma a_1' a_2 \tag{2.33}$$

$$\text{with } \Delta\Phi = \arg(a_3) - \arg(a_2) - \arg(a_1') \tag{2.34}$$

The transformation could equally well have been done to one of the other fields, or the phase term could have been distributed on two or three fields. The same transformation can be done with the equations for the amplitudes b or e.

If one of the fields, say a_1, is initially zero, and $\Delta k = 0$, we can transform the equations to only real variables. Let

$$a_3 = d_3 \exp(i\phi_3) \tag{2.35}$$
$$a_2 = d_2 \exp(i\phi_2) \tag{2.36}$$
$$a_1 = id_1 \exp(i\phi_1) \tag{2.37}$$
$$\text{where } \phi_1 = \phi_3 - \phi_2 \tag{2.38}$$

The real amplitudes d_m are governed by the equations

$$\partial d_1/\partial z = \omega_1 \gamma d_3 d_2 \tag{2.39}$$
$$\partial d_2/\partial z = \omega_2 \gamma d_3 d_1 \tag{2.40}$$
$$\partial d_3/\partial z = -\omega_3 \gamma d_2 d_1 \tag{2.41}$$

If the phase relation (2.38) happened to be satisfied, these transformations could be done even if a_1 was nonzero.

Now consider the degenerate case. We define $E_1 = E(\omega)$ and $E_2 = E(2\omega)$. As explained in connection with Equation (2.7), a factor 2 in the driving polarization P_2 disappears, so the degenerate equations corresponding to (2.14-2.16) are

$$\frac{\partial e_1}{\partial z} = i\frac{\omega}{n_1 c}\chi e_2 e_1^* \exp(i\Delta k z) \tag{2.42}$$
$$\frac{\partial e_2}{\partial z} = \frac{1}{2} i\frac{2\omega}{n_2 c}\chi e_1^2 \exp(-i\Delta k z) \tag{2.43}$$

where $\Delta k = k_2 - 2k_1$. Apart from the small difference between n_1 and n_2, both equations have the same coupling constant. This is different from the nondegenerate case. The equations for the a- and b-fields can easily be found by analogy.

2.3.2 Conserved quantities

Consider the total intensity $I = I_1 + I_2 + I_3$. Using Equations (2.19–2.21) we see that

$$\frac{\partial I}{\partial z} = a_3^* \frac{\partial a_3}{\partial z} + a_2^* \frac{\partial a_2}{\partial z} + a_1^* \frac{\partial a_1}{\partial z} + cc = 0 \tag{2.44}$$

This result reflects the conservation of optical energy in a parametric process in a lossless medium.

Using Equations (2.23–2.25), we find for the photon rates

$$\frac{\partial N_1}{\partial z} = \frac{\partial N_2}{\partial z} = -\frac{\partial N_3}{\partial z} \quad \text{where} \quad \frac{\partial N_1}{\partial z} = b_1^* \frac{\partial b_1}{\partial z} + cc \quad \text{etc} \tag{2.45}$$

These equations are called the Manley-Rowe relations. They show that the parametric process can absorb a photon at ω_3 and create a pair of photons at ω_1 and ω_2, or vice versa.

2.3.3 Solutions

The coupled amplitude equations can be solved exactly using Jacobi elliptic functions [4]. However, these solutions are so complicated that numerical solution is often more efficient in practice. In this section, we present solutions for some simple special cases and then discuss the qualitative features of the general solutions. More detailed treatment of the equations can be found in [4] and [1, Chapter 2]. A pedagogical presentation of the analytic solution is given in [5].

The phase mismatch factor $\exp(i\Delta kz)$ is a very important feature of the equations. If L is the interaction length and $\Delta k \cdot L$ is large, the driving polarizations at different positions will cancel and the resulting frequency conversion will be weak. Techniques for achieving phase matching, i.e. making Δk small, will be discussed in Section 2.4.

Consider first DFG with small conversion. The ω_2 and ω_3 waves are assumed to be undepleted, i.e. they do not change with z, and the incident ω_1 waves is assumed to have zero intensity. We use the equations for the photon number amplitudes, (2.23–2.25), because these lead to the simplest form of the solutions. For b_1, we find

$$b_1(z) = \frac{2i\eta b_3 b_2^*}{\Delta k} \sin(\Delta kz/2) \exp(i\Delta kz/2) \tag{2.46}$$

and

$$N_1(z) = \eta^2 N_3 N_2 z^2 \mathrm{sinc}^2(\Delta kz/2) \tag{2.47}$$

This solution may not be very useful for practical frequency conversion, but it is important because phase matching acceptance intervals are usually defined in terms of the width of the sinc^2 factor (Section 2.4). For SFG with small conversion, where b_3 is generated from b_1 and b_2 that are taken to be constant, the solution has exactly the same form:

$$b_3(z) = \frac{2i\eta b_1 b_2}{\Delta k} \sin(\Delta kz/2) \exp(-i\Delta kz/2) \tag{2.48}$$

and

(2.49)

$$N_3(z) = \eta^2 N_1 N_2 z^2 \mathrm{sinc}^2(\Delta kz/2) \tag{2.50}$$

Now consider the more complicated case where only one wave is taken to be undepleted. If this wave is b_3, we find for the other waves

$$b_1(z) = \left[b_1(0)(\cosh(gz) - \frac{i\Delta k}{2g} \sinh(gz)) + b_2^*(0) \frac{i\eta b_3}{g} \sinh(gz) \right] \exp(i\Delta kz/2) \tag{2.51}$$

$$b_2(z) = \left[b_2(0)(\cosh(gz) - \frac{i\Delta k}{2g} \sinh(gz)) + b_1^*(0) \frac{i\eta b_3}{g} \sinh(gz) \right] \exp(i\Delta kz/2) \tag{2.52}$$

$$\text{where } g = \sqrt{\eta^2 N_3 - (\Delta k/2)^2} \tag{2.53}$$

If g is imaginary, the hyperbolic functions can be replaced by the corresponding trigonometric functions, and g by g/i. In the low gain limit, i.e. when $\eta^2 N_3$ is small, the result

reproduces Equation (2.46) when $b_1(0) = 0$. For higher gain, the tolerance to phase mismatch is increased compared to (2.46). A small phase mismatch reduces the gain g, but as long as g is real there is still exponential growth. Both signals grow exponentially because b_3 supplies energy to them both. If the undepleted wave is one of the signals, say b_2, the solutions are qualitatively different because $b_1(0)$ and $b_3(0)$ both limit the amount of energy that can be exchanged between the waves. The solutions are always oscillating:

$$b_1(z) = \left[b_1(0)(\cos(gz) - \frac{i\Delta k}{2g}\sin(gz)) + b_3(0)\frac{i\eta b_2^*}{g}\sin(gz)\right]\exp(i\Delta kz/2) \tag{2.54}$$

$$b_3(z) = \left[b_3(0)(\cos(gz) + \frac{i\Delta k}{2g}\sin(gz)) + b_1(0)\frac{i\eta b_2}{g}\sin(gz)\right]\exp(-i\Delta kz/2) \tag{2.55}$$

$$\text{where } g = \sqrt{\eta^2 N_2 + (\Delta k/2)^2} \tag{2.56}$$

The general solutions show oscillatory behaviour with periodic exchange of energy between the three waves. The period and amplitude of the oscillations depend and the phase mismatch and on the relative phase of the incident waves. If the phase mismatch is large, the oscillations have short period and small amplitude. The amplitude and period of the oscillations are maximized if the phase mismatch is zero and the relative phase of the waves is $\Delta\Phi = \Phi_3 - \Phi_2 - \Phi_1 = \pm\pi$. In this case, the photon numbers N_1, N_2, and N_3 oscillate in the ranges $[\max(0, N_{10} - N_{20}),\ N_{10} + N_{30}]$, $[\max(0, N_{20} - N_{10}),\ N_{20} + N_{30}]$, and $[0,\ N_{30} + \min(N_{10}, N_{20})]$ respectively, where N_{10}, N_{20}, and N_{30} are the initial photon numbers in each wave.

2.3.4 Nonlinear processes

The solutions to the coupled amplitude equations can describe a number of useful nonlinear processes. If signals at ω_1 and ω_2 are incident, the sum frequency ω_3 can be generated. This is called sum frequency generation (SFG). A special case is second harmonic generation (SHG) where $\omega_1 = \omega_2$. On the other hand, if a strong signal at ω_3 is incident, signals at ω_1 (or ω_2) can be amplified while the difference frequency ω_2 (or ω_1) is also generated. This process is called optical parametric amplifcation (OPA) or difference frequency generation (DFG), depending on the application. Note that the abbreviations OPA, DFG, etc. are also used for the corresponding devices, i.e. optical parametric amplifiers, difference frequency generators etc. If an OPA is placed in a resonator, and the gain of the OPA is sufficient to overcome the loss of the resonator, we have an optical parametric oscillator (OPO). In the context of OPAs and OPOs, the wave at ω_3 is usually called the pump wave, while the other waves are called signal or idler waves.

The oscillatory behaviour of the solutions of the amplitude equations have important consequences for nonlinear devices. When one of the input waves is zero, as is often the case in an OPA, all the energy can be transferred from the pump wave a_3 to the signal waves. But after this has happened, back conversion, i.e. transfer of energy back to a_3 takes place. Back conversion is a major problem in practical devices because the period of the oscillations depend on the intensities. Thus if the pump pulse has a nonuniform profile in space or time, it is difficult to achieve good conversion efficiency

over the whole spatial or temporal profile of the pulse. Since back conversion is limited by the number of photons in the a_1 or the a_2 wave, it can be reduced by attenuating one of these waves while keeping the other.

If all three signals have nonzero initial amplitudes, the relative phase of the signals determines the point on the oscillation period where the nonlinear process starts, i.e. if the nonlinear process starts as SFG (amplifying wave 3) or DFG (amplifying waves 1 and 2).

2.4 Phase matching and tuning

As explained in Section 2.3.3, efficient second order interaction requires that the phase mismatch is small. The condition that needs to be satisfied for three collinear waves is

$$|\Delta k\, L| < 2.78 \tag{2.57}$$

where L is the length of the crystal and the figure 2.78 is the half-value point of the $\mathrm{sinc}^2(\Delta k\, L/2)$ factor in Equation (2.47). This value is of course somewhat arbitrary, and some authors use π instead, e.g. [6]. For collinear waves, the phase matching condition can be written

$$\Delta k \equiv (n_3\omega_3 - n_2\omega_2 - n_1\omega_1)/c = 0 \tag{2.58}$$

where n_i is the refractive index for wave i, which in general depends on wavelength and polarization. In an isotropic medium with normal dispersion, the refractive index increases with frequency. This makes phase matching impossible. On the other hand, in birefringent media, it is sometimes possible to achieve phase matching by using the birefringence to cancel the dispersion. Many materials with second order nonlinearity are birefringent. For a given propagation direction, there is a slow and a fast polarization eigenmode. If the highest frequency has the fast polarization, while one or both of the lower frequencies has the slow polarization, phase matching may be achieved for propagation in a certain direction in the crystal. Birefringent phase matching is denoted type 1, 2 or 3, according to the table below [3]. Some literature uses the classification I and II, with type II meaning both types 2 and 3.

Type	ω_1	ω_2	ω_3
1	Slow	Slow	Fast
2	Fast	Slow	Fast
3	Slow	Fast	Fast

Phase matching is also possible for non-collinear waves. In this case, the phase mismatch is given by the vector equation

$$\Delta\mathbf{k} = \mathbf{k}_3 - \mathbf{k}_1 - \mathbf{k}_2 \tag{2.59}$$

For non-collinear phase matching, there is a condition similar to Equation (2.57) for the transverse part of $\Delta\mathbf{k}$. The transverse dimension of the interacting beams is often much smaller than the interaction length, so a relatively large transverse phase mismatch may be acceptable. In the so-called Čerenkov configuration, non-collinear cones of beams interact, and the angle between the beams can adapt to eliminate longitudinal phase

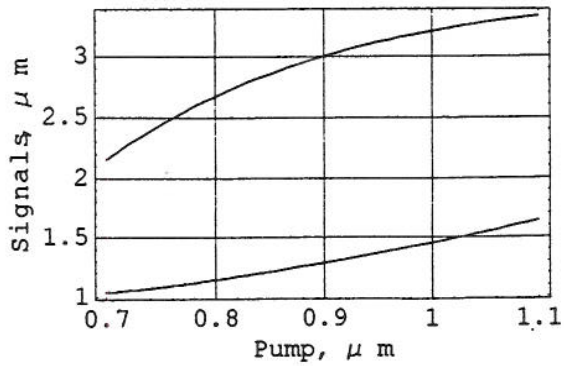

Figure 2.1 *Tuning curves show signal wavelengths as functions of pump wavelength for type 3 phase matching in KTP with propagation in the x-direction*

mismatch [7]. Čerenkov phase matching has been exploited in a wave guide device where one of the signals radiated out of the wave guide [8]. Because of the small transverse dimension of the wave guide, this device accepted a large transverse phase mismatch. Noncollinear phase matching is often called *vector* phase matching. It is discussed in more detail in Section 2.4.4.

2.4.1 Tuning

The set of wavelengths that satisfies the phase matching condition depends on the propagation direction in the crystal. Therefore an OPO can be tuned by rotating the crystal. Tuning can also be achieved by changing any parameter that changes the birefringence of the crystal, like temperature [9] or electric field [10]. Temperature and electro-optic tuning have the advantage of leaving the crystal in one position, but the tuning range is usually smaller than for angle tuning. If the pump source is tunable, e.g. a Ti:sapphire laser, the OPO can be tuned by changing the pump wavelength.

Tuning curves giving signal wavelengths as functions of angle or pump wavelength can be computed by solving the equation for the phase matching condition using Sellmeier equations to model the dispersion. An example of pump tuning is shown in Figure 2.1, and tuning curves for angle tuning are given in Chapter 3.

Temperature tuning must often be treated differently because dispersion equations with temperature dependence are only rarely available. However, individual thermo-optic coefficients for particular wavelengths and temperatures are more common, and these can be used for computing temperature tuning curves for limited temperature intervals. For fixed wavelengths, the phase mismatch changes with temperature according to

$$\frac{\partial \Delta k}{\partial T} = \frac{1}{c}\left(\frac{\partial n_3(\omega_3)}{\partial T}\omega_3 - \frac{\partial n_2(\omega_2)}{\partial T}\omega_2 - \frac{\partial n_1(\omega_1)}{\partial T}\omega_1\right) \tag{2.60}$$

where n_3 is the fast index for the pump and n_1 and n_2 can be fast or slow depending on the type of phase matching. For the general case of propagation outside the principal planes, all the n_i depend on all three principal indices. When the temperature changes and the pump wavelength is fixed, the signal wavelengths will adjust to compensate

for the temperature induced mismatch. Thus

$$\frac{\partial \Delta k}{\partial \omega_2}\Delta\omega_2 + \frac{\partial \Delta k}{\partial T}\Delta T = 0 \tag{2.61}$$

or

$$\Delta\omega_2 = -\Delta T \frac{(\partial \Delta k/\partial T)}{(\partial \Delta k/\partial \omega_2)} \tag{2.62}$$

where it is understood that $\omega_1 = \omega_3 - \omega_2$.

2.4.2 Acceptance intervals

Since phase matching depends on propagation direction, temperature and wavelengths, any 2. order nonlinear process has a limited tolerance to variation in these parameters. In processes with two input signals (SFG, DFG or OPA), the third wavelength is determined by the two input wavelengths. Changing the temperature, crystal orientation, or one of the input wavelengths, will induce a phase mismatch which in turn reduces the efficiency of the nonlinear process. In an OPO, on the other hand, the two signal wavelengths are free to drift, and in absence of other frequency selective elements, they adjust to minimize phase mismatch. Therefore, changing the operating parameters of an OPO tends to tune it, without necessarily reducing the output power. If one wants stable operation, the OPO, like the other nonlinear processes, has limited tolerance to variation in operating parameters.

The tolerance to parameter variation is often expressed in terms of acceptance intervals. The acceptance interval of a parameter is the interval within which inequality (2.57) is satisfied. Because the interaction length L appears as a factor in the inequality, acceptance intervals are usually given for the product of L and the parameter. For example, the pump acceptance bandwidth $L\,\Delta\omega_3$ in an OPA designed to amplify ω_2 is given by

$$L\frac{d\Delta k(\omega_3 - \omega_2, \omega_2, \omega_3)}{d\omega_3}\Delta\omega_3 = 2 \cdot 2.78 \quad \text{or} \quad L\,\Delta\omega_3 = 5.56/\left(\frac{d\Delta k}{d\omega_3}\right) \tag{2.63}$$

It is understood that ω_2 is held fixed while ω_1 is allowed to adapt to satisfy energy conservation. For signal bandwidth (gain bandwidth) we have similarly

$$L\,\Delta\omega_2 = 5.56/\left(\frac{d\Delta k}{d\omega_2}\right) \tag{2.64}$$

where ω_3 is fixed and $\omega_1 = \omega_3 - \omega_2$. Consider collinear type 1 phase matching with a fixed pump frequency. The derivative

$$\begin{aligned}\frac{d\Delta k}{d\omega_2} =& \frac{1}{c}\left(-n_2 - \omega_2\frac{dn_2}{d\omega_2} + n_1 + \omega_1\frac{dn_1}{d\omega_1}\right) = \\ & \frac{1}{c}\left(-n_2 + \lambda_2\frac{dn_2}{d\lambda_2} + n_1 - \lambda_1\frac{dn_1}{d\lambda_1}\right)\end{aligned} \tag{2.65}$$

vanishes at degeneracy, i.e. when $\lambda_1 = \lambda_2$. This makes the gain bandwidth very large. At this point, the sensitivity to angle tuning is also very large because

$$\frac{d\omega_2}{d\theta} = \frac{d\omega_2}{d\Delta k}\frac{d\Delta k}{d\theta} \tag{2.66}$$

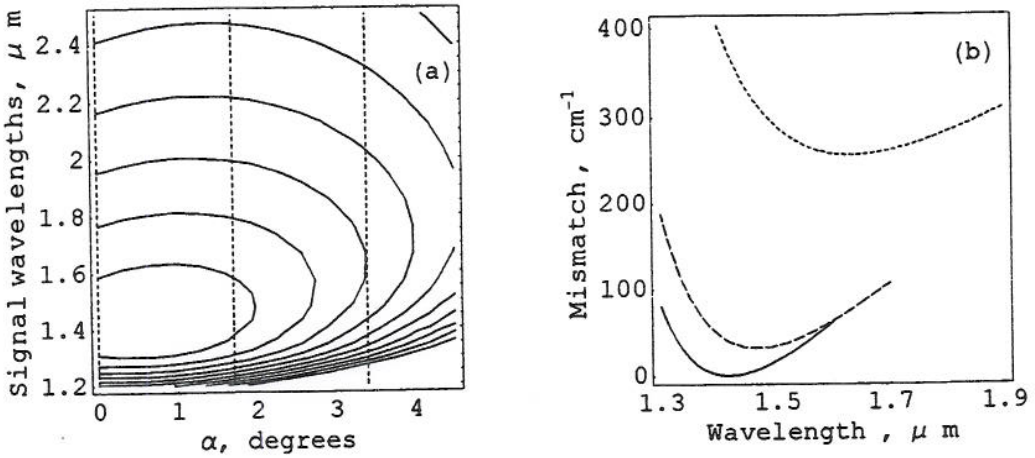

Figure 2.2 *(a) Contours of the surface Δk as a function of signal wavelength and the angle α between signal and pump wave vectors. The pump wavelength is $\lambda_3 = 1.06\,\mu m$, and phase matching is type 2. The dotted lines indicate the positions of the profiles shown in part (b). (b) Profiles of the surface for $\alpha = 0$ (solid), $\alpha = 1.7°$ (dashed), and $\alpha = 3.4°$ (dotted)*

This situation is illustrated by Figure 3.12 on page 56 where the tangent to the tuning curve is vertical at the degenerate point.

The situation with $d\Delta k/d\omega_2 = 0$ can also arise in type 2 or 3 phase matching, but then away from degeneracy. As with type 1 phase matching, it leads to very strong sensitivity to angle tuning. An example is seen at the turning points of the tuning curve in Figure 3.4 on page 43.

With non-collinear phase matching, the wide bandwidth points occur at other wavelengths than with collinear phase matching. To understand non-collinear phase matching, it is useful to consider the surface Δk as a function of ω_2 and the angle α between $\mathbf{k}_2$ and $\mathbf{k}_3$. ω_3 is fixed and ω_1 and $\mathbf{k}_1$ are allowed to adapt. Phase matching is satisfied at the contour $\Delta k = 0$. Tuning by changing one of the angles, say θ, while keeping α fixed, corresponds to shifting the Δk surface vertically. The bandwidth is greatest at the points where $d\Delta k/d\omega_2 = 0$. Figure 2.2 shows the contours and some profiles of the Δk surface for KTA with propagation in the xz-plane, type 2 phase matching, and $\lambda_3 = 1.06\,\mu$m. The wide bandwidth points correspond to the ridge of the contour surface or the minima of the profiles. For collinear phase matching ($\alpha = 0$), we can see the wide bandwidth point corresponding to Figure 3.4. For $\alpha \neq 0$, we see that the wide bandwidth point is shifted.

The wide bandwidth point for non-collinear type 1 phase matching in BBO has been exploited in an OPO with 100 nm gain bandwidth [11]. The OPO was tuned with an external grating, without turning the crystal.

At the wide bandwidth point, the actual bandwidth of a type 1 phase matched OPA is determined by the $|dn/d\omega|$, as can be seen from (2.65). Thus the bandwidth is maximized if this derivative has a minimum at the signal wavelength. This was demonstrated experimentally in [12]. It is illustrated in Figure 3.12, where tuning curves are shown for different pump frequencies. The gain bandwidth is greatest at $\lambda_3 = 900\,$nm, because the index has an inflexion point near $1.8\,\mu$m.

The temperature acceptance interval is defined similarly to the spectral acceptance interval:

$$L\,\Delta T = 5.56/\left(\frac{d\Delta k}{dT}\right) \tag{2.67}$$

Nonuniform temperature distribution in the nonlinear crystal can make the phase mismatch vary across the interacting beams. Such local phase mismatch can reduce beam quality and efficiency. In high power OPOs, even a small absorption in the nonlinear crystal can lead to a temperature gradient that severely degrades performance. The temperature acceptance depends on propagation direction, and it is sometimes possible to reduce the problem by finding a direction that satisfies phase matching while having a large temperature acceptance interval [13].

Acceptance angles give information about tolerance to misaligned crystals, misaligned beams or divergent beams. Compared to the temperature and frequency acceptance intervals, the concept of acceptance angles is more complicated because changing the direction of a beam affects both the magnitude and direction of the phase mismatch vector $\Delta\mathbf{k}$. In many devices, one of the beams can adapt its direction to cancel the transverse part of the phase mismatch. Otherwise, the tolerance to transverse phase mismatch is determined by the width of the beams. When specifying acceptance angles, one must be careful to state which beams change directions, which beams are fixed, and if one beam is allowed to vary freely to minimize phase mismatch. Otherwise an acceptance angle is not meaningful.

As an example of acceptance angle, we consider an OPO with divergent beams. If the beams have the same divergence angle, they can be regarded as locally collinear, with different parts of the beams having different propagation directions in the crystal. Then the local change of propagation direction has the same effect as a rotation of the crystal. The full acceptance interval of the angle θ is

$$L\,\Delta\theta = 5.56/\left(\frac{d\Delta k}{d\theta}\right) \tag{2.68}$$

and similarly for the other angle ϕ. If the modes are not matched, the beams can be regarded as locally non-collinear. If only one signal is resonant, the other signal is free to propagate in the direction that minimizes transverse phase mismatch. If we assume that propagation is in the z-direction, the acceptance angle $\Delta\theta_3$ for the pump is

$$L\,\Delta\theta_3 = 5.56/\left(\frac{d\Delta k_z}{d\theta_3}\right) \tag{2.69}$$

where the wavelengths are fixed, and it is understood that the direction of the nonresonant signal can vary to eliminate the transverse part of $\Delta\mathbf{k}$. Acceptance angles for the signal are similarly defined.

The sensitivity of Δk to variation in the direction or divergence of one of the beams depends strongly on the geometry and on which of the other two beams is held fixed and which is allowed to adapt. A change in direction of a beam will tune the OPO, while divergence can reduce efficiency. Consider for example collinear type 2 phase matcing in the xz-plane of a crystal. Suppose that beam 2 is extraordinary (polarized in the xz-plane) while beams 1 and 3 are ordinary (polarized along y). When the angle

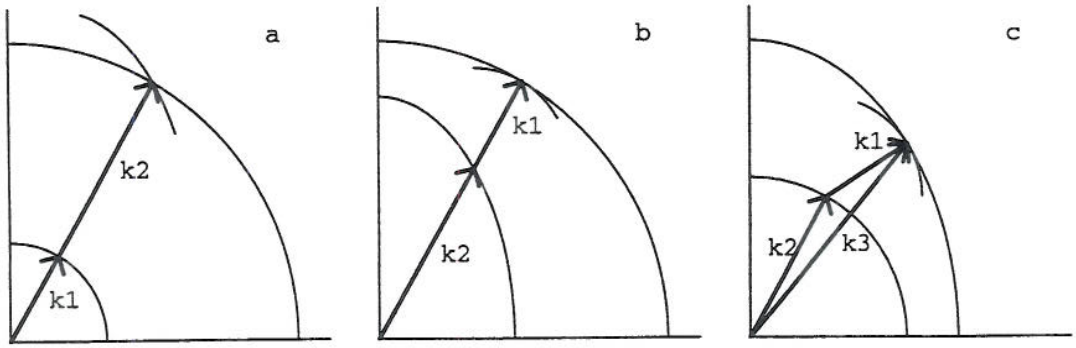

Figure 2.3 *(a) Non-tangential collinear type 2 phase matching. (b) Tangential collinear type 2 phase matching. (c) Tangential non-collinear type 1 phase matching. In parts (a) and (b),* $\mathbf{k}_3 = \mathbf{k}_2 + \mathbf{k}_1$ *is not shown because the vectors overlap*

θ between the propagation direction and the z-axis is varied, n_1 and n_3 remain constant while n_2 changes as the radius of an ellipse, as shown in Figure 2.3(a). Phase matching is satisfied because $\mathbf{k}_3$ (not shown) is exactly equal to $\mathbf{k}_1 + \mathbf{k}_2$. Suppose now that the direction of $\mathbf{k}_3$ changes slightly (phase matching becomes slightly non-collinear), while beam 1 is fixed and beam 2 is allowed to adapt to minimize phase mismatch. The end of $\mathbf{k}_3$ follows the outer circle in Figure 2.3(a). The end of $\mathbf{k}_2$ follows the ellipse in the figure. The resulting phase mismatch is represented by the distance between the ellipse and the outer circle. Figure 2.3(b) illustrates the situation where beam 2 is fixed and beam 1 is allowed to adapt. When beam 1 adapts, the end of $\mathbf{k}_1$ describes a circle that is tangential to the circle of $\mathbf{k}_3$. The figure shows that the resulting phase mismatch is much smaller than in part (a) for the same change of the direction of $\mathbf{k}_3$. This situation is called tangential phase matching (TPM) [6]. TPM is also possible with non-collinear phase matching. In fact, the possibilities for TPM are richer because, for example, a circle may be tangent to an ellipse as shown in Figure 2.3(c), where beams 1 and 2 are ordinary and beam 3 is extraordinary.

These examples illustrate the fact that TPM always applies to a paricular pair of beams. In collinear phase matching, we always have TPM for the two beams with the same polarization (ordinary or extraordinary). In the examples here with type 2 phase matching, one of these beams was the pump wave. In type 1 collinear phase matching, the two signal beams are tangential. This can lead to large divergence of the signal beams. This divergence can be reduced by using non-collinear phase matching [14].

There are at least two other interpretations of TPM. The phase mismatch Δk can be expanded in a Taylor series in the relevant angle parameter, $\Delta\theta$ or $\Delta\phi$, for the beam that changes direction. If the first order term in this series vanishes, phase matching is tangential. The Poynting vectors are always normal to the index surface. Therefore the Poynting vectors of two tangentially phase matched waves are parallel.

A special case of TPM is when all beams propagate along a crystal axis. This is called non-critical phase matching (NCPM), and it satisfies the TPM condition regardless of which beam is held fixed, i.e. all three pairs of beams are tangentially phase matched. Examples of acceptance angles for TPM and non-TPM are given in Section 3.3.7.

2.4.3 Problems with birefringent phase matching

With birefringent phase matching, the phase matching condition, (2.58), determines which propagation and polarization directions must be used for a given set of interacting wavelengths. In some cases, it may be possible to phase match the same set of wavelengths with more than one type of phase matching. In uniaxial crystals, the propagation direction that satisfies the phase matching condition is not unique. Even in biaxial crystals, there may be more solutions for the same type of phase matching. On the other hand, it happens that there is no solution that satisfies phase matching for a given set of wavelengths, even if they are all within the transparent range of the crystal. The number of solutions is determined by the dispersion and birefringence properties of the crystal.

Equation (2.6) shows that χ_{eff} depends on the propagation direction and polarizations of the interacting waves. In other words, χ_{eff} is determined by the phase matching type and propagation direction used. For some combinations, χ_{eff} is small or even zero, so the possibility of phase matching in a crystal is not sufficient for an efficient nonlinear interaction. If more than one phase matching type or propagation direction is possible, the choice can be made to maximize χ_{eff}.

When a wave propagates in a birefringent crystal, the electric field vector $\mathbf{E}$ and the displacement $\mathbf{D}$ are parallel only in special cases: They are parallel when polarization is along a crystal axis, and in uniaxial crystals they are always parallel for the ordinary polarization (polarization in a plane normal to the optic axis). The displacement $\mathbf{D}$ and the magnetic field $\mathbf{H}$ are always normal to the propagation vector $\mathbf{k}$, and the Poynting vector is defined by $\mathbf{S} = \mathbf{E} \times \mathbf{H}$. Thus the angle between $\mathbf{S}$ and $\mathbf{k}$ is equal to the angle between $\mathbf{E}$ and $\mathbf{D}$. This leads to the phenomenon called *walk-off*, the transverse intensity distribution of a beam walks away from the propagation direction. Since the beams interacting in a nonlinear process with birefringent phase matching have different polarizations, they do not all have the same walk-off. For narrow beams, this limits the interaction length. Walk-off also affects the quality of the generated beams. The problem with walk-off can be reduced by using one crystal after another, with the second crystal reversed with respect to the propagation vector. Then the beams walk away from each other in the first crystal and together in the second crystal.

Walk-off does not occur in non-critical phase matching. Unfortunately, NCPM can only be used for the special sets of wavelengths that happen to be phase matched along one of the axes. Temperature tuning is possible, but the tuning range is small. If the pump laser is tunable, a noncritically phase matched OPO can be tuned by tuning the pump.

2.4.4 Non-collinear phase matching

The performance of an OPO can sometimes be improved by the use of non-collinear phase matching. Reduced threshold, improved conversion efficiency and greater pump acceptance angle was reported in [15]. The disadvantage was that the signal spectrum was wider. The reasons for the improvement were that the non-collinearity partly compensated for walk-off, and that phase matching conditions could be made near tangential, increasing the pump acceptance angle. The polarization directions in non-

collinear phase matching differ from those in collinear phase matching of the same frequencies. In some cases, this can increase d_{eff}.

2.4.5 Quasi phase matching

Quasi phase matching (QPM) is another way to avoid the problems inherent in birefringent phase matching. As the name implies, $\Delta k \neq 0$ in QPM. Normally the driving term in the coupled amplitude equations would oscillate as $\exp(i\Delta kz)$. The trick of QPM is to "rectify" these oscillations by changing the sign of χ for each half-period of the oscillations. Thus the relative magnitude of the driving term oscillates between 0 and 1, but it always has the same sign. When the QPM period is optimal, the oscillation introduces a factor $2/\pi$ in χ_{eff}, but this reduction is small compared to the advantages gained. An alternative interpretation of QPM is that modulation of χ with period Λ provides wave vectors $K = \pm 1/\Lambda$ that can cancel Δk. QPM has several attractive features: It can work for any wavelengths within the transparent range of the material by appropriate choice of QPM period. Walk-off can be avoided by choosing the propagation direction along a crystal axis. QPM can be used with any polarizations of the interacting waves. Thus one is free to choose the polarizations that interact through the greatest element of the χ tensor. In many common nonlinear materials, like the KTP-family and $LiNbO_3$, χ_{333} is much greater than any of the other elements. This element can be used with QPM, but not with birefringent phase matching.

Early experiments on QPM were done by slicing and reassembling crystals. These experienced problems with losses and damage at the interfaces. More recently, work on QPM has focused on periodic poling of ferroelectric crystals. Inverting the ferroelectric domain orientation in such a crystal has the effect of changing the sign of χ. Domains can be inverted by modification of the growth process, exposure to electron beams, or, most commonly, application of a strong electric field [16]. Since the domain walls have to be parallel to the unique direction of spontaneous polarization, the propagation direction must be normal to this direction. This does not give full freedom in choice of polarizations, but it usually allows the greatest χ-element to be used. More details on QPM can be found in [17, 18, 19].

Periodic poling has been demonstrated in $LiNbO_3$, $LiTaO_3$, KTP, RTA, RTP, and CTA. See Chapter 3 for more details on QPM in specific materials.

2.5 Coupled amplitude equations with transverse effects

In real nonlinear devices, transverse effects are important, and the plane wave equations discussed in Section 2.3 cannot give a quantitatively correct description. In detailed models, it is necessary to include diffraction, walk-off, transverse variations of the beams and divergence of the beams. Coupled amplitude equations including these effects are derived in Appendix A. The equations are

$$\begin{aligned}\frac{\partial e_3(x,y,z)}{\partial z} = &\tan\rho_x \frac{\partial e_3}{\partial x} + \tan\rho_y \frac{\partial e_3}{\partial y} - \frac{i}{2k_0}\nabla^2 e_3 + \\ &i\omega_3 \frac{\chi_{\text{eff}}}{cn_3} e_1 e_2 \exp(-i(k_3 - k_2 - k_1)z)\end{aligned} \tag{2.70}$$

and similarly for the other waves. These resemble the plane wave equations, but the walk-off terms ($\tan\rho(\partial e/\partial x)$) and diffraction terms ($i/(2k_0)\nabla^2 e$) have been added. ρ_x and ρ_y are the walk-off angles in the two directions.

2.6 Signal bandwidth

As explained in Section 2.4.2, phase matching determines the gain bandwidth of an OPA. This bandwidth is often in the order of 100 GHz. Nevertheless, single frequency operation of CW OPOs is relatively simple because the OPA acts like a homogeneously broadened laser. When one mode reaches threshold, depletion of the pump reduces the gain of the competing modes. A recent experiment compared line widths of OPOs with ring and linear cavities [20]. The ring OPO had the predicted small linewidth, but the spectrum of the linear OPO was much broader. The reason for this was not understood.

Pulsed OPOs tend to have large bandwidth because many modes are amplified to significant intensities before depletion takes place. Even though many modes are oscillating, output signals tend to be smooth because saturation reduces intensity fluctuations [21]. Thus the output signal is mainly phase modulated.

OPO linewidth can be controlled using frequency selective elements or injection seeding like in lasers. If there is a choice of phase matching types, this can also affect the linewidth. For example, as explained in Section 2.4.2, type 1 phase matching near degeneracy leads to large bandwidth. A detailed experimental and numerical study of linewidth and injection seeding of a pulsed OPO is reported in [22]. They studied a BBO OPO pumped by the third harmonic of a Nd:YAG laser. The spectrum of the unseeded OPO had large pulse to pulse fluctuations, with 100% variation of the energy in individual modes. The fluctuation in the total signal energy was only 6–8%. 2 nJ of seed light was enough to cause single mode operation.

The width of the resonant signal of an OPO is not necessarily increased by a multi longitudinal mode pump. Each pump mode can in principle interact with a separate mode of the non-resonant signal and drive the same resonant signal, possibly a single mode. However, the width of the non-resonant signal will increase corresponding to the pump width.

2.7 Noise initiation of parametric oscillation

We are primarily interested in OPOs as wavelength converters. Thus we work with macroscopic fields, and we are not concerned with the quantum properties of the fields. For our purpose, most OPO calculations can be done classically. However, the classical equations cannot describe how the OPO starts. Equations (2.23–2.25) shows that if the signal fields are initially zero, they will remain zero. An OPO starts from spontaneous parametric emission, which is a quantum phenomenon. When simulating OPOs numerically, it is usual to add a noise term to the classical equations to approximate the effect of spontaneous emission. This noise term makes the OPO start, but of course it does not model other quantum properties of the generated fields.

The correct magnitude of the noise terms can be estimated by comparing classical and quantum solutions to the OPO equations and selecting noise terms that make the results agree. We do this for the case with plane waves and perfect phase matching. When the OPO starts, the pump beam is intense and can be modelled classically. After the signal waves have grown to macroscopic amplitudes, classical and quantum behaviour are essentially equal. Therefore we only need to compare the solutions for the initial parts of OPO operation, before pump depletion becomes important. Thus we can use simplified equations like (2.25), and the corresponding solutions like (2.52). If we take b_3 to be real, the classical solutions for the photon numbers become

$$\begin{aligned} N_1(z) = b_1 b_1^* =& N_1(0)\cosh^2(\eta z) + N_2(0)\sinh^2(\eta z) \\ & - i(b_1(0)b_2(0) - b_1^*(0)b_2^*(0))\cosh(\eta z)\sinh(\eta z) \end{aligned} \tag{2.71}$$

and similarly for N_2. In quantum optics, the equations for the field operators correspond to the classical equations for the fields. The solutions are also very similar, see [23, Section 22.4.1]. In our case, the field operators are simply

$$\hat{b}_1(z) = \hat{b}_1(0)\cosh(\eta z) + i\hat{b}_2^\dagger(0)\sinh(\eta z) \tag{2.72}$$

$$\hat{b}_2(z) = \hat{b}_2(0)\cosh(\eta z) + i\hat{b}_1^\dagger(0)\sinh(\eta z) \tag{2.73}$$

We now take both fields to have zero photons initially and find the expectation value of the number operator:

$$\langle \hat{N}_1(z) \rangle = \langle \hat{N}_2(z) \rangle = \sinh^2(\eta z) \tag{2.74}$$

For large ηz, cosh $\approx$ sinh. Classical and quantum results correspond if we take $b_1(0) = 1$, $b_2(0) = 0$ or $b_1(0) = 0$, $b_2(0) = 1$ in the classical equations. Another alternative is $|b_1(0)| = 1/2$, $b_2(0) = ib_1(0)$. Noise terms become more complicated when transverse modes are taken into account. In practice, it turns out that simulation results are not very sensitive to the exact values of the noise terms.

References

[1] R.W. Boyd. *Nonlinear optics.* Academic Press, San Diego, 1992.

[2] Y.R. Shen. *The principles of nonlinear optics.* Wiley, 1984.

[3] D.A. Roberts. Simplified characterization of uniaxial and biaxial nonlinear optical crystals: A plea for standardization of nomenclature and conventions. *IEEE J. Quantum Electron.*, 28:2057–2074, 1992.

[4] J.A. Armstrong, N. Bloembergen, J. Ducuing, and P.S. Pershan. Light waves in a nonlinear dielectric. *Phys. Rev.*, 127:1918–1939, 1962.

[5] T. Debuisschert, J. Raffy, and J.P. Pocholle. Semi-analytical model of the pulsed optical parametric oscillator; comparison with experiment. In S.A. Payne and C.R. Pollock, editors, *Advanced Solid State Lasers*, volume 1 of *OSA Trends in Optics and Photonics*, pages 182–187, 1996.

[6] N.P. Barnes and V.J. Corcoran. Parametric generation processes: spectral bandwidth and acceptance angles. *Appl. Opt.*, 15:696–699, 1976.

[7] M.K. Pandit and F.P. Payne. Cerenkov second-harmonic generation by nondiffracting bessel beams in bulk optical crystals. *Opt. Quantum Electron.*, 29:35–51, 1997.

[8] K. Thyagarajan, V. Rastogi, M.R. Shenoy, D.B. Ostrowsky, M. De Micheli, and P. Baldi. Modeling of parametric amplification in the cerenkov-idler configuration in planar waveguides. *Opt. Lett.*, 21:1631–1633, 1996.

[9] R.C. Eckardt, C.D. Nabors, W.J. Kozlovsky, and R.L. Byer. Optical parametric oscillator frequency tuning and control. *J. Opt. Soc. Am. B*, 8:646–667, 1991.

[10] M.D. Ewbank, M.J. Rosker, and G.L. Bennett. Frequency tuning a mid-infrared optical parametric oscillator by the electro-optic effect. *J. Opt. Soc. Am. B*, 14:666–671, 1997.

[11] J. Wang, M.H. Dunn, and C.F. Rae. Polychromatic optical parametric generation by simultaneous phasematching over a large spectral bandwidth. In *CLEO Europe 1996, Post deadline papers*, 1996. Paper CPD1.1.

[12] J. Raffy, T. Debuisschert, and J.P. Pocholle. Widely tunable OPO without crystal rotation. In C.R. Pollock and W.R. Bosenberg, editors, *Advanced solid-state lasers*, volume 10 of *OSA Trends in Optics and Photonics*, pages 185–188, 1997.

[13] K. Kato. Temperature insensitive SHG at 0.5321 μm in KTP. *IEEE J. Quantum Electron.*, 28:1974–1976, 1992.

[14] C.D. Nabors and G. Frangineas. Optical parametric oscillator with bi-noncollinear, porro prism cavity. In C.R. Pollock and W.R. Bosenberg, editors, *Advanced solid-state lasers*, volume 10 of *OSA Trends in Optics and Photonics*, pages 90–93, 1997.

[15] L.A.W. Gloster, Z.X. Jiang, and T.A. King. Characterization of an Nd:YAG-pumped β-BaB_2O_4 optical parametric oscillator in collinear and noncollinear phase-matched configurations. *IEEE J. Quantum Electron.*, 30:2961–2969, 1994.

[16] L.E. Myers, R.C. Eckardt, M.M. Fejer, R.L. Byer, W.R. Bosenberg, and J.W. Pierce. Quasi-phase-matched optical parametric oscillators in bulk periodically poled $LiNbO_3$. *J. Opt. Soc. Am. B*, 12:2102–2116, 1995.

[17] S.K. Wong. Effects of plate thickness and stack distribution of quasi-phase-matched materials on nonlinear frequency generation. *IEEE J. Quantum. Electron.*, 32:1560–1569, 1996.

[18] M.M. Fejer, G.A. Magel, D.H. Jundt, and R.L. Byer. Quasi-phase-matched second harmonic generation: tuning and tolerances. *IEEE J. Quantum. Electron.*, 28:2631–2654, 1992.

[19] K.C. Rustagi, S.C. Mehendale, and S. Meenakshi. Optical frequency conversion in quasi-phase-matched stacks of nonlinear crystals. *IEEE J. Quantum. Electron.*, 18:1029–1041, 1982.

[20] W.R. Bosenberg, A. Drobshoff, J.I. Alexander, L.E. Myers, and R.L. Byer. 93% pump depletion, 3.5W continuous-wave, singly resonant optical parametric oscillator. *Opt. Lett.*, 21:1336–1338, 1996.

[21] D.J. Armstrong and A.V. Smith. Tendency of nanosecond optical parametric oscillators to produce purely phase-modulated light. *Opt. Lett.*, 21:1634–1636, 1996.

[22] A. Fix and R. Wallenstein. Spectral properties of pulsed nanosecond optical parametric oscillators: Experimental investigation and numerical analysis. *J. Opt. Soc. Am. B*, 13:2484–2497, 1996.

[23] L. Mandel and E. Wolf. *Optical coherence and quantum optics.* Cambridge University Press, 1995.

3 MATERIALS FOR SECOND ORDER PROCESSES

In this section, we review the materials KTP, KTA, RTP, RTA, CTA, $LiNbO_3$, $LiIO_3$, $KNbO_3$, $LiTaO_3$, $AgGaS_2$, $AgGaSe_2$, $ZnGeP_2$, CdSe, $CdGeAs_2$, GaSe and GaAs. These materials are the most promising for OPO operation in the 3–5 μm or 8–12 μm bands.

3.1 Material parameters

The crystal data most important to OPO design are

- Transmission spectrum
- Dispersion data for phase matching calculation
- Second order nonlinear coefficients
- Optical damage thresholds
- Availability and cost
- If the OPO is operated at high power at a wavelength with non-negligible absorption, thermal conductivity, thermal expansion and the temperature dependence of the refractive indices also become important.
- For very high intensity, typical of picosecond and femtosecond pulses, the nonlinear refractive index n_2 becomes relevant. This has been measured only in a few crystals.
- Robustness with respect to mechanical stress, temperatures and moisture.

For some materials, we include examples with tuning curves, d_{eff}, walk-off and acceptance intervals. We also include examples of published experiments and results with the material.

A problem when reporting material properties is that some crystals exist in multiple varieties. Variation in composition, doping or growth technique can affect the crystal properties. Phase matching conditions (angle and temperature) can be sensitive to very small changes in the material.

3.1.1 Transmission range

Published transmission ranges differ widely for some materials. One reason is that the definition of transmission range is somewhat arbitrary. For definite information, we need the full absorption spectrum, not only the ends of the so-called transparent range. We have not found such spectra for all materials. Sometimes the spectrum of the transmission through a particular crystal is shown, instead of the spectrum of the absorption coefficient. If the crystal length is known, the absorption coefficient can be computed from the transmission.

Absorption data are further complicated by variation between samples. The spectrum can be sensitive to small impurities or water content. In some crystals, the transmission depends on the propagation direction and polarization. The conclusion is that the transmission spectrum should be measured for the actual crystals to be used in experiments.

3.1.2 Refractive index data

The refractive index depends on wavelength and temperature. The wavelength dependence is normally represented by Sellmeier equations. Such equations can be derived directly from measured index data, or from indirect data in the form of phase matching angles. Roberts [1] recently proposed a new technique for combining data of both these types, and weighting them according to confidence. Using this technique, he obtained new Sellmeier equations for KDP, $AgGaSe_2$ and $AgGaS_2$. Like the transmission spectrum, the dispersion data may vary between different samples of the same material.

The temperature dependence of the refractive indices is important for temperature tuning and temperature acceptance intervals. In general the temperature dependence of the refractive index is complicated, and it cannot be decoupled from the dispersion. Nevertheless, it is common to approximate it by a linear change in the refractive indices within a temperature range:

$$n_i(T) = n_i(T_0) + \frac{dn_i}{dT}(T - T_0) \tag{3.1}$$

Published values of dn/dT (the thermo-optic coefficients) vary wildly, and the wavelength at which they were measured, is not always specified. Thermo-optic coefficients for unspecified wavelength and temperature should be treated with great suspicion. For some materials, like $LiNbO_3$ and $KNbO_3$, there exist modified Sellmeier equations that include temperature dependence. In some cases, thermo-optic coefficients can be fitted to a model-based equation of the form

$$2n\frac{dn}{dT} = GR + HR^2 \tag{3.2}$$

where $R = \lambda^2/(\lambda^2 - \lambda_{ig}^2)$ and λ_{ig} is a bandgap that was introduced in the model [2, 3].

3.1.3 Nonlinear coefficients

As explained in Section 2.1.4, the d-matrix notation is commonly used for reporting the second order susceptibility. We follow this convention when citing other peoples work, but we emphasize that care must be exercised when using these data at three different wavelengths. Dispersion of the d-tensor can be approximately modelled by Miller's rule (see Section 2.1.3). This is typically more accurate than the nonlinear susceptibility data themselves [4].

Methods for measuring the d-coefficients include phase matched SHG [5], Maker fringes (using non-phase matched SHG) [6], phase matched parametric gain [7], and parametric

fluorescence [8]. In the Maker fringe method, the interaction length is varied by rotating the crystal. A variation of this method is the wedge technique, where the interaction length is changed by translation of a wedge shaped crystal. In our tables, we abbreviate the measurement methods: spontaneous parametric generation = SPG, Maker fringes = MF, phase matched second harmonic generation = PM SHG, wedge technique = WT. Accurate data for nonlinear coefficients are exceptions, and published data often differ by 50% or more. There are several reasons for this:

- Different methods of measurement give different results. For example, it has been found that parametric fluorescence consistently leads to higher d-values than second harmonic generation [5, 9]. This problem is currently unresolved.
- The nonlinear coefficients depend on wavelengths. Some workers are not careful to report the wavelengths used in the measurement.
- The elements of the d-matrix are not always measured individually. When the propagation direction is not along a crystal axis, two or more elements may contribute to the measured effective nonlinearity. Deconvolution of these results may introduce errors.
- All the measurement methods are difficult to implement experimentally with high accuracy. For instance, the results may be sensitive to the transverse and temporal profiles of the pump pulses.
- Many experiments measure only some elements of the d-matrix. This makes it difficult to find consistent and complete data. If only an effective value is measured, it is common to use ratios from earlier reports to estimate the values of the individual d-matrix elements. Thus new reports are not always independent of former data, and errors may propagate.
- d-coefficients are often measured relative to another material. Therefore the reported data depend on the accuracy of the d-coefficients of the reference material.
- Some experiments determine only the magnitudes of the d-elements, and not the signs. The relative signs are important when d_{eff} for an interaction is a linear combination of d-elements.

In the SI system, when using the convention in Equation (2.3), d has units m/V. Some authors report the d-coefficients in esu (electrostatic units). For conversion, use the formula

$$1\,\text{m/V} = \frac{4\pi}{3 \cdot 10^4}\text{esu}$$

from [6, Appendix A].

3.1.4 Damage thresholds

Data on damage thresholds are often uncertain. There can be significant differences between samples due to minor defects in the crystal or surface. Data obtained at different wavelengths or pulse lengths are difficult to compare.

References

[1] D.A. Roberts. Dispersion equations for nonlinear optical crystals: KDP, $AgGaSe_2$ and $AgGaS_2$. *Appl. Opt.*, 35:4677–4688, 1996.

[2] G. Ghosh. Thermo-optic coefficients of $LiNbO_3$, $LiIO_3$, and $LiTaO_3$ nonlinear crystals. *Opt. Lett.*, 19:1391–1393, 1994.

[3] G.T. Johnston. Wavelength dependence of dn/dT in infrared-transmitting semiconductor materials. *Appl. Opt.*, 16:1796–1797, 1977.

[4] D.A. Roberts. Simplified characterization of uniaxial and biaxial nonlinear optical crystals: A plea for standardization of nomenclature and conventions. *IEEE J. Quantum Electron.*, 28:2057–2074, 1992.

[5] R.C. Eckardt, H. Masuda, Y.X. Fan, and R.L. Byer. Absolute and relative nonlinear optical coefficients of KDP, KD*P, BaB_2O_4, $LiIO_3$, MgO:$LiNbO_3$, and KTP measured by phase-matched second-harmonic generation. *IEEE J. Quantum Electron.*, 26:922–933, 1990.

[6] R.W. Boyd. *Nonlinear optics.* Academic Press, San Diego, 1992.

[7] D.J. Armstrong, W.J. Alford, T.D. Raymond, and A.V. Smith. Absolute measurements of the effective nonlinearities of KTP and BBO crystals by optical parametric amplification. *Appl. Opt.*, 35:2032–2040, 1996.

[8] K. Koch, E.C. Cheung, G.T. Moore, S.H. Chakmakjian, and J.M. liu. Hot spots in parametric fluorescence with a pump beam of finite cross section. *IEEE J. Quantum Electron.*, 31:769–781, 1995.

[9] E.C. Cheung, K. Koch, G.T. Moore, and J.M. liu. Measurement of second-order nonlinear optical coefficients from the spectral brightness of parametric fluorescence. *Opt. Lett.*, 19:168–170, 1994.

3.2 The KTP isomorphs

These are a family of materials with formula $M\mathrm{TiO}X\mathrm{O}_4$, where M is K, Rb, Tl, NH_4 or Cs and X is P or As [1]. Five of them, KTiOPO_4 (KTP), $\mathrm{KTiOAsO}_4$ (KTA), $\mathrm{RbTiOPO}_4$ (RTP), $\mathrm{RbTiOAsO}_4$ (RTA), and $\mathrm{CsTiOAsO}_4$ (CTA) have been used in nonlinear optics. KTP is very much used for OPOs and second harmonic generation. KTA has also been used in a number of devices, while experience with the other materials is relatively small. The materials share a number of desirable features: High nonlinear coefficients, high damage thresholds, mechanical robustness, and they are nonhygroscopic.

The KTP isomorphs are all positive biaxial with point group mm2 (C_{3v}). Most of the literature on KTP isomorphs reports nonlinear coefficients in a frame XYZ that coincides with the principal dielectric axes xyz. Z is the axis of rotational symmetry. We follow this convention although it swaps X and Y-axes relative to the standard [2]. Note that some literature follows the standard. With point group mm2, the only nonzero elements of the d-matrix are d_{15}, d_{24}, d_{31}, d_{32}, and d_{33}. If Kleinman symmetry is valid, $d_{31} = d_{15}$ and $d_{32} = d_{24}$.

The KTP isomorphs have similar refractive indices and nonlinear coefficients. However, small differences in dispersion can be very important in particular applications. For example, different materials allow noncritical phase matching at different wavelengths. Reported d-coefficients for the 5 materials differ, but not more than different measurements in the same material. When comparing the KTP isomorphs, reference [1] is useful because it contains measurements of all the 5 materials, apparently carried out in the same laboratory and with the same methods. The KTP isomorphs are ferroelectric, with spontaneous polarization along the $z = Z$ axis. Periodic poling has been done in KTP, RTP, RTA, and CTA.

The form of the d-matrix restricts the possible polarization directions of the interacting waves. The interacting polarizations can be ZZZ, ZXX, ZYY, and permutations of these. The ZZZ interaction is not very useful in birefringent phase matching because not all the waves can have large field components in the Z direction. The ZXX and ZYY interactions require that one of the waves has a significant polarization component in the Z-direction. Thus θ should not be too small. For $\theta > \Omega$, where Ω is the angle between the Z-axis and the optics axes, it is the slow wave that has polarization in the Z-direction. To satisfy phase matching, this has to be one of the signal waves. Because of this, type 2 or 3 phase matching is most common in the KTP isomorphs. Type 1 is also possible, but d_{eff} is relatively small.

References

[1] L.K. Cheng, L.T. Cheng, J. Galperin, P.A.Morris Hotsenpiller, and J.D. Bierlein. Crystal growth and characterization of KTiOPO_4 isomorphs from the self-fluxes. *J. Crystal Growth*, 137:107–115, 1994.

[2] D.A. Roberts. Simplified characterization of uniaxial and biaxial nonlinear optical crystals: A plea for standardization of nomenclature and conventions. *IEEE J. Quantum Electron.*, 28:2057–2074, 1992.

3.3 KTP ($KTiOPO_4$)

3.3.1 Transmission range

Most of the literature, including suppliers' data sheets, state that the transparency range is 350-4500 nm [1, 2, 3]. Litton [4] claims only 350-3500 nm, and they also state that there is an absorption band near 2800 nm. The transmission spectrum published in [5] shows large absorption for $\lambda > 3$ μm, and it is slightly different for polarizations along the y- and z-axes. The crystal was x-cut and 15 mm long. We have measured the transmission spectra of two 20 mm long x-cut flux-grown KTP crystals from different suppliers, and they both agree well with [5]. Transmission spectra of KTP are shown in Figure 3.1.

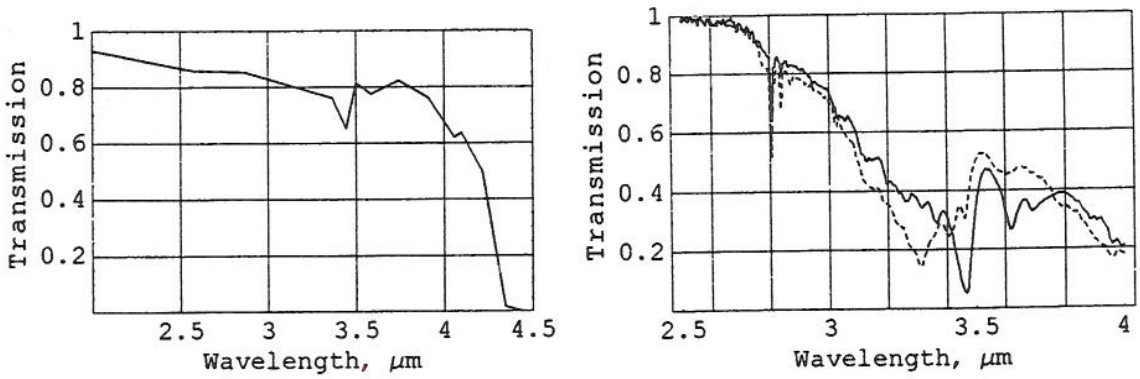

Figure 3.1 *Left: Transmission spectrum of 3 mm long KTP crystal with z-polarized light propagating in the x-direction. Data from [6]. Right: Transmission spectra of 20 mm long KTP crystal from Casix, propagation in the x-direction. Solid curve: z-polarized light. Dotted curve: y-polarized light. Data were measured by us. The absolute level is uncertain, so the transmission was scaled to unity at $\lambda = 2.5\mu m$*

In spite of the absorption, KTP OPOs have generated wavelengths as large as $\lambda = 3.96$ μm. Absorption in the crystal reduced the power for $\lambda > 3.5$ μm [7]. This result indicates that some KTP crystals may have better IR transmission than the crystals we measured.

3.3.2 Refractive index

There are numerous published Sellmeier equations for KTP [8, 9, 10, 11, 12, 5]. The latter two cover the widest wavelength range and appear to be the most accurate. The equations in [12] are based on minimum deviation measurements in hydrothermal KTP, in the wavelength range 350-2400 nm. In [2], the authors claim that these Sellmeier equations are valid for the whole transparency range up to about 4500 nm. The equations in [5] are based on phase matching angles in flux grown KTP. The wavelength range is not explicitly stated, but the equations seem to perform well at least in the range from 450-3300 nm. Many Sellmeier equations were compared with experimental phase matching angles in flux grown KTP in [13]. The equations in [12] agreed very well with experimental data at least to 2800 nm. The equations in [5] had deviations of up to 1.5° in phase matching angle, while the other equations were

worse. Dmitriev et.al. [3], recommend the Sellmeier equations in [11] for the whole transparency range. These equations appear to us to be less accurate than [12]. Litton [4] uses the equations from [12], and Casix [14] and Castech [15] use those from [5]. Cristal Laser [16] provide their own Sellmeier equations. The Sellmeier equations in [12] have the form

$$n^2 = A + \frac{B\lambda^2}{\lambda^2 - C^2} - D\lambda^2$$

where

Axis	A	B	C	D
x	2.1146	0.89188	0.20861	0.01320
y	2.1518	0.87862	0.21801	0.01327
z	2.3136	1.00012	0.23831	0.01679

The Sellmeier equations in [5] are

$$n^2 = A + \frac{B}{\lambda^2 - C} - D\lambda^2$$

where

Axis	A	B	C	D
x	3.0065	0.03901	0.04251	0.01327
y	3.0333	0.04154	0.04547	0.01408
z	3.3134	0.05694	0.05658	0.01682

Reported thermo-optic coefficients differ widely. This is not surprising, because the temperature derivatives of the refractive indices depend on both temperature and wavelength [17]. Reference [18] gives expressions for the thermo-optic coefficients obtained by fitting experimental data for the wavelength range 502–1129 nm and the temperature range 15–40°C to the following function:

$$dn/dT = (A\lambda^{-3} + B\lambda^{-2} + C\lambda^{-1} + D)10^{-6}\mathrm{K}^{-1} \tag{3.3}$$

where

Axis	A	B	C	D
x	1.427	-4.735	8.711	0.952
y	4.269	-14.761	21.232	-2.113
z	12.415	-44.414	59.129	-12.101

The same equations were fitted to other experimental data in [19], leading to somewhat different coefficients. Some other example thermo-optic coefficients are given in Table 3.1.

Reported values of the nonlinear index are shown in Table 3.2.

Source	x	y	z	λ, μm
[18]	0.61	0.83	1.45	1.064
[2]	1.1	1.3	1.6	
[19]	1.65	2.5	3.4	1.064
[3]	2	2.7	4	
[17]	1.9	2.5	3.7	1.064
[16]	0.56	0.65	1.12	

Table 3.1 Thermo-optic coefficients of KTP. The table shows $10^5\, dn/dT$ for each of the principal axes x, y, and z. Some of the sources did not specify λ

Reference	n_2, 10^{-16}cm^2/W	λ, nm	Polarization
[20]	46	532	z or y
[21]	23	532	z or y
[21]	23	1064	z
[22]	14–21	1064	in xy-plane

Table 3.2 Nonlinear refractive index of KTP

3.3.3 Nonlinear coefficients

Nonlinear coefficients also differ widely. The early data from [1] are often quoted, but most of their coefficients are much higher than more recent results. The most common method to measure d is phase matched type 2 second harmonic generation in the xy-plane. This yields an effective value d_{eff} which is a linear combination of d_{24} and d_{15}. Using type 1 phase matching outside the xy-plane it is also possible to measure d_{33} in this way. By Kleinman symmetry, $d_{31} = d_{15}$ and $d_{32} = d_{24}$. References [23, 19, 24] argue for Kleinman symmetry. With the Maker fringe method, all the 5 nonzero d-coefficients can be measured independently. These data do not support the assumption of Kleinman symmetry, but the discrepancies may be due to measurement errors. Measured values of the d-matrix elements are summarized in Table 3.3.

Source	d_{15}	d_{24}	d_{31}	d_{32}	d_{33}	Method	Wavelength, μm
[1]	6.1	7.6	6.5	5	13.7	MF	Probably 1.064
[23]	1.4	2.65	1.4	2.65	10.7	PM SHG	1.064
[5, 19]	1.9	3.4	1.9	3.4	8.1	PM SHG	Near 1
[25]	1.9	3.6	2.54	4.35	16.9	MF	Measured at 0.88, scaled to 1.064
[15]	2.6	3.3	1.9	3.5	13.7		
[26]		4.1				SPG	0.527, 0.9, 1.269

Table 3.3 Nonlinear coefficients of KTP, in pm/V

The values of d_{15} and d_{24} found by [25] are supported by many reports of d_{eff} [27, 13, 28]. Reference [28] measured d_{eff} for SHG for many different KTP crystals and found that some crystals had multiple ferroelectric domains, leading to reduced d_{eff}.

3.3.4 Damage

The threshold is lower for surface damage than for bulk damage. Casix [14] and Castech [15] state that the surface damage threshold is at least 450 MW/cm^2 for 10 ns pulses (4.5 J/cm^2) at 1.06 μm. Ahmed [29] report thresholds at least twice as high. For more data on damage thresholds under various conditions, see [3, 30] and references therein.

KTP is also susceptible to temporary damage in the form of grey tracks [23, 31], but this damage is only induced by intense visible light, e.g. in SHG experiments, so it is not a problem in IR OPOs.

3.3.5 Thermal data

Sources agree that the specific heat is about 700 J/(kg·K). Reference [2] states that the thermal conductivity is 0.02 to 0.033 W/(cm·K), depending on direction. This is supported by a recent report [32] of values in the range 0.022–0.026 W/(cm·K). Casix and Castech state 0.13 W/(cm·K), but this must be wrong. For thermal expansion, see [2].

3.3.6 Price and availability

KTP can be grown with hydrothermal or flux processes. The difference between crystals grown with different processes appears to be small [2]. Hydrothermal KTP is supplied by Litton Airtron, all other suppliers use flux processes. We have purchased a $3 \times 3 \times 20$ mm crystal from Casix for \$950. Litton charges at least 5 times as much. Crystal Associates quotes \$1100 for $5 \times 5 \times 15$ mm.

3.3.7 Tuning calculations

Figure 3.2 shows tuning curves for a KTP OPO with type 2 or 3 phase matching in the XZ-plane for 3 different pump wavelengths. The curves are based on the Sellmeier equations in [12]. In this phase matching geometry, $d_{\text{eff}} = d_{24} \sin\theta$. For $\lambda_3 = 1.064\,\mu$m and $\lambda_1 = 3.8\,\mu$m, walk-off of the λ_1-wave is 2.8°, and the acceptance intervals are $L\,\Delta T = 19.5$ cm K, $L\,\Delta\theta = 1.5$ cm mrad, $L\,\Delta\phi = 9500$ cm mrad, $L\,\Delta\lambda_3 = 4.3$ cm nm, and $L\,\Delta\lambda_1 = 930$ cm nm. Note that the gain bandwidth is large because the tuning curve is steep at this point.

The difference between tangential and non-tangential phase matching can be illustrated by the pump-acceptance angles in type 2 phase matching when the signal wavelengths are 3 μm and 1.64 μm. If wave 1 (3 μm, polarized along y) is fixed, $L\,\Delta\theta_3 = 1.1$ cm mrad. On the other hand, if wave 2 (1.65 μm, polarized in the xz-plane) is fixed, $L\,\Delta\theta_3 = 59$ cm mrad.

Noncritical phase matching is possible at 1.57 μm and 3.3 μm in the x-direction and at 1.52 μm and 3.54 μm in the y-direction. For the x-direction ($\theta = 90°$, $\phi = 0$) and with thermo-optic coefficients from [19], we find $d\Delta k/dT = -9.5\,\text{m}^{-1}/\text{K}$. We also find that

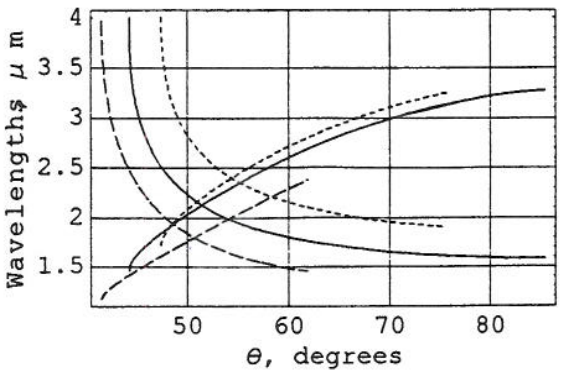

Figure 3.2 *Tuning curves for KTP for different pump wavelengths. Solid:* $\lambda_3 = 1.064\,\mu m$, *dashed:* $\lambda_3 = 0.9\,\mu m$, *dotted:* $\lambda_3 = 1.2\,\mu m$

$d\Delta k/d\lambda_2 = 284\,\mathrm{m}^{-1}/\mathrm{nm}$. Combining these with Equation (2.62) we find $d\lambda_2/dT = -0.034\,\mathrm{nm/K}$. This is in reasonable agreement with a directly measured temperature tuning coefficient of $-0.022\mathrm{nm/K}$ [32]. The temperature acceptance interval is $L\,\Delta T = 58\,\mathrm{K\,cm}$. The acceptance bandwidth for the pump is about 1 cm nm. The acceptance bandwidth for the 1.57 μm signal (i.e. the gain bandwidth) is about 2 cm nm. The acceptance angle is about 3500 cm mrad. This is large because of the noncritical phase matching.

3.3.8 Examples

A large number of papers on KTP-based OPOs have been published, e.g. [33, 5, 34, 7]. Marshall and Kaz [33] achieved 47% conversion from 1.064 μm Nd:YAG radiation to 1.61 μm in a noncritically phase matched OPO. The KTP crystal was 20 mm long, and the peak pump fluence was 2.3 J/cm^2. The output energy at 1.61 μm was 10 mJ. With an x-cut crystal the output wavelength was measured to be 1.61 μm, and with a y-cut crystal it was 1.54 μm. These differ from the wavelengths that we calculated in Section 3.3.7. KTP and KTA based OPOs designed for ruggedized laser systems are reported in [35]. Reference [36] compares a NCPM KTP OPO and stimulated Raman scattering for conversion of Nd:YAG radiation to eye-safe wavelengths. A KTP based OPO for use in airborne military systems was described in [37].

McCahon et.al. generated 175 fs pulses in a synchronously pumped OPO. The pump source was a mode-locked Ti:sapphire laser giving 750 mW at 830 nm. The hydrothermally grown KTP crystal was 2 mm long and cut at $\theta = 43°$ in the xz-plane. The resonant signal could be angle tuned from 1.05–1.16 μm, and the nonresonant signal from 2.9–3.96 μm. Output was 22 mW at 3.55 μm or 13 mW at 3.96 μm. The angle between the wave-vectors of the pump and the resonant signal was about 1° to partly compensate for walk-off. Power was reduced at the long wavelength because of absorption in the crystal.

Periodic poling has been done in hydrothermal KTP[38]. A period of only 4 μm was achieved with a sample thickness of 1 mm. Flux grown KTP is difficult to pole because of greater conductivity, but it has recently been achieved [39].

References

[1] F.C. Zumsteg, J.D. Bierlein, and T.E. Gier. $K_xRb_{1-x}TiOPO_4$: A new nonlinear optical material. *J. Appl. Phys.*, 47:4980–4985, 1976.

[2] J.D. Bierlein and H. Vanherzeele. Potassium titanyl phosphate: properties and new applications. *J. Opt. Soc. Am. B*, 6:622–633, 1989.

[3] V.G. Dmitriev, G.G. Gurzadyan, and D.N. Nikogosyan. *Handbook of nonlinear optical crystals.* Springer-Verlag, Heidelberg, 1991.

[4] Litton Airtron - SYNOPTICS Group, Charlotte, NC, USA. *KTP Data sheet*, 1994.

[5] K. Kato. Parametric oscillation at 3.2 μm in KTP pumped at 1.064 μm. *IEEE J. Quantum Electron.*, 27:1137–1140, 1991.

[6] L.K. Cheng and J.D. Bierlein. Crystal growth of $KTiOPO_4$ isomorphs from tungstate and molybdate fluxes. *J. Crystal Growth*, 110:697–703, 1991.

[7] S.W. McCahon, S.A. Anson, D.J. Jang, and T.F. Boggess. Generation of 3-4 μm femtosecond pulses from a synchronously pumped, critically phase-matched KTP OPO. *Opt. Lett.*, 20:2309–2311, 1995.

[8] T.Y. Fan, C.E. Huang, B.Q. Hu, R.C. Eckardt, R.L. Byer, and R.S. Feigelson. Second harmonic generation and accurate index of refraction measurements in flux-grown $KTiOPO_4$. *Appl. Opt.*, 26:2390–2394, 1987.

[9] K. Kato. Second-harmonic and sum-frequency generation to 4950 and 4589 å in KTP. *IEEE J. Quantum Electron.*, 24:3–4, 1988.

[10] D.W. Anthon and C.D. Crowder. Wavelength dependent phase matching in KTP. *Appl. Opt.*, 27:2650–2652, 1988.

[11] V.A. Dyakov and V.V. Krasnikov. Sellmeier equation and tuning characteristics of KTP crystal frequency converters in the 0.4 - 4.0 μm range. *Sov. J. Quantum Electron.*, 18:1059–1060, 1988.

[12] H. Vanherzeele, J.D. Bierlein, and F.C. Zumsteg. Index of refraction measurements and parametric generation in hydrothermally grown $KTiOPO_4$. *Appl. Opt.*, 27:3314–3316, 1988.

[13] J.J. Zondy, M. Abed, and A. Clairon. Type-II frequency doubling at 1.30 μm and 2.53 μm in flux-grown potassium titanyl phosphate. *J. Opt. Soc. Am. B*, 11:2004–2015, 1994.

[14] Casix, Inc, Fujian, China. *Crystal Guide*, 1996.

[15] Fujian Castech Crystals, Inc, Fujian, China. *Crystals.*

[16] Cristal Laser, SA, Chaligny, France. *Cristal Laser Catalog*, 1996.

[17] D.J. Gettemy, W.C. Harker, G. Lindholm, and N.P. Barnes. Some optical properties of KTP, $LiIO_3$, and $LiNbO_3$. *IEEE J. Quantum Electron.*, 24:2231–2237, 1988.

[18] W. Wiechmann, S. Kubota, T. Fukui, and H. Masuda. Refractive-index temperature derivatives of potassium titanyl phosphate. *Opt. Lett.*, 18:1208–1210, 1993.

[19] K. Kato. Temperature insensitive SHG at 0.5321 μm in KTP. *IEEE J. Quantum Electron.*, 28:1974–1976, 1992.

[20] W. Ji, H.P. Li, F. Zhou, and N. Zhai. Picosecond z-scan investigation of two-photon absorption and bound electronic self-focusing in second-harmonic-generation crystals. In M. Eich, B.H.T. Chai, and M. Jiang, editors, *Electro-optic and second harmonic generation materials, devices, and applications*, volume 2897 of *Proc. SPIE*, pages 414–423, 1996.

[21] R. DeSalvo, A.A. Said, D.J. Hagan, E.W. van Stryland, and M. Sheik-Bahae. Infrared to ultraviolet measurements of two-photon absorbtion and n_2 in wide bandgap solids. *IEEE J. Quantum. Electron.*, 32:1324–1333, 1996.

[22] R. DeSalvo, M. Sheik-Bahae, A.A. Said, D.J. Hagan, and E.W. van Stryland. Z-scan measurement of the anisotropy of nonlinear refraction and absorption in crystals. *Opt. Lett.*, 18:194–196, 1993.

[23] B. Boulanger, M.M. Fejer, R. Blachman, and P.F. Bordui. Study of $KTiOPO_4$ gray-tracking at 1064, 532 and 355 nm. *Appl. Phys. Lett.*, 65:2401–2403, 1994.

[24] D.A. Roberts. Simplified characterization of uniaxial and biaxial nonlinear optical crystals: A plea for standardization of nomenclature and conventions. *IEEE J. Quantum Electron.*, 28:2057–2074, 1992.

[25] H. Vanherzeele and J.D. Bierlein. Magnitude of the nonlinear-optical coefficients of $KTiOPO_4$. *Opt. Lett.*, 17:982–984, 1992.

[26] E.C. Cheung, K. Koch, G.T. Moore, and J.M. liu. Measurement of second-order nonlinear optical coefficients from the spectral brightness of parametric fluorescence. *Opt. Lett.*, 19:168–170, 1994.

[27] R.C. Eckardt, H. Masuda, Y.X. Fan, and R.L. Byer. Absolute and relative nonlinear optical coefficients of KDP, KD*P, BaB_2O_4, $LiIO_3$, MgO:$LiNbO_3$, and KTP measured by phase-matched second-harmonic generation. *IEEE J. Quantum Electron.*, 26:922–933, 1990.

[28] D.J. Armstrong, W.J. Alford, T.D. Raymond, and A.V. Smith. Absolute measurements of the effective nonlinearities of KTP and BBO crystals by optical parametric amplification. *Appl. Opt.*, 35:2032–2040, 1996.

[29] F. Ahmed. Laser damage threshold of $KTiOPO_4$. *Appl. Opt.*, 28:119–122, 1989.

[30] R.J. Bolt and M. Mooren. Single shot bulk damage threshold and conversion efficiency measurements on flux grown KTP. *Opt. Commun.*, 100:399–410, 1993.

[31] M.P. Scripsick and G.J. Edwards. The role of point defects in optical damage of nonlinear crystals. In B.H. Chai, editor, *Growth, Characterization, and Applications of Laser Host and Nonlinear Crystals II*, volume 1863 of *Proc. SPIE*, pages 170–180, 1993.

[32] C.A. Ebbers and S.P. Velsko. Optical and thermo-optical characterization of KTP and its isomorphs for 1.06μm pumped opos. In M.C. Gupta, W.J. Kozlovsky, and D.C. MacPherson, editors, *Nonlinear frequency generation and conversion*, volume 2700 of *Proc. SPIE*, pages 227–239, 1996.

[33] L.R. Marshall and A. Kaz. Eye-safe output from noncritically phase-matched parametric oscillators. *J. Opt. Soc. Am. B*, 10:1730–1736, 1993.

[34] F. Huisken, M. Kaloudis, and J. Marquez. Single-mode $KTiOPO_4$ optical parametric oscillator. *Opt. Lett.*, 20:2306–2308, 1995.

[35] R.P. Jones. Parametric oscillation in KTP and KTA at 1064 nm. In G.J. Quarles, L. Esterowitz, and L.K. Cheng, editors, *Solid State Lasers and Nonlinear Crystals*, volume 2379 of *Proc. SPIE*, pages 357–360, 1995.

[36] G. Roy and P. Mathieu. Comparison of raman and degenerated optical parametric oscillators for a high-energy and high-repetition-rate eye-safe laser. *Opt. Eng.*, 35:3579–3584, 1996.

[37] G.A. Grabon, W.L. Moon, G. Witt, and L. Jones. Solid state eyesafe converter for multi-mode yag lasers. In N. Peygambarian, H. Everitt, R.C. Eckardt, and D.D. Lowenthal, editors, *Nonlinear Optics for High-Speed Electronics and Optical Frequency*, volume 2145 of *Proc. SPIE*, pages 299–308, 1994.

[38] Q. Chen and W.P. Risk. Periodic poling of $KTiOPO_4$ using an applied electric

field. *Electron. Lett.*, 30:1516–1517, 1994.

[39] H. Karlsson and F. Laurell. Periodic poling of flux grown KTP. In C.R. Pollock and W.R. Bosenberg, editors, *Advanced solid-state lasers*, volume 10 of *OSA Trends in Optics and Photonics*, pages 61–63, 1997.

3.4 KTA ($KTiOAsO_4$)

KTA is not as much developed as KTP, but it is a very promising material. KTA shares most of the good properties of KTP, and it has better IR transmission. Some reports indicate that is has higher nonlinear coefficients and damage threshold [1]. KTA is often doped to promote growth of single domain crystals [2, 3]. Doping may affect crystal properties.

3.4.1 Transmission range

Most sources agree that the transmission range starts at 350 nm, but there is some disagreement about the longer end of the wavelength range. Reports vary from 4 to 5.3 μm. Figure 3.3 shows two transmission spectra of KTA.

The material $KTi_{1-x}Zr_xOAsO_4$ for x up to 0.3, has been reported to have somewhat better IR transmission the pure KTA [4].

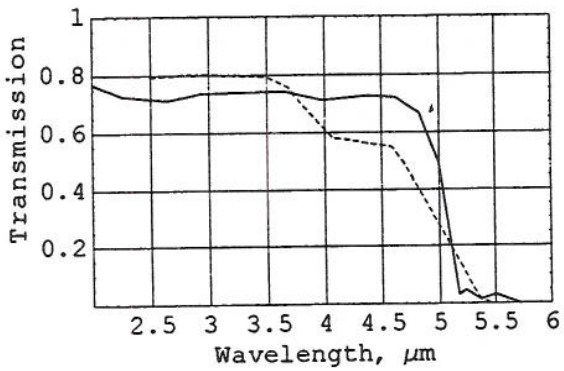

Figure 3.3 *Transmission spectra of KTA. Solid curve: 3 mm long crystal, z-polarized light propagating in the x-direction. Data from [5]. Dotted curve: 5 mm long crystal, propagation along $\theta = 23°$ in the xz-plane. Data from [6]*

3.4.2 Refractive index

Sellmeier equations for KTA are reported in [7]. They are based on minimum deviation measurements in the range 0.41–3.6 μm. The equations have the form:

$$n^2 = A + \frac{B\lambda^2}{\lambda^2 - C^2} - D\lambda^2$$

where

Axis	A	B	C	D
x	1.90713	1.23522	0.19692	0.01025
y	2.15912	1.00099	0.21844	0.01096
z	2.14786	1.29559	0.22719	0.01436

These equations are for (nominally) undoped KTA. The dispersion of KTA can vary significantly because of small impurities [8]. A set of Sellmeier equations given in [9] is probably inaccurate because it used data from contaminated crystals [10].

3.4.3 Nonlinear coefficients

Measured values of the d-matrix elements are summarized in Table 3.4. These data are consistent with Kleinman symmetry.

Source	d_{15}	d_{24}	d_{31}	d_{32}	d_{33}	Method	Wavelength, μm
[2, 3]			2.8	4.2	16.3	MF	Near 1
[9]	2.5	4.5				PM SHG	Near 1

Table 3.4 Nonlinear coefficients of KTA, in pm/V

3.4.4 Damage

Bosenberg et.al. [1] report at least 1.2 GW/cm^2 for 7 ns pulses at 1064 nm. They tested several KTA and KTP crystals and found that all the KTA crystals had higher damage threshold than any of the KTP crystals.

3.4.5 Thermal data

Thermal expansion is reported in [11]. Thermal conductivity is in the range 0.018–0.021 W/(cm·K), depending on direction [12].

3.4.6 Price and availability

Crystal Associates can supply standard sizes up to $5 \times 5 \times 15$ mm. For this size, they charge $1350.

3.4.7 Tuning calculations

Figure 3.4 shows tuning curves for a KTA OPO with type 2 or 3 phase matching in the XZ-plane. The pump wavelength is 1.0642 μm. The curve is based on the Sellmeier equations in [7]. In this phase matching geometry, $d_{\text{eff}} = d_{24} \sin\theta$. Note that with type 2 phase matching and θ in the vicinity of 41°, two pairs of signal wavelengths are simultaneously phase matched. This is possible because the refractive index changes rapidly near 4 μm and slowly near 1.45 μm, so that the left hand side of the phase matching condition $\omega_1 n_1 + \omega_2 n_2 = \omega_3 n_3$ has a maximum near $\lambda_2 = 1.45$ μm. It is possible that this effect is a result of using the Sellmeier equations outside the range of wavelengths in which they were fitted to experimental data. Nevertheless, the effect is worth the comment because it may occur in other crystals even if it is not really present in KTA.

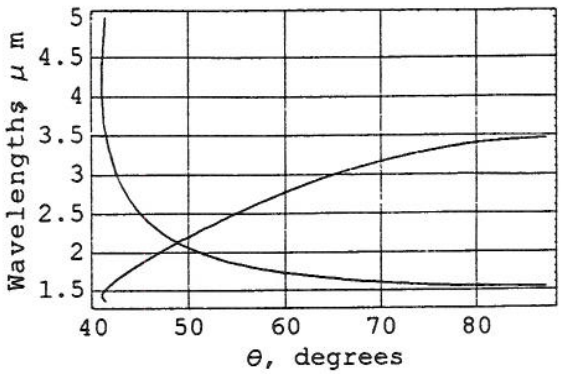

Figure 3.4 Tuning curve for KTA

Noncritical phase matching is possible at 1.53 μm and 3.47 μm in the x-direction and at 1.50 μm and 3.64 μm in the y-direction.

3.4.8 Examples

A KTA-based OPO is reported in [1]. The KTA crystal was x-cut and 10 mm long. The OPO was noncritically phase matched and had a flat-flat cavity with two-pass pump. The pump was a Nd:YAG laser giving 7 ns pulses. With 60 mJ pump, the OPO gave 9 mJ at 1.5 μm.

References

[1] W.R. Bosenberg, L.K. Cheng, and J.D. Bierlein. Optical parametric frequency conversion properties of $KTiOAsO_4$. *Appl. Phys. Lett.*, 65:2765–2767, 1994.

[2] L.K. Cheng, L.T. Cheng, J.D. Bierlein, F.C. Zumsteg, and A.A. Ballman. Properties of doped and undoped crystals of single domain $KTiOAsO_4$. *Appl. Phys. Lett.*, 62:346–348, 1993.

[3] L.K. Cheng, L.T. Cheng, J. Galperin, P.A.Morris Hotsenpiller, and J.D. Bierlein. Crystal growth and characterization of $KTiOPO_4$ isomorphs from the self-fluxes. *J. Crystal Growth*, 137:107–115, 1994.

[4] L. Isaenko, A. Merkulov, V. Tyurikov, S. Gromilov, and R. Mashkovtsev. Growth and characterization of $KTi_{1-x}Zr_xAsO_5$ single crystals. *J. Crystal Growth*, 166:502–506, 1996.

[5] L.K. Cheng and J.D. Bierlein. Crystal growth of $KTiOPO_4$ isomorphs from tungstate and molybdate fluxes. *J. Crystal Growth*, 110:697–703, 1991.

[6] G.M. Loiacono, D.N. Loiacono, J.J. Zola, R.A. Stolzenberger, T. McGee, and R.G. Norwood. Optical properties and ionic conductivity of $KTiOAsO_4$ crystals. *Appl. Phys. Lett.*, 61:895–897, 1992.

[7] D.L. Fenimore, K.L. Schepler, U.B. Ramabadran, and S.R. McPherson. Infrared corrected sellmeier coefficients for potassion titanyl arsenate. *J. Opt. Soc. Am. B*, 12:794–796, 1995.

[8] J.D. Bierlein and H. Vanherzeele. Erratum: "linear and nonlinear optical properties of flux-grown $KTiOAsO_4$" [Appl. Phys. Lett. 54, 783 (1989)]. *Appl. Phys. Lett.*, 61:3193, 1992.

[9] K. Kato. Second-harmonic and sum-frequency generation in $KTiOAsO_4$. *IEEE J. Quantum Electron.*, 30:881–883, 1994.

[10] J.D. Bierlein and H. Vanherzeele. Potassium titanyl phosphate: properties and new applications. *J. Opt. Soc. Am. B*, 6:622–633, 1989.

[11] Z. Zhong, P.K. Gallagher, D.L. Loiacono, and G.M. Loiacono. The thermal expansion and stability of $KTiOAsO_4$ and related compounds. *Thermochimica Acta*, 234:255–261, 1994.

[12] C.A. Ebbers and S.P. Velsko. Optical and thermo-optical characterization of KTP and its isomorphs for 1.06μm pumped opos. In M.C. Gupta, W.J. Kozlovsky, and D.C. MacPherson, editors, *Nonlinear frequency generation and conversion*, volume 2700 of *Proc. SPIE*, pages 227–239, 1996.

3.5 RTP ($RbTiOPO_4$)

There is relatively little information on RTP. We obtain data from [1, 2], and [3], which cites a Russian report. We are not aware of any commercial supplier of RTP, and we have not found reports on any OPO using it.

3.5.1 Transmission range

A transmission spectrum of RTP is shown in Figure 3.5.

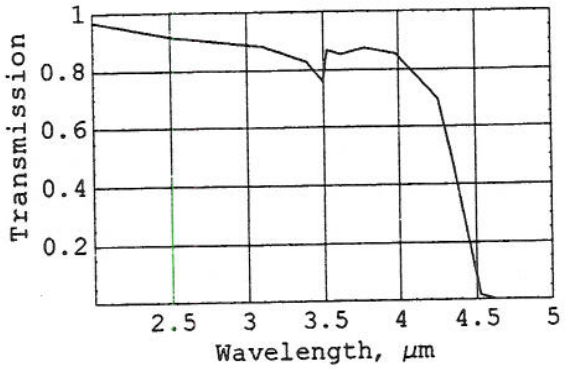

Figure 3.5 *Transmission spectrum of RTP. 3 mm long crystal, z-polarized light propagating in the x-direction. Data from [1]*

3.5.2 Refractive index

From [3], wavelength range not specified:

$$n^2 = A + \frac{B\lambda^2}{\lambda^2 - C} - D\lambda^2$$

where

Axis	A	B	C	D
x	2.56666	0.53842	0.06374	0.01666
y	2.34868	0.77949	0.05449	0.0211
z	2.77339	0.63961	0.08151	0.02237

From [2], wavelength range 0.45–1.5 μm:

$$n^2 = A + \frac{B\lambda^2}{\lambda^2 - C^2} - D\lambda^2$$

where

Axis	A	B	C	D
x	2.15559	0.93397	0.20994	0.01452
y	2.38494	0.73603	0.23891	0.01583
z	2.27723	1.11030	0.23454	0.01995

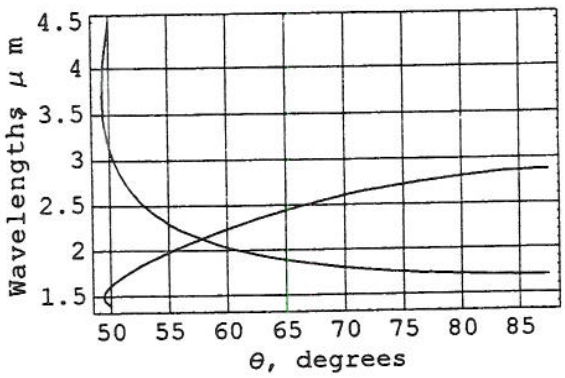

Figure 3.6 Tuning curve for RTP

3.5.3 Nonlinear coefficients

Cheng et.al. [2] measured $d_{31} = 3.3$ pm/V, $d_{32} = 4.1$ pm/V, and $d_{33} = 17.1$ pm/V using Maker fringes at 1.064 μm. Zumsteg et.al. [4] measured the same d-coefficients for RTP and KTP, but these data are much higher than more recent measurements of d in KTP, so they are probably not reliable for RTP either.

3.5.4 Damage

900 MW/cm^2 for 17 ns pulses at 1.06 μm [3].

3.5.5 Tuning calculations

Figure 3.6 shows tuning curves for an RTP OPO with type 2 or 3 phase matching in the XZ-plane. The pump wavelength is 1.0642 μm. The curve is based on the Sellmeier equations in [2]. In this phase matching geometry, $d_{\text{eff}} = d_{24} \sin\theta$. The tuning curve may be inaccurate because the Sellmeier equations are used outside their range.

Noncritical phase matching is possible at 1.69 μm and 2.87 μm in the x-direction and at 1.61 μm and 3.15 μm in the y-direction.

3.5.6 Examples

Periodically poled RTP has been used for frequency doubling [5]. A 3 mm long and 0.7 mm thick crystal was poled with 6.6 μm period.

References

[1] L.K. Cheng and J.D. Bierlein. Crystal growth of $KTiOPO_4$ isomorphs from tungstate and molybdate fluxes. *J. Crystal Growth*, 110:697–703, 1991.

[2] L.K. Cheng, L.T. Cheng, J. Galperin, P.A.Morris Hotsenpiller, and J.D. Bierlein. Crystal growth and characterization of $KTiOPO_4$ isomorphs from the self-fluxes. *J. Crystal Growth*, 137:107–115, 1994.

[3] V.G. Dmitriev, G.G. Gurzadyan, and D.N. Nikogosyan. *Handbook of nonlinear optical crystals.* Springer-Verlag, Heidelberg, 1991.

[4] F.C. Zumsteg, J.D. Bierlein, and T.E. Gier. $K_xRb_{1-x}TiOPO_4$: A new nonlinear optical material. *J. Appl. Phys.*, 47:4980–4985, 1976.

[5] H. Karlsson, F. Laurell, and L.K. Cheng. Diode laser frequency doubling in periodically poled $RbTiOPO_4$. In *CLEO Europe 1996, post deadline papers*, 1996. Paper CPD1.2.

3.6 RTA ($RbTiOAsO_4$)

3.6.1 Transmission range

Transmission spectra of RTA are shown in Figures 3.7.

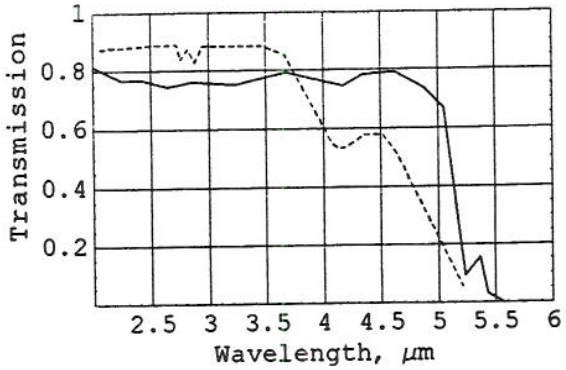

Figure 3.7 *Transmission spectra of RTA. Solid curve: 3 mm long crystal, z-polarized light propagating in the x-direction. Data from [1]. Dotted curve: 10 mm long crystal, propagation along $\theta = 42°$ in the xz-plane, polarization not specified. Data from [2]*

3.6.2 Refractive index

The following Sellmeier equations are based on measurements with the minimum deviation method in the wavelength range 0.4–3.6 μm [2]:

$$n^2 = A + \frac{B\lambda^2}{\lambda^2 - C^2} - D\lambda^2$$

where

Axis	A	B	C	D
x	2.04207	1.17785	0.20157	0.01035
y	2.14941	1.09267	0.21462	0.01067
z	2.18962	1.30103	0.22809	0.01390

Sellmeier equations for the range 0.4–1.5 μm are given in [3]. These equations agree in their wavelength range.

3.6.3 Nonlinear coefficients

Cheng et.al. [3] measured $d_{31} = 2.3$ pm/V, $d_{32} = 3.8$ pm/V, and $d_{33} = 15.8$ pm/V using Maker fringes at 1.064 μm.

3.6.4 Damage

Crystal Associates [4] states 400 MW/cm^2 for 10 ns pulses at 1064 nm.

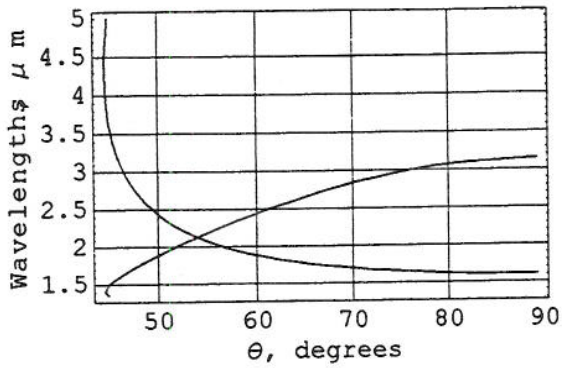

Figure 3.8 Tuning curve for RTA

3.6.5 Thermal data

Thermal conductivity is in the range 0.016–0.017 W/(cm·K), depending on direction [5].

3.6.6 Price and availability

Crystal Associates can supply standard sizes up to $5 \times 5 \times 15$ mm. For this size, they charge $2250.

3.6.7 Tuning calculations

Figure 3.8 shows tuning curves for an RTA OPO with type 2 or 3 phase matching in the XZ-plane. The pump wavelength is 1.0642 μm. The curve is based on the Sellmeier equations in [2]. In this phase matching geometry, $d_{\text{eff}} = d_{24} \sin\theta$.

Noncritical phase matching is possible at 1.61 μm and 3.15 μm in the x-direction and at 1.54 μm and 3.42 μm in the y-direction.

3.6.8 Examples

Reid et.al. [6] built a femtosecond OPO with a 2 mm RTA crystal. When pumped with 880 mW at 825 nm, it generated 185 mW at 1.27 μm. The other signal was at 2.4 μm. Powers et.al. [7] made a femtosecond OPO that was tunable from 2.15–3.65 μm.

Periodic poling has been done in flux grown RTA, and frequency doubling was done in a 1 mm thick crystal with 4.2 μm period [8, 9]. RTA has much lower conductivity than KTP, and this makes poling easier.

References

[1] L.K. Cheng and J.D. Bierlein. Crystal growth of $KTiOPO_4$ isomorphs from tungstate and molybdate fluxes. *J. Crystal Growth*, 110:697–703, 1991.

[2] D.L. Fenimore, K.L. Schepler, D. Zelmon, S. Kück, U.B. Ramabadran, P. Von Richter, and D. Small. Rubidium titanyl arsenate difference-frequency generation and validation of new sellmeier coefficients. *J. Opt. Soc. Am. B*, 13:1935–1940, 1996.

[3] L.K. Cheng, L.T. Cheng, J. Galperin, P.A.Morris Hotsenpiller, and J.D. Bierlein. Crystal growth and characterization of $KTiOPO_4$ isomorphs from the self-fluxes. *J. Crystal Growth*, 137:107–115, 1994.

[4] Crystal Associates, Inc., Waldwick, NJ, USA. *Nonlinear optical crystals data sheet*, 1994.

[5] C.A. Ebbers and S.P. Velsko. Optical and thermo-optical characterization of KTP and its isomorphs for 1.06μm pumped opos. In M.C. Gupta, W.J. Kozlovsky, and D.C. MacPherson, editors, *Nonlinear frequency generation and conversion*, volume 2700 of *Proc. SPIE*, pages 227–239, 1996.

[6] D.T. Reid, M. Ebrahimzadeh, and W. Sibbett. Design criteria and comparison of femtosecond optical parametric oscillators based on $KTiOPO_4$ and $RbTiOAsO_4$. *J. Opt. Soc. Am. B*, 12:2168–2179, 1995.

[7] P.E. Powers, C.L. Tang, and L.K. Cheng. High-repetition-rate femtosecond optical parametric oscillator based on $RbTiOAsO_4$. *Opt. Lett.*, 19:1439–1441, 1994.

[8] H. Karlsson, F. Laurell, P. Henriksson, and G. Arvidsson. Frequency doubling in periodically poled $RbTiOAsO_4$. *Electron. Lett.*, 32:556–557, 1996.

[9] Z.W. Hu, P.A. Thomas, J. Webjörn, and G.M. Loiacono. Domain inversion in $RbTiOAsO_4$ using electric field poling. *J. Phys. D: Appl. Phys.*, 29:1681–1684, 1996.

3.7 CTA ($CsTiOAsO_4$)

3.7.1 Transmission range

A transmission spectrum of CTA is shown in Figure 3.9.

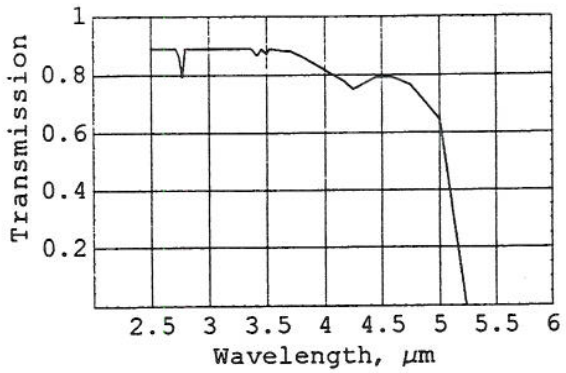

Figure 3.9 *Transmission spectrum of CTA, 5 mm long crystal, propagation in the x-direction, polarization not specified. Data from [1]*

3.7.2 Refractive index

From [2, 3], wavelength range 0.45–1.5 μm:

$$n^2 = A + \frac{B\lambda^2}{\lambda^2 - C^2} - D\lambda^2$$

where

Axis	A	B	C	D
x	2.34498	1.04863	0.22044	0.01483
y	2.74440	0.70733	0.26033	0.01526
z	2.53666	1.10600	0.24988	0.01711

A recent report [4] indicates that these may be somewhat inaccurate.

3.7.3 Nonlinear coefficients

Cheng et.al. [3] measured $d_{31} = 2.1$ pm/V, $d_{32} = 3.4$ pm/V, and $d_{33} = 18.1$ pm/V using Maker fringes at 1.064 μm. Boulanger et.al. [4] measured $d_{15} = 1.09$ pm/V and $d_{24} = 1.7$ pm/V with phase matched SHG at 1.32 μm.

3.7.4 Damage

Crystal Associates [5] states 400 MW/cm^2 for 10 ns pulses at 1064 nm.

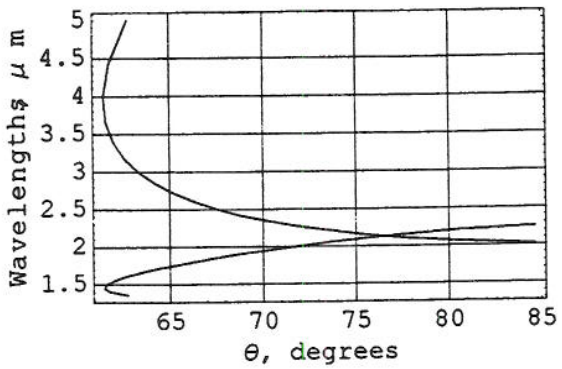

Figure 3.10 Tuning curve for CTA

3.7.5 Price and availability

Crystal Associates can supply CTA on a research basis.

3.7.6 Tuning calculations

Figure 3.10 shows tuning curves for a CTA OPO with type 2 or 3 phase matching in the XZ-plane. The pump wavelength is 1.0642 μm. The curve is based on the Sellmeier equations in [3]. In this phase matching geometry, $d_{\text{eff}} = d_{24} \sin\theta$. The tuning curve may be inaccurate because the Sellmeier equations are used outside their range.

Noncritical phase matching is possible at 2.0 μm and 2.27 μm in the x -direction and at 1.71 μm and 2.81 μm in the y -direction.

3.7.7 Examples

A femtosecond OPO which was tunable from 2.59–4.12 μm is reported in [6]. It was pumped by 1.12 W at 809 nm and generated 235 mW at 1.12 μm.

CTA has been periodically poled by Karlsson et.al., but the results have not been published yet.

References

[1] G.M. Loiacono, D.N. Loiacono, and R.A. Stolzenberger. Crystal growth and characterization of ferroelectric $CsTiOAsO_4$. *J. Crystal Growth*, 131:323–330, 1993.

[2] L.T. Cheng, L.K. Cheng, J.D. Bierlein, and F.C. Zumsteg. Nonlinear optical and electro-optical properties of single crystal $CsTiOAsO_4$. *Appl. Phys. Lett.*, 63:2618–2620, 1993.

[3] L.K. Cheng, L.T. Cheng, J. Galperin, P.A.Morris Hotsenpiller, and J.D. Bierlein. Crystal growth and characterization of $KTiOPO_4$ isomorphs from the self-fluxes. *J. Crystal Growth*, 137:107–115, 1994.

[4] B. Boulanger, J.P. Feve, G. Marnier, G.M. Loiacono, D.N. Loiacono, and C. Bonnin. SHG and internal conical refraction experiments in $CsTiOAsO_4$: Comparison with $KTiOPO_4$ and $KTiOAsO_4$ for 1.32 μm type 2 SHG. *IEEE J. Quantum. Electron.*, 33:945–949, 1997.

[5] Crystal Associates, Inc., Waldwick, NJ, USA. *Nonlinear optical crystals data sheet*, 1994.

[6] G.R. Holtom, R.A. Crowell, and L.K. Cheng. Femtosecond mid-infrared optical parametric oscillator based on $CsTiOAsO_4$. *Opt. Lett.*, 20:1880–1882, 1995.

3.8 $LiNbO_3$ (LNO)

$LiNbO_3$ has been used in nonlinear optics since the 1960s, and it is one of the best developed nonlinear materials. Several varieties of LNO are in use. Congruently grown LNO contains 48.6% Li and 51.4% Nb (atomic percent). (Congruent growth means that the crystal and the melt has the same composition. This is only possible for one particular composition.) Stoichiometric LNO contains 50% Li [1]. The reason for using different varieties is that LNO is susceptible to photorefractive (PR) damage. This means that light changes the refractive index of the material, thereby reducing the optical quality. Such damage is temporary, and it can be erased by heating the crystal to the damage annealing temperature, which is in the range 100 – 200°C. PR damage can be avoided by operating the crystal at high temperature. Congruent LNO allows noncritical phase matching for SHG of 1.064 μm at room temperature, but not at the temperatures required to avoid PR damage. To allow NCPM at high temperature, crystals with higher Li content (e.g. Stoichiometric) were grown. Later it has been found that MgO doping removes the problem of PR damage even at room temperature. Doping concentrations of 4.5–7 mol% are common. ZnO doping is also used [2]. When using reported data on LNO, one must be aware of the difference between LNO of different compositions. Analysis of LNO composition is discussed in [3].

LNO is negative uniaxial with point group 3m (C_{3v}). The axes are chosen so that xyz = XYZ, with $n_z < n_x = n_y$.

3.8.1 Transmission range

Transmission spectra of MgO:LNO and pure LNO are shown in Figure 3.11. The absorption depends on polarization direction, with better IR transmission for polarization along the z-axis (extraordinary). Although absorption starts at about 4μm, an LNO OPOs was operated with one signal at 4.83μm [4], but the power was reduced for long wavelengths.

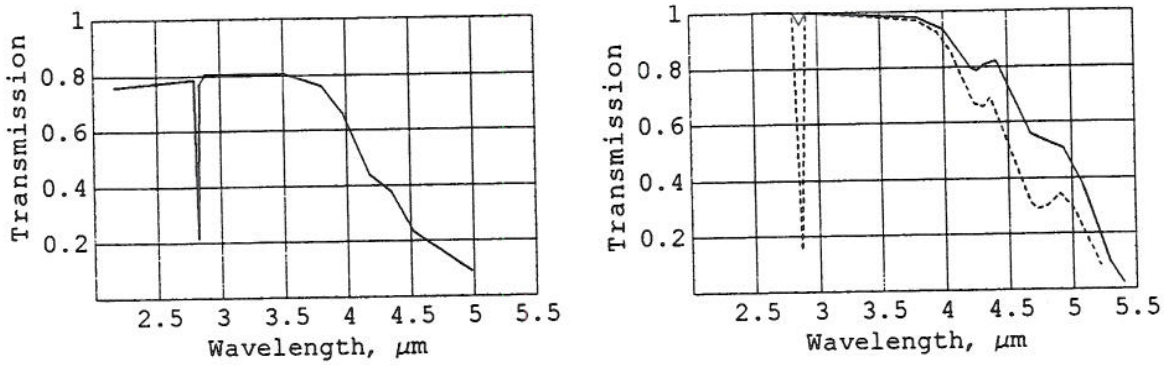

Figure 3.11 *Left: Transmission spectrum of 7% MgO:LNO, 20 mm crystal, unspecified polarization. Data from [5]. Right: Transmission spectra of pure congruent LNO, 9 mm crystal. Solid curve: e-polarization. Dotted curve: o-polarization. Data from [4]*

3.8.2 Refractive index

Edwards and Lawrence [6] provide dispersion equations with temperature dependence for congruent LNO in the wavelength range 0.4–3.2 μm:

$$n^2 = A_1 + \frac{A_2 + B_1 F}{\lambda^2 - (A_3 + B_2 F)^2} + B_3 F - A_4 \lambda^2 \tag{3.4}$$

where $F = T^2 - T_0^2$, T is the temperature in Kelvin, $T_0 = 297.5$K, and the coefficients are

Coefficient	Ordinary (x,y)	Extraordinary (z)
A_1	4.9048	4.5820
A_2	0.11775	0.09921
A_3	0.21802	0.21090
A_4	0.027153	0.021940
B_1	$2.2314 \cdot 10^{-8}$	$5.2716 \cdot 10^{-8}$
B_2	$-2.9671 \cdot 10^{-8}$	$-4.9143 \cdot 10^{-8}$
B_3	$2.1429 \cdot 10^{-8}$	$2.2971 \cdot 10^{-8}$

There is evidence that these equations are inaccurate for high temperatures and long wavelengths [7, 8]. Eckardt et.al. suggested a modification of these equations for LNO with 5% MgO [9]: By changing A_1 for the extraordinary polarization to 4.55207, the computed results agreed with their experimental phase matching temperature. Jundt et.al. [10] provide equations of the same form as (3.4) for stoichiometric LNO in the wavelength range 325–1064 nm. Yao et.al. [11] provide Sellmeier equations for (7 mol %)MgO:LNO. The coefficients for the o-polarization were later improved [5] by fitting to phase matching angles in the range 2.2–3.4 μm. Note that for type 1 phase matching in LNO, the long wavelengths are o-polarized while the short wavelength is e-polarized, so the limited range of the Sellmeier equation for e-polarization is not a problem. The equations have the form

$$n^2 = A + \frac{B}{\lambda^2 - C} - D\lambda^2$$

where

Source	Polarization	A	B	C	D
[11]	o (x,y)	4.87615	0.11554	0.04673	0.03378
[5]	o (x,y)	4.86687	0.11916	0.04263	0.02751
[11]	e (z)	4.54686	0.09478	0.04539	0.02672

Composition dependent Sellmeier equations for LNO are proposed in [12]. More Sellmeier equations and references are given in [13, 6].

Ghosh [14] provides equations for the thermo-optic coefficients according to Equation (3.2) with the coefficients

Polarization	$10^6 G$	$10^6 H$	λ_{ig}, μm
o (x,y)	-173.556	163.038	0.280
e (z)	-23.966	177.681	0.281

Reported values of the nonlinear index are shown in Table 3.5.

Reference	n_2, 10^{-16}cm^2/W	λ, nm	Polarization
[15]	53	532	x
[16]	82	532	z
[16]	9	1064	z
[17]	39		x

Table 3.5 Nonlinear refractive index of $LiNbO_3$

3.8.3 Nonlinear coefficients

The nonzero d-coefficients are $d_{31} = d_{32}$, $d_{15} = d_{24}$, $d_{22} = -d_{21} = d_{16}$, and d_{33}. If Kleinman symmetry holds, $d_{15} = d_{31}$. d-matrix elements are given in Table 3.6.

Source	d_{15}	d_{22}	d_{31}	d_{33}	Doping	Method	Wavelength, μm
[18]		2.1	4.4	33			
[13]	-5.44	-2.76	-5.95	-34		SPG	
[19]	-4.3	2.1	-4.3	-27		PM SHG	
[20]			-4.7		5% MgO	PM SHG	1.064

Table 3.6 Nonlinear coefficients for LNO, in pm/V

3.8.4 Damage

The threshold for permanent optical damage in pure (probably congruent) LNO is reported to be about 3 J/cm^2 [21]. The threshold could be significantly higher on small spots. MgO doped LNO has higher damage threshold. Casix [2] and Castech [18] claim 5 GW/cm^2 for 12 ns pulses at 1064 nm, but these data seem very optimistic.

LNO is susceptible to two types of temporary damage. Photorefractive (PR) damage is local, light-induced changes in the refractive index. These changes destroy the optical quality of the crystal. PR damage is only induced by visible light [22]. Nevertheless, such damage is a problem in IR OPOs pumped at 1064 nm because of the green second harmonic of the pump. The intensity can be sufficient to cause PR damage even though the SHG process is not phase matched. PR damage can be erased by heating the crystal to the damage annealing temperature, which is usually in the range 100–200°C, depending on the material composition. PR damage can be avoided by operating the OPO crystal at high temperature, 60–200°C is usual for periodically poled LNO. PR damage is also avoided in MgO or ZnO doped LNO.

The other type of temporary damage is dark traces [23, 24]. These too are induced only by visible light, and they occur in frequency doublers for 1064 nm. Dark traces have not been a problem in IR OPOs, so the threshold for this damage appears to be higher than for PR damage. Dark traces occur in pure and doped crystals.

3.8.5 Thermal data

Reviews of thermal properties are given in [25] and other chapters in the same book. All thermal properties depend on the exact composition of the material, and they may

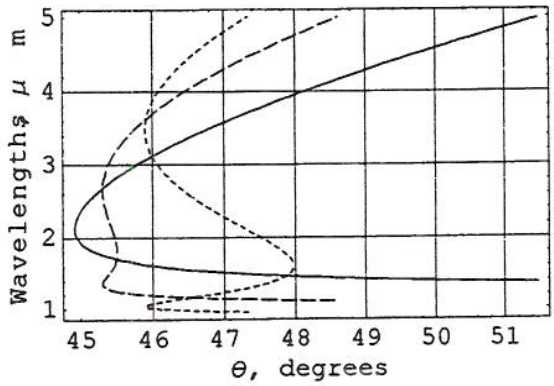

Figure 3.12 *Tuning curves for LNO. The pump wavelengths are* 1.0642 μm *(solid curve),* 0.9 μm *(dashed), and* 0.8 μm *(dotted). Gain bandwidths are very large near degeneracy, especially for the* 0.9 μm *pump*

also depend on temperature. Reported data differ widely, and in many reports the composition of the sample is not specified. Thermal conductivity seems to be about 0.04 W/(cm·K) at room temperature, and it decreases at higher temperatures. Specific heat is about 650 J/(kg·K) at room temperature, increasing with temperature.

3.8.6 Price and availability

LNO is available from most crystal suppliers and in large sizes. Casix quotes $850 for $10 \times 10 \times 50$ mm. Crystal Technologies supplies periodically poled LNO. The price for a single 50 mm long, 0.5 mm thick crystal with 8 different gratings is about £2000, dropping to £800 a piece for more than 5 pieces.

3.8.7 Tuning calculations

Type 1 phase matching using the d_{31}-element (ZXX) is most common in LNO, although type 2/3 phase matching using the smaller d_{16} (XYX) is also possible. Figure 3.12 shows tuning curves for an LNO OPO with type 1 phase matching and three different pump wavelengths. The curve is based on the Sellmeier equations for 7% mol MgO:LNO in [5]. In this phase matching geometry, $d_{\text{eff}} = d_{31} \sin\theta$. For $\lambda_3 = 1.064\,\mu$m and $\lambda_1 = 3.8\,\mu$m, pump walk-off is about 2°, and the acceptance intervals are $L\,\Delta\theta = 1.2$ cm mrad, $L\,\Delta\lambda_3 = 5.6$ cm nm, and $L\,\Delta\lambda_1 = 25$ cm nm. $L\,\Delta\phi$ is infinite because LNO is uniaxial.

3.8.8 Examples

LNO is particularly interesting because of the possibility of quasi phase matching by periodic poling. Samples up to 53 mm long and 0.5 mm thick with period 6.5 μm have been fabricated and used in an OPO [7]. Periodically poled LNO (PPLN) retains the transmission and power handling capability of bulk LNO. It appears to be less susceptible to photo refractive damage [22], but it is still necessary to operate at high temperature to avoid it. Temperature tuning is possible. Tuning can also be implemented by fabricating multiple gratings with different periods on the same substrate

[4]. The poling is along the z-axis, which is the extraordinary axis. QPM makes it possible to use the d_{33}-element, which is much greater than the other d-elements. Another advantage is that the IR transmission is better for polarization in the z-direction than in other directions. Increasing the crystal thickness by diffusion bonding PPLN plates has recently been reported [26], but there are still problems with this technology.

Although electric poling is the most common method, QPM crystals have also been made by modifying the growth process [27]. Quasi phase matching in MgO:LNO was demonstrated by [28]. They fabricated a 1.2 mm long crystal by changing the temperature during growth. More recently, electric poling of MgO:LNO was demonstrated [29]. The QPM period was 5.2 μm, and the thickness of the crystal was 0.4 mm. Periodic poling of MgO:LNO has also been reported by [30].

References

[1] D.A. Bryan, R. Gerson, and H.E. Tomaschke. Increased optical damage resistance in lithium niobate. *Appl. Phys. Lett.*, 44:847–849, 1984.

[2] Casix, Inc, Fujian, China. *Crystal Guide*, 1996.

[3] M. Wöhlecke, G. Corradi, and K. Betzler. Optical methods to characterise the composition and homogeneity of lithium niobate single crystals. *Appl. Phys. B*, 63:323–330, 1996.

[4] L.E. Myers, R.C. Eckardt, M.M. Fejer, R.L. Byer, and W.R. Bosenberg. Multigrating quasi-phase-matched optical parametric oscillator in periodically poled $LiNbO_3$. *Opt. Lett.*, 21:591–593, 1996.

[5] S. Lin, Y. Tanaka, S. Takeuchi, and T. Suzuki. Improved dispersion equation for MgO:$LiNbO_3$ crystal in the infrared spectral range derived from sum and difference frequency mixing. *IEEE J. Quantum Electron.*, 32:124–126, 1996.

[6] G.J. Edwards and M. Lawrence. A temperature-dependent dispersion equation for congruently grown lithium niobate. *Opt. Quantum Electron.*, 16:373–375, 1984.

[7] R.G. Batchko, D.R. Weise, T. Plettner, G.D. Miller, M.M. Fejer, and R.L. Byer. 532nm-pumped continuous wave singly resonant optical parametric oscillator based on periodically poled lithium niobate. In C.R. Pollock and W.R. Bosenberg, editors, *Advanced solid-state lasers*, volume 10 of *OSA Trends in Optics and Photonics*, pages 182–184, 1997.

[8] G. Hansson and D.D. Smith. 2 μm wavelength pumped optical parametric oscillator using periodically poled $LiNbO_3$. In C.R. Pollock and W.R. Bosenberg, editors, *Advanced solid-state lasers*, volume 10 of *OSA Trends in Optics and Photonics*, pages 238–240, 1997.

[9] R.C. Eckardt, C.D. Nabors, W.J. Kozlovsky, and R.L. Byer. Optical parametric oscillator frequency tuning and control. *J. Opt. Soc. Am. B*, 8:646–667, 1991.

[10] D.H. Jundt, M.M. Fejer, and R.L. Byer. Optical properties of lithium-rich lithium niobate fabricated by vapor transport equilibration. *IEEE J. Quantum Electron.*, 26:135–138, 1990.

[11] J.Q. Yao, W.Q. Shi, J.D. Millerd, G.F. Xu, E. Garmire, and M. Birnbaum. Room-temperature 1.06-0.53-μm second-harmonic generation with MgO:$LiNbO_3$. *Opt. Lett.*, 15:1339–1341, 1990.

[12] U. Schlarb and K. Betzler. Refractive indices of lithium niobate as a function of wavelength and composition. *J. Appl. Phys.*, 73:3472–3476, 1993.

[13] V.G. Dmitriev, G.G. Gurzadyan, and D.N. Nikogosyan. *Handbook of nonlinear optical crystals.* Springer-Verlag, Heidelberg, 1991.

[14] G. Ghosh. Thermo-optic coefficients of $LiNbO_3$, $LiIO_3$, and $LiTaO_3$ nonlinear crystals. *Opt. Lett.*, 19:1391–1393, 1994.

[15] W. Ji, H.P. Li, F. Zhou, and N. Zhai. Picosecond z-scan investigation of two-photon absorption and bound electronic self-focusing in second-harmonic-generation crystals. In M. Eich, B.H.T. Chai, and M. Jiang, editors, *Electro-optic and second harmonic generation materials, devices, and applications*, volume 2897 of *Proc. SPIE*, pages 414–423, 1996.

[16] R. DeSalvo, A.A. Said, D.J. Hagan, E.W. van Stryland, and M. Sheik-Bahae. Infrared to ultraviolet measurements of two-photon absorbtion and n_2 in wide bandgap solids. *IEEE J. Quantum. Electron.*, 32:1324–1333, 1996.

[17] J.J. Wynne. Nonlinear optical spectroscopy of $\chi^{(3)}$ in $LiNbO_3$. *Phys. Rev. Lett*, 29:650–653, 1972.

[18] Fujian Castech Crystals, Inc, Fujian, China. *Crystals.*

[19] D.A. Roberts. Simplified characterization of uniaxial and biaxial nonlinear optical crystals: A plea for standardization of nomenclature and conventions. *IEEE J. Quantum Electron.*, 28:2057–2074, 1992.

[20] R.C. Eckardt, H. Masuda, Y.X. Fan, and R.L. Byer. Absolute and relative nonlinear optical coefficients of KDP, KD*P, BaB_2O_4, $LiIO_3$, MgO:$LiNbO_3$, and KTP measured by phase-matched second-harmonic generation. *IEEE J. Quantum Electron.*, 26:922–933, 1990.

[21] S.J. Brosnan and R.L. Byer. Optical parametric oscillator threshold and linewidth studies. *IEEE J. Quantum Electron.*, 15:415–431, 1979.

[22] L.E. Myers, R.C. Eckardt, M.M. Fejer, R.L. Byer, W.R. Bosenberg, and J.W. Pierce. Quasi-phase-matched optical parametric oscillators in bulk periodically poled $LiNbO_3$. *J. Opt. Soc. Am. B*, 12:2102–2116, 1995.

[23] J. Li, X. Chen, B. Wu, B. Li, and S. Pan. Laser-induced dark traces in doped $LiNbO_3$ crystals. *Appl. Phys. Lett.*, 67:3384–3386, 1995.

[24] J. Deng, Y. Kong, J. Li, J. Wen, and B. Li. Reduction of laser-induced dark traces in $LiNbO_3$:Mg and $LiNbO_3$:Zn by heat treatment. *J. Appl. Phys.*, 79:9334–9337, 1996.

[25] T.H. Lin and S.H. Lee. Thermal conductivity of lithium niobate. In *Properties of Lithium Niobate*, pages 49–51. INSPEC, London, 1989.

[26] L.E. Myers, R.C. Eckardt, C. Littell, M. Missey, and V. Dominic. High energy opo based on a diffusion-bonded stack of ppln plates. In C.R. Pollock and W.R. Bosenberg, editors, *Advanced solid-state lasers*, volume 10 of *OSA Trends in Optics and Photonics*, pages 247–252, 1997.

[27] D. Feng, N.B. Ming, J.F. Hong, Y.S. Yang, J.S. Zhu, Z. Yang, and Y.N. Wang. Enhancement of second-harmonic generation in $LiNbO_3$ crystals with periodic laminar ferroelectric domains. *Appl. Phys. Lett.*, 37:607–609, 1980.

[28] D.H. Jundt, G.A. Magel, M.M. Fejer, and R.L. Byer. Periodically poled $LiNbO_3$ for high-efficiency second-harmonic generation. *Appl. Phys. Lett.*, 59:2657–2659, 1991.

[29] A. Harada and Y. Nihei. Bulk periodically poled MgO-$LiNbO_3$ by corona discharge method. *Appl. Phys. Lett.*, 69:2629–2631, 1996.

[30] K. Mizuuchi, K. Yamamoto, and M. Kato. Harmonic blue light generation in bulk periodically poled MgO:$LiNbO_3$. *Electron. Lett.*, 32:2091–2092, 1996.

3.9 $LiIO_3$ (LIO)

$LiIO_3$ is negative uniaxial with point group 6 (C_6). The axes are chosen so that xyz = XYZ, with $n_z < n_x = n_y$. LIO is highly hygroscopic, and it must be mounted in a sealed housing.

3.9.1 Transmission range

Transmission and absorption spectra are reported in [1]. Figure 3.13 shows the transmission spectrum.

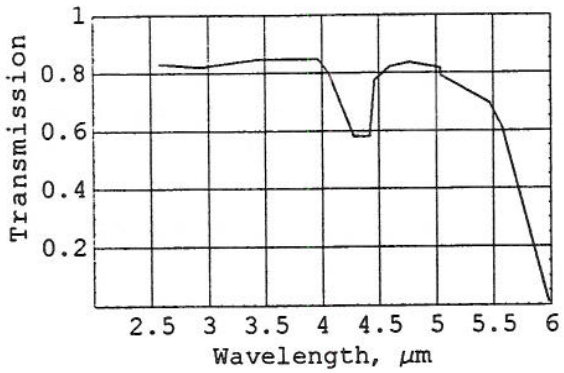

Figure 3.13 *Transmission spectrum of LIO. 3 mm long crystal, ordinary polarization. Data from [1]*

LIO has been used for DFG at 5.7 μm [2], but absorption was significant at that wavelength. There is a second transmission window a longer wavelengths, and DFG in the range 6.8–7.2 μm has been reported [3].

3.9.2 Refractive index

Kato [2] provides Sellmeier equations, which are also used by Casix:

$$n^2 = A + \frac{B}{\lambda^2 - C} - D\lambda^2$$

where

Polarization	A	B	C	D
o (x,y)	3.415716	0.047031	0.035306	0.008801
e (z)	2.918692	0.035145	0.028224	0.003641

These equations are transformed version of those in [4]. The D-coefficient for ordinary polarization was adjusted to give better agreement with observed tuning curves. These equations agreed with experimental OPO tuning up to 5.8 μm.

Gettemy et.al. [5] gives relatively detailed information on the refractive index temperature dependence and absorption. At 1064 nm and 35°C, the thermo-optic coefficients

are $-7.52 \cdot 10^{-5}$ for e-polarization and $-8.93 \cdot 10^{-5}$ for o-polarization. Thermo-optic for the wavelength 532 nm, 660 nm and 1320 nm are also reported. Webb [6] measured the temperature dependence of the phase matching angles for SHG at 1.064 μm. The results did not agree with these thermo-optic coefficients.

Ghosh [7] provides equations for the thermo-optic coefficients according to Equation (3.2) with the coefficients

Polarization	$10^6 G$	$10^6 H$	λ_{ig}, μm
o (x,y)	-203.885	-131.800	0.13
e (z)	-323.460	53.575	0.19

3.9.3 Nonlinear coefficients

Point group 6 allows the following d-elements to be nonzero: $d_{31} = d_{32}$, d_{33}, $d_{24} = d_{15}$, and $d_{14} = -d_{25}$. If Kleinman symmetry is valid, $d_{31} = d_{24}$ and $d_{14} = 0$. Reference [8] reports $d_{31} = 7.11$ pm/V and $d_{33} = 7.02$ pm/V for SHG at 1064 nm. These are based on parametric fluorescence measurements. In phase matched SHG experiments, $d_{31} = -4.1$ pm/V [9].

3.9.4 Damage

Damage thresholds at 1064 nm are shown in Table 3.7.

Source	Damage threshold	Pulse length
[10]	60–250 MW/cm^2	20–100 ns
[11]	1.4 J/cm^2	120 ps
[12]	80 MW/cm^2	Q-switched
[2]	120 MW/cm^2	12 ns

Table 3.7 Damage thresholds for $LiIO_3$

Reference [11] presents a thorough study of damage thresholds for short pulses. They found that the threshold was higher at 1064 nm than at 532 nm, and that bulk damage at 1064 nm was related to generation of the second harmonic. Casix [13] comments that the damage threshold is low and that LIO is not suitable for high power devices.

3.9.5 Price and availability

Casix Casix supplies sizes up to $10 \times 10 \times 20$ mm^2. They quote \$400 for $10 \times 10 \times 15$ mm.

3.9.6 Tuning calculations

Phase matching requires the highest frequency wave to have the e-polarization, while at least one of the lower frequency waves must have o-polarization, i.e. in the xy-plane. The form of the d-tensor shows that the last wave must also be polarized

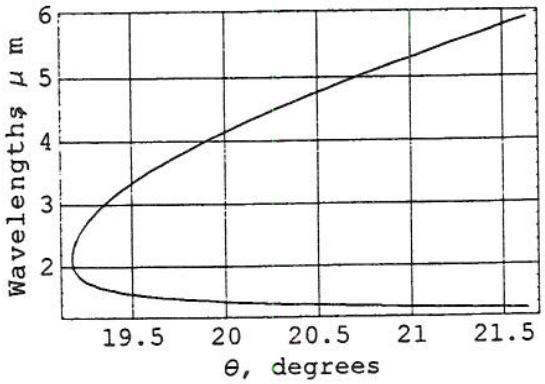

Figure 3.14 Tuning curve for LIO

in the xy-plane for d_{eff} to be nonzero, so only type 1 phase matching can be used. Figure 3.14 shows tuning curves for a LIO OPO. The pump wavelength is 1.0642 μm. The curve is based on the Sellmeier equations in [2]. In this phase matching geometry, $d_{\text{eff}} = d_{31} \sin\theta$. For $\lambda_1 = 3.8\,\mu$m, pump walk-off is about 3°, and the acceptance intervals are $L\,\Delta\theta = 1.0$ cm mrad, $L\,\Delta\lambda_3 = 25$ cm nm, $L\,\Delta\lambda_1 = 85$ cm nm. The tuning curve shows that $\theta \approx 20°$, so d_{eff} is relatively small.

3.9.7 Examples

An OPO based on LIO is described in [12]. They used noncollinear waves to increase θ and thereby d_{eff}. The angles given in this paper are not consistent with our calculations. The OPO was pumped at 1.064 μm and generated about 2.12 μm. LIO has been used for difference frequency generation in the range 4.4–5.7 μm [2], but there was absorption above 5 μm. Pump intensity was 80 MW/cm^2, and the crystal was 19 mm long.

References

[1] M.S. Cafferty. Absorption of $LiIO_3$ in the infrared and the ordinary direction of propagation. *Infrared Phys. Technol.*, 35:801–805, 1994.

[2] K. Kato. High-power difference-frequency generation at 4.4-5.7 μm in $LiIO3_3$. *IEEE J. Quantum Electron.*, 21:119–120, 1985.

[3] U. Chatterjee, A.M. Rudra, and G.C. Bhar. Generation of 6.8-7.7 μm radiation in lithium iodate. *Appl. Phys. B*, 61:489–491, 1995.

[4] V.I. Kabelka, A.S. Piskarskas, A.Y. Stabinis, and R.L. Sher. Group matching of interacting light pulses in nonlinear crystals. *Sov. J. Quantum Electron.*, 5:255–256, 1975.

[5] D.J. Gettemy, W.C. Harker, G. Lindholm, and N.P. Barnes. Some optical properties of KTP, $LiIO_3$, and $LiNbO_3$. *IEEE J. Quantum Electron.*, 24:2231–2237, 1988.

[6] M.S. Webb and S.P. Velsko. Temperature sensitivity of phase-matched second-harmonic generation in $LiIO_3$. *IEEE J. Quantum Electron.*, 26:1394–1398, 1990.

[7] G. Ghosh. Thermo-optic coefficients of $LiNbO_3$, $LiIO_3$, and $LiTaO_3$ nonlinear crystals. *Opt. Lett.*, 19:1391–1393, 1994.

[8] M.M. Choy and R.L. Byer. Accurate second-order susceptibility measurements of visible and infrared nonlinear crystals. *Phys. Rev. B*, 14:1693–1706, 1976.

[9] R.C. Eckardt, H. Masuda, Y.X. Fan, and R.L. Byer. Absolute and relative nonlinear optical coefficients of KDP, KD*P, BaB_2O_4, $LiIO_3$, MgO:$LiNbO_3$, and KTP measured by phase-matched second-harmonic generation. *IEEE J. Quantum Electron.*, 26:922–933, 1990.

[10] V.G. Dmitriev, G.G. Gurzadyan, and D.N. Nikogosyan. *Handbook of nonlinear optical crystals.* Springer-Verlag, Heidelberg, 1991.

[11] E.W. van Stryland, W.E. Williams, M.J. Soileau, and A.L. Smirl. Laser induced damage, nonlinear absorption, and doubleing efficiency of $LiIO_3$. *IEEE J. Quantum Electron.*, 20:434–439, 1984.

[12] A.A. Babin, Y.N. Belyaev, V.N. Petryakov, M.M. Sushchik, and G.I. Freidman. Parametric oscillator utilizing an $LiIO_3$ crystal pumped by neodymium laser radiation. *Sov J. Quantum Electron.*, 6:613–614, 1976.

[13] Casix, Inc, Fujian, China. *Crystal Guide*, 1996.

3.10 $KNbO_3$ (KNO)

$KNbO_3$ is negative biaxial with point group mm2 (C_{2v}). For the axes, we follow the convention used in [1], with $xyz = ZXY$ and $n_x < n_y < n_z$. This is common in the literature, but differs from the standard [2]. KNO has larger nonlinear coefficients than other inorganic materials for the same wavelength range, but is looses its crystal structure outside the temperature range -50–220°C. Ferroelectric domains can be formed by shaking or stressing the crystal [3]. Domain formation has also been reported at a temperature of only 40°C [4]!

3.10.1 Transmission range

We have not found an absorption spectrum for the relevant wavelength range, but KNO is claimed to be transparent from 0.4–4.5 μm [5, 3]. There are OH absorption features at 1.46, 2.2, and 2.85 μm [6]. MgO doping reduces absorption of short wavelengths [7], but its effect on long wavelengths has not been not reported.

3.10.2 Refractive index

Zysset et.al. [8] provide Sellmeier equations for the range 400–3400 nm, with coefficients for 6 different temperatures in the range 22–180°C. The accuracy is $2.5 \cdot 10^{-4}$. The equations have the form

$$n^2 = 1 + \frac{S_1\lambda_1^2\lambda^2}{\lambda^2 - \lambda_1^2} + \frac{S_2\lambda_2^2\lambda^2}{\lambda^2 - \lambda_2^2} - D\lambda^2$$

where wavelengths are in μm and the coefficients at 22°C are

Polarization	$S_1(\mu\text{m})^{-2}$	E_1(eV)	$S_2(\mu\text{m})^{-2}$	E_2(eV)	$D(\mu\text{m})^{-2}$
y = X	20.05519	4.802660	149.8408	9.604319	0.02517432
z = Y	19.37347	4.545782	135.4992	9.049686	0.02845018
x = Z	16.09170	4.857787	165.4431	10.356684	0.01943289

λ_i is found from E_i by $\lambda_i = a/E_i$, where $a = ch/e = 1.23985 \cdot 10^{-6}$mV, c is the speed of light, h is Plank's constant, and e is the electron charge. Later, temperature dependent Sellmeier equations were fitted to the same data [9]. These equations are claimed to valid for the entire temperature range of the orthorhombic phase of KNO, (−50°C to 223°). The equations have the form

$$\begin{aligned} n^2 = 1 &+ (S_1 + b_1F + b_2G)\frac{\lambda^2\lambda_1^2}{\lambda^2 - (\lambda_1 + b_3F + b_4G)^2} \\ &+ (S_2 + b_5F)\frac{\lambda^2\lambda_2^2}{\lambda^2 - (\lambda_2 + b_6F)^2} - (D + b_7F)\lambda^2 + b_8F\lambda^4 \end{aligned} \tag{3.5}$$

where $G = T - T_0$, $F = T^2 - T_0^2$, $T_0 = 295.15$K, T is the temperature in Kelvin, λ is the wavelength in μm, and the coefficients are

Parameter	y = X	z = Y	x = Z
S_1	17.381	19.456	16.086
E_1	4.7288	4.5492	4.8553
S_2	142.40	134.95	166.258
E_2	9.1082	9.0392	10.3834
D	0.02513	0.02837	0.01939
$10^5 b_1$	-2.018	-5.263	-3.267
$10^3 b_2$	-1.32	-1.65	-2.8
$10^7 b_3$	1.231	2.38	1.89
$10^5 b_4$	-1.82	-6.78	-2.48
$10^5 b_5$	9.017	20.536	19.90
$10^8 b_6$	7.96	17.67	17.5
$10^9 b_7$	-5.58	-12.2	-2.7
$10^{10} b_8$	-4.4	-3.3	-5.7

Ghosh [10] fitted the data from [8] to a different Sellmeier equation which he claims is physically more meaningful. He also reports thermo-optic coefficients according to Equation (3.2) with the coefficients (note the precision!)

Polarization	$10^6 G$	$10^6 H$	λ_{ig}, μm
y=X	-52.63636	152.12376	0.2846
z=Y	-152.53160	26.67160	0.3486
x=Z	-5.04307	264.82864	0.2541

Hsu [11] measured thermo-optic coefficients interferometrically. The results were in reasonable agreement with the data from [8].

3.10.3 Nonlinear coefficients

Nonlinear coefficients, in XYZ axes, are given in Table 3.8.

Source	d_{15}	d_{24}	d_{31}	d_{32}	d_{33}	Method	Wavelength, μm
[12]	-16.5	-17.1	-15.8	-18.3	-27.4	MF, WT	1.064
[12] (Scaled)	-12.4	-12.8	-11.9	-13.7	-20.6	MF, WT	1.064
[13, 14]			10.5	-12	-18.3	MF	1.064
[15]				10.2		PM SHG	1.064

Table 3.8 Nonlinear coefficients for KNO, in pm/V

The data in [12] are based on $d_{11}(SiO_2) = 0.4$ pm/V as reference. A more recent recommended reference value is 0.3 pm/V [2], so the rescaled results are also shown in the table. The data in [14] are also given relative to $d_{11}(SiO_2)$, and they have been converted to pm/V using the reference value 0.3 pm/V. Work on type 2 phase matching in KNO indicates that all the d-elements have the same sign [16]. Pliska et.al. [15] studied the uniformity of KNO crystals using SHG. Most of the samples had good uniformity.

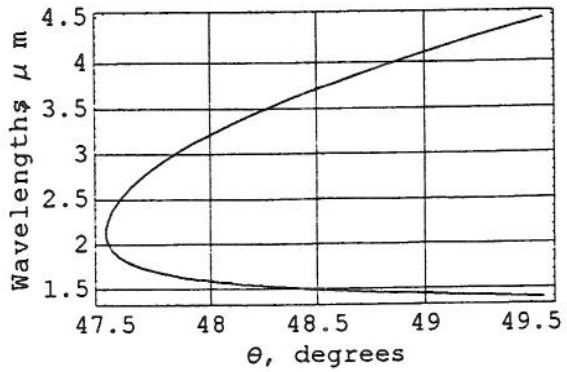

Figure 3.15 Tuning curve for KNO

3.10.4 Damage

Damage thresholds:

Source	Damage threshold	Conditions
[17]	150–180 MW/cm^2	1064 nm, 10 ns
[16]	> 240 MW/cm^2	1064 nm, 7 ns
[1]	10 J/cm^2	1064 nm, 100 ps
[18]	6 J/cm^2	1054 nm, 700 ps

Table 3.9 Damage thresholds for KNO

3.10.5 Price and availability

Casix quotes $950 for $3 \times 3 \times 5$ mm.

3.10.6 Tuning calculations

Figure 3.15 shows a tuning curve for Type 1 phase matching in the YZ = zx plane, based on the Sellmeier equations in [8]. The pump wavelength is 1.064 μm. In this phase matching geometry, $d_{\text{eff}} = d_{31} \sin\theta$. For $\lambda_1 = 3.8\,\mu$m, walk-off of the pump is about 3.5° and the acceptance intervals are $L\,\Delta T = 30$ K cm, $L\,\Delta\theta = 0.7$ mrad cm, $L\,\Delta\phi = 1300$ mrad cm, $L\,\Delta\lambda_3 = 9.8$ nm cm, and $L\,\Delta\lambda_1 = 33$ nm cm. The latter corresponds to a gain bandwidth of 680 GHz cm.

Phase matching is also possible in the XZ = yx plane, but the θ is about 17°, leading to small d_{eff}. On the other hand, walk-off is reduced to 1.6°. Many more tuning examples can be found in [1].

3.10.7 Examples

A KNO based OPO pumped by a Q-switched Nd:YAG laser is described in [19]. The two output wavelengths were tunable in the ranges 1.45–2.01 μm and 2.27–4.0 μm respectively. Type 1 phase matching was used, and the crystal was 7.8 mm long. The

pump pulse was 9 ns long, and the pump fluence was 1.3 J/cm^2. Output energy at 1.9 μm was 6 mJ for 80 mJ pump. Pump beam divergence was 0.5 mrad, close to the calculated acceptance angle of 0.45 mrad.

KNO has also been used in a Ti:sapphire pumped femtosecond OPO [20, 21]. Wavelengths up to 5.2 μm were generated. A type 2 phase matched OPO was demonstrated by [16]. It had smaller line width than a comparable type 1 OPO.

References

[1] I. Biaggio, P. Kerkoc, L.S. Wu, and P. Günter. Refractive indices of orthorhombic $KNbO_3$. II. phase-matching configurations for nonlinear-optical interactions. *J. Opt. Soc. Am. B*, 9:507–517, 1992.

[2] D.A. Roberts. Simplified characterization of uniaxial and biaxial nonlinear optical crystals: A plea for standardization of nomenclature and conventions. *IEEE J. Quantum Electron.*, 28:2057–2074, 1992.

[3] Casix, Inc, Fujian, China. *Crystal Guide*, 1996.

[4] J.J.E. Reid. Resonantly enhanced, frequency doubling of an 820 nm GaAlAs diode laser in a potassium lithium niobate crystal. *Appl. Phys. Lett.*, 62:19–21, 1993.

[5] V.G. Dmitriev, G.G. Gurzadyan, and D.N. Nikogosyan. *Handbook of nonlinear optical crystals.* Springer-Verlag, Heidelberg, 1991.

[6] X. Tong, A. Yariv, M. Zhang, and A. Agranat. Three dimensional polarization dependence of OH bands absorption in potassium niobate crystals. *Appl. Phys. Lett.*, 70:429–431, 1997.

[7] L.E. Busse, L. Goldberg, M.R. Surette, and G. Mizell. Absorption losses in MgO-doped and undoped potassium niobate. *J. Appl. Phys.*, 75:1102–1110, 1994.

[8] B. Zysset, I. Biaggio, and P. Günter. Refractive indices of orthorhombic $KNbO_3$. I. dispersion and temperature dependence. *J. Opt. Soc. Am. B*, 9:380–386, 1992.

[9] D.H. Jundt, P. Günter, and B. Zysset. A temperature dependent dispersion equation for $KNbO_3$. *Nonlinear optics*, 4:341–345, 1993.

[10] G. Ghosh. Dispersion of thermo-optic coefficients in a potassium niobate nonlinear crystal. *Appl. Phys. Lett.*, 65:3311–3313, 1994.

[11] C.C. Hsu, T.H. Huang, T.H. Wei, S. Chang, and C.Y. Leaung. Temperature variation of the refractive index of potassium niobate. *J. Appl. Phys.*, 77:3399–3402, 1995.

[12] J.C. Baumert, J. Hoffnagle, and P. Günter. Nonlinear optical effects in $KNbO_3$ crystals at $Al_xGa_{1-x}As$, dye, ruby, and Nd:YAG laser wavelengths. In B. Bölger and H.A. Ferwerda, editors, *1984 European conference on optics, optical systems and applications*, volume 492 of *Proc. SPIE*, pages 374–385, 1984.

[13] Y. Uematsu. Nonlinear optical coefficients of $KNbO_3$ single crystal. *Japan J. Appl. Phys.*, 12:1257–1258, 1973.

[14] Y. Uematsu. Nonlinear optical properties of $KNbO_3$ single crystal in the orthorhombic phase. *Japan J. Appl. Phys.*, 13:1362–1368, 1974.

[15] T. Pliska, F. Mayer, D. Fluck, P. Günter, and D. Rytz. Nonlinear optical investigation of the optical homogeneity of $KNbO_3$ bulk crystals and ion-implanted waveguides. *J. Opt. Soc. Am. B*, 12:1878–1887, 1995.

[16] W.R. Bosenberg and R.H. Jarman. Type-II phase matched $KNbO_3$ optical parametric oscillator. *Opt. Lett.*, 18:1323–1325, 1993.

[17] V.A. Dyakov, V.I. Pryalkin, and A.I. Kholodnykh. Potassium niobate optical parametric oscillator pumped by the second harmonic of a garnet laser. *Sov. J. Quantum Electron.*, 11:433–436, 1981.

[18] U. Ellenberger, R. Weber, J.E. Balmer, B. Zysset, D. Ellgehausen, and G.J. Mizell. Pulsed optical damage threshold of potassium nioate. *Appl. Opt.*, 31:7563–7569, 1992.

[19] R. Urschel, A. Fix, R. Wallenstein, D. Rytz, and B. Zysset. Generation of tunable narrow-band midinfrared radiation in a type i potassium niobate optical parametric oscillator. *J. Opt. Soc. Am. B*, 12:726–730, 1995.

[20] D.E. Spence, S. Wielandy, C.L. Tang, C. Bosshard, and P. Günter. High-repetition-rate femtosecond optical parametric oscillator based on $KNbO_3$. *Opt. Lett.*, 20:680–682, 1995.

[21] D.E. Spence, S. Wielandy, C.L. Tang, C. Bosshard, and P. Günter. High average power, high-repetition rate femtosecond pulse generation in the 1-5 μm region using an optical parametric oscillator. *Appl. Phys. Lett.*, 68:452–454, 1996.

3.11 $LiTaO_3$ (LTA) and other related materials

LTA has been much used in quasi phase matched waveguide devices, but there are also reports on QPM in bulk LTA. Gupta et.al. [1] report a 0.5 mm thick sample with a 2 mm long QPM region with period of only 3.6 μm. They found $d_{33} = 20$ pm/V. Mizuuchi [2] had a 0.2 mm thick sample with a 10 mm long QPM region. Temperature dependent Sellmeier equations for LTA are reported in [3].

There are also other materials related to LNO, KNO, and LTA. $K_3Li_2Nb_5O_{15}$ (KLN) has higher damage resistance, lower loss and better mechanical robustness than KNO [4, 5]. Introducing Tantalum ($K_3Li_2(Ta_xNb_{1-x})_5O_{15}$, KLTNO) has improved UV transmission even more [5]. The IR transmission was not reported.

References

[1] M.C. Gupta, W.J. Kozlovsky, and A.C.G. Nutt. Second-harmonic generation in bulk and waveguided $LiTaO_3$ with domain inversion induced by electron beam scanning. *Appl. Phys. Lett.*, 64:3210–3212, 1994.

[2] K. Mizuuchi and K. Yamamoto. Generation of 304-nm light by frequency doubling of a laser diode in bulk periodically poled $LiTaO_3$. *Opt. Lett.*, 21:107–109, 1996.

[3] K.S. Abedin and H. Ito. Temperature-dependent dispersion relation of ferroelectric lithium tantalate. *J. Appl. Phys.*, 80:6561–6563, 1996.

[4] J.J.E. Reid. Resonantly enhanced, frequency doubling of an 820 nm GaAlAs diode laser in a potassium lithium niobate crystal. *Appl. Phys. Lett.*, 62:19–21, 1993.

[5] Y. Furukawa, S. Makio, T. Miyai, M. Sato, H. Kitayana, Y. Urata, T. Tamiuchi, and T. Fukuda. Growth and characterization of $K_3Li_2(Ta_xNb_{1-x})_5O_{15}$ crystals for blue second-harmonic-generation applications. *Appl. Phys. Lett.*, 68:744–746, 1996.

3.12 $AgGaS_2$

Silver Thiogallate (AGS) has a wide transparency and phase matching range and a moderately high nonlinearity. It is commonly used for 8-12 μm generation, and can be used for direct conversion from 1 μm to 8 μm. It can also be used for direct conversion from 1 μm to 3-5 μm. It is a negative uniaxial crystal ($n_o > n_e$) with point group $\bar{4}2m$. The material has a bandgap at 0.5 μm and there is no absorption in the material at 1 μm.

3.12.1 Transmission range

AGS has high transmission in the entire range from 1 μm to 12 μm. In Figure 3.16 a measured absorption spectrum of AGS is shown.

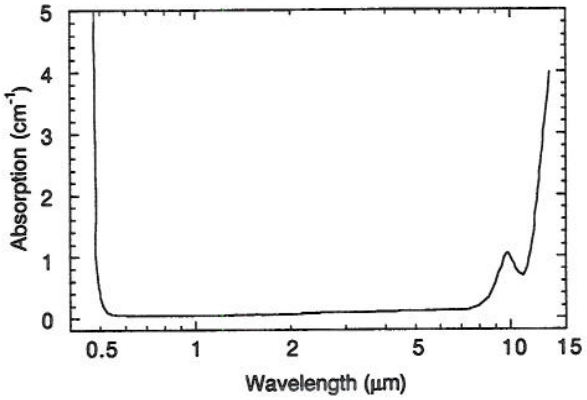

Figure 3.16 Measured absorption coefficient in AGS [1]

3.12.2 Refractive index

The refractive indices of AGS are in the range 2.3-2.4 for wavelengths in the range 1-10 μm. Roberts [2] recently published an improved set of Sellmeier equations for AGS which use the formula

$$n^2 = A + \frac{B}{\lambda^a - C} + \frac{F}{\lambda^b - G} + \frac{J}{\lambda^c - K} + \frac{D}{1 - E/\lambda^d}$$

For wavelengths in the range 0.5-12 μm, he found the coefficients to be

	A	B	C	D	F	G
n_o	5.824100	0.0867547	0.0356502	176380	112586795	-0.315646
n_e	5.530050	0.0510941	0.141109	4253.78	4304927.0	-0.0910735
	J	K	a	b	c	d
n_o	0.506566	-6.582197	3.156983	4.430430	6.604280	2.225043
n_e	0	0	2.359877	2.566664	0	2.383834

Other published measurements of the dispersion in AGS can be found in [3-8].

3.12.3 Temperature dependence

The temperature dependence of the refractive indices of AGS has been found to be [9, 10]:

Wavelength	dn_o/dT (10^{-6} /K)	dn_e/dT (10^{-6} /K)	Source
1.06 μm	167	176	[9]
	173	175	[10]
10.6 μm	149	156	[9]
	154	156	[10]

3.12.4 Nonlinear second order coefficients

There are only three elements of the d-matrix that are nonzero, and when Kleinman symmetry is valid these are equal:

$$d_{14} = d_{25} = d_{36}$$

The magnitude of this element has been measured to be:

Source	d_{36} (pm/V)	Method	Wavelength
[11, 12]	17.5	SHG	1.064 μm
[12, 13]	11.1	DFG	(1.06, 1.3, 6) μm
[11, 12]	11.2	SHG	10.6 μm
[14, 15]	13.4 ± 2.5	MF	10.6 μm
[16]	9 ± 2	DFG	(0.88, 1.06, 5.1) μm
[17]	31 ± 5	SPE	(0.6, 0.85, 7.8) μm
[18]	32.0 ± 4	SHG	10.6 μm

A summary and brief comparison of the measured values is given in [17, 18]. Although a value for d_{36} in the range of 18 pm/V is most frequently used in the literature, the two most recent (and independent) measurements found the value to be in the range 27-36 pm/V [17, 18].

3.12.5 Effective nonlinearity

The expression for the effective nonlinearity for second order processes is given by the crystal's point group.

Type 1 phase matching: $d_{eff} = d_{36}\sin(\theta)\sin(2\phi)$

Type 2/3 phase matching: $d_{eff} = d_{36}\sin(2\theta)\cos(2\phi)$

where θ is the angle between the direction of propagation and the crystal z-axis, and ϕ is the angle between the projection of the direction of propagation on the xy-plane and the crystal x-axis.

3.12.6 Optical damage

The threshold for optical damage on the surfaces has been reported to be 25 MW/cm² in 10-35 ns pulses (i.e. 0.25-0.9 J/cm²) [4, 9] and 3 GW/cm² in a 20 ps pulse (60 mJ/cm²) [19] for wavelengths between 1 μm and 10 μm. In a recent measurement, the damage threshold was found to be 0.25 J/cm² for 180 ns pulses at 2 μm and 2.2 J/cm² for 50 ns pulses at 10 μm [18].

3.12.7 Phase matching

Calculated phase matching curves for 1 μm and 2 μm pump wavelengths are shown in Figure 3.17.

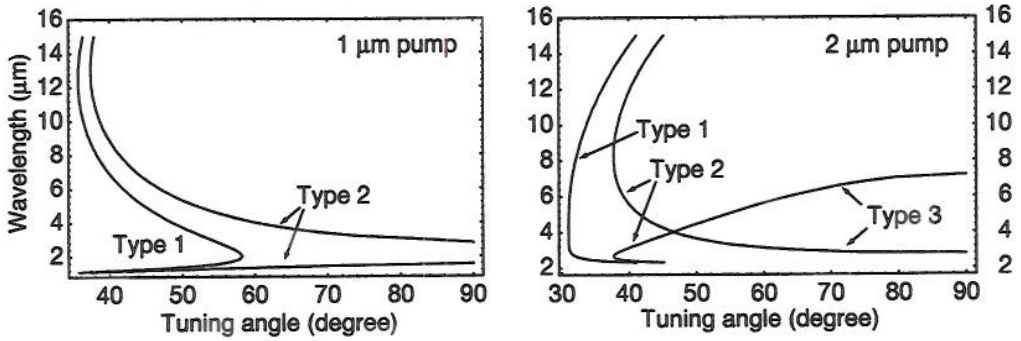

Figure 3.17 Calculated tuning curves for $AgGaS_2$

We note the extremely wide phase matching region where 1 μm pump can be directly converted to 8-12 μm radiation both with type 1 and type 2 phase matching.

3.12.8 Noncritical phase matching

Noncritical phase matching ($\theta = 90^\circ$) is not possible in AGS ($d_{eff} = 0$ for type 2/3 phase matching).

3.12.9 Example: Calculations

Results from calculations with various OPO configurations with AGS are listed in Table 3.10. In calculations of d_{eff}^2/n^3 we have assumed that $d_{36} = 18$ pm/V and n = 2.4.

3.12.10 Example: Experiment

Cheung et *al.* [20] recently reported on a singly resonant AGS OPO. The pump source was a cw mode-locked Nd:YAG laser at 1.064 μm. With 625 mW of pump power, they obtained 100 mW on 1.319 μm and 6 mW on 5.505 μm. To avoid thermal lensing in AGS, the pump was chopped at a 32 to 1 duty cycle.

Pump	Signals (μm)	PM	θ	ϕ	d_{eff}/d_{36}	d_{eff}^2/n^3	Walkoff
1.0 μm	1.3 4.0	1	48.7°	45°	0.75	13 (pm/V)^2	1.3°
1.0 μm	1.3 4.0	2	60.0°	0°	0.87	18 (pm/V)^2	1.1°
2.0 μm	4.0 4.0	1	31.0°	45°	0.52	6 (pm/V)^2	1.2°
2.0 μm	4.0 4.0	2	46.6°	0°	1.00	23 (pm/V)^2	1.3°
1.0 μm	1.1 8.0	1	38.3°	45°	0.62	9 (pm/V)^2	1.3°
1.0 μm	1.1 8.0	2	41.5°	0°	0.99	22 (pm/V)^2	1.3°
2.0 μm	2.7 8.0	1	32.0°	45°	0.53	7 (pm/V)^2	1.2°
2.0 μm	2.7 8.0	2	37.7°	0°	0.97	22 (pm/V)^2	1.3°

Table 3.10 Calculations of tuning angles and effective nonlinearity for vaious AGS OPOs

3.12.11 Price and availability

AGS crystals can be acquired from Cleveland Crystals (Cleveland, OH). In their March 1996 price list, they charge USD 4368 for a 5 x 5 x 15 mm^3 sample and USD 12574 for a 10 x 10 x 20 mm^3 sample.

References

[1] R S Feigelson and R K Route. Recent development in the growth of chalcopyrite crystals for nonlinear infrared applications. In *SPIE Conference Proceedings*, vol. 567, SPIE, 1985, pp. 2-10.

[2] D A Roberts. Dispersion equations for nonlinear optical crystals: KDP, $AgGaSe_2$, and $AgGaS_2$. *Appl. Opt.*, 35: 4677-4688, 1996.

[3] G C Bhar. Refractive index interpolation in phase-matching. *Appl. Opt.*, 15: 305-307, 1976.

[4] G C Bhar and R C Smith. Silver Thiogallate ($AgGaS_2$)-Part II: Linear Optical Properties. *IEEE J. Quantum Electron.*, 10: 546-550, 1974.

[5] Y X Fan, R C Eckardt, R L Byer, R K Route, and R S Feigelson. $AgGaS_2$ infrared parametric oscillator. *Appl. Phys. Lett.*, 45: 313-315, 1984.

[6] T Itabe and J L Bufton. Phase-matching measurements for 10-μm upconversion in $AgGaS_2$. *Appl. Opt.*, 23: 3044-3047, 1984.

[7] K Kato and H Shirahata. Nonlinear IR generation in $AgGaS_2$. *Jpn. J Appl. Phys. Part 1*, 35: 4645-4648, 1996.

[8] D S Chemla, P J Kupecek, D S Robertson, and R G Smith. Silver thiogallate, a new material with potential for infrared devices. *Opt. Commun.*, 3: 29-31, 1971.

[9] *Silver gallium selenide and silver gallium sulfide.* Information sheet, Cleveland Crystals, Cleveland, OH, 1994.

[10] G C Bhar, D K Ghosh, P S Ghosh, and D Schmitt. Temperature effects in $AgGaS_2$ nonlinear devices. *Appl. Opt.*, 22: 2492-2494, 1983.

[11] G D Boyd, H Kasper, and J H McFee. Linear and nonlinear optical properties of $AgGaS_2$, $CuGaS_2$, and $CuInS_2$, and theory of the wedge technique for the measurement of nonlinear coefficients. *IEEE J. Quantum Electron.*, 7: 563-573, 1971.

[12] D A Roberts. Simplified characterization of uniaxial and biaxial nonlinear optical crystals: A plea for standardization of nomenclature and conventions. *IEEE J. Quantum Electron.*, 28: 2057-2074, 1992.

[13] K Kato. High-power difference-frequency generation at 5-11 μm in $AgGaS_2$. *IEEE J. Quantum Electron.*, 20: 698-699, 1984.

[14] B F Levine and C G Bethea. Nonlinear susceptibility of GaP; relative measurement and use of measured values to determine a better absolute value. *Appl. Phys. Lett.*, 20: 272-257, 1972.

[15] P J Kupecek, C A Schwartz, and D S Chemla. Silver thiogallate ($AgGaS_2$)-Part I: Nonlinear optical properties. *IEEE J. Quantum Electron.*, 10: 540-545, 1974.

[16] A G Yodh, H W K Tom, G D Aumiller, and R S Miranda. Generation of tunable mid-infrared picosecond pulses at 76 MHz. *J. Opt. Soc. Am. B*, 8: 1663-1667, 1991.

[17] P Canarelli, Z Benko, A H Hielscher, R F Curl, and F K Tittel. Measurement of nonlinear coefficient and phase matching characteristics of $AgGaS_2$. *IEEE J. Quantum Electron.*, 28: 52-55, 1992.

[18] A Harasaki and K Kato. New data on the nonlinear optical constant, phase-matching, and optical damage of $AgGaS_2$. *Jpn. J Appl. Phys. Part 1*, 36: 700-703, 1997.

[19] T Elsaesser, A Seilmeiler, and W Kaiser. Parametric generation of tunable picosecond pulses in the medium infrared using $AgGaS_2$ crystals. *Appl. Phys. Lett.*, 44: 383-385, 1984.

[20] E C Cheung, K Koch, and G T Moore. Silver thiogallate, singly resonant optical parametric oscillator pumped by a continuous-wave mode-locked Nd:YAG laser. *Opt. Lett.*, 19: 631-633, 1994.

3.13 $AgGaSe_2$

Silver Gallium Selenide (AGSe) has a wide transparency range and a high nonlinearity. It is a popular material for both 3-5 μm and 8-12 μm generation. It is a negative uniaxial crystal ($n_o > n_e$) with point group $\bar{4}2m$. The material has a bandgap at 0.73 μm and there is some absorption in the material at 1 μm. Therefore the material is usually pumped at wavelengths above 1.3 μm, for instance in a 2-step OPO configuration or with a 2 μm pump laser.

3.13.1 Transmission range

AGSe has high transmission in the entire range from 2 μm to 15 μm. In Figure 3.18 a measured absorption spectrum of AGSe is shown. Recent materials research has increased the transparency in both ends of the transmission range.

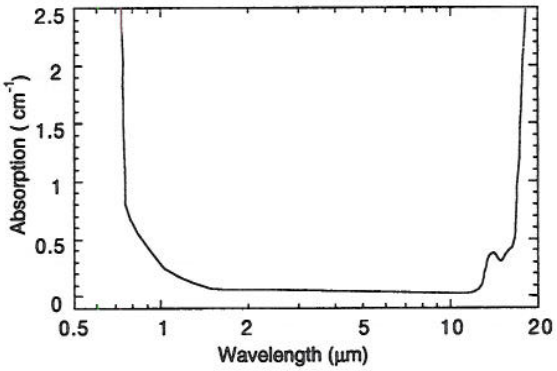

Figure 3.18 Measured absorption coefficient in AGSe [1]

3.13.2 Refractive index

The refractive indices of AGSe are in the range 2.55-2.65 for wavelengths between 2 μm and 10 μm. Roberts [2] recently published an improved set of Sellmeier equations for AGSe which use the formula

$$n^2 = A + \frac{B}{\lambda^a - C} + \frac{D}{\lambda^b - E} + \frac{F \cdot \lambda^c}{\lambda^c - G} \quad .$$

For wavelengths in the range 0.73-13.5 μm, he found the coefficients to be

	A	B	C	D	F
n_o	6.849065	0.417863	0.198080	0.000442	0.889242
n_e	6.675232	0.436579	0.229775	0.012063	0.213957
	G	H	a	b	c
n_o	1.209374	915.345	1.970203	0.340096	1.921292
n_e	3.252722	3129.32	1.893694	4.369152	2.04724

Other published measurements of the dispersion relation for AGSe can be found in [3, 4].

3.13.3 Temperature dependence

The temperature dependence of the refractive indices of AGSe have been found to be:

Wavelength	dn_o/dT (10^{-6} /K)	dn_e/dT (10^{-6} /K)	Reference
1.06 μm	98	66	[5]
3.39 μm	74±10	43±10	[6]
10.6 μm	58	46	[5]

This indicates that an AGSe OPO can be temperature tuned.

3.13.4 Nonlinear second order coefficients

There are only three elements of the d-matrix that are nonzero, and when Kleinman symmetry is valid these are equal:

$$d_{14} = d_{25} = d_{36}$$

To the best of our knowledge, all published measurements of the nonlinearity are over 20 years old.

Source	d_{36} (pm/V)	Method	Wavelength
[7, 8]	33±3	SHG	10.6 μm
[9]	32±5	SHG	10.6 μm
[10]	67.7±13	Wedge	2.12 μm
[10]	57.7	MD*	10.6 μm

*) This value was calculated by use of Millers Δ from the value at 2.12 μm.

In the literature the latter measurement often is neglected and it is commonly assumed that d_{36} = 33 pm/V [11]. However, Choy and Byer [10] state that the discrepancy between the published values may be explained with better material quality in their experiments.

3.13.5 Effective nonlinearity

The expression for the effective nonlinearity for second order processes is given by the point group of the crystal.

Type 1 phase matching: $d_{eff} = d_{36}\sin(\theta)\sin(2\phi)$

Type 2/3 phase matching: $d_{eff} = d_{36}\sin(2\theta)\cos(2\phi)$

where θ is the angle between the direction of propagation and the crystal z-axis, and ϕ is the angle between the projection of the direction of propagation in the xy-plane and the crystal x-axis.

3.13.6 Optical damage

Recent reports indicate a threshold for optical damage on the crystal surface in the range 2-3 J/cm² (180 ns pusles) [12]. At kilohertz pulse rates and pulse lengths of 15 ns, the threshold level is reduced to 0.35 J/cm² [13]. For longer pulses (20 μs) a damage threshold of 37 MW/cm² (i.e. 720 J/cm²) on an AR-coated AGSe surface has been reported [14].

3.13.7 Phase matching

Calculated phase matching curves for 2 μm pump wavelength are shown in Figure 3.19.

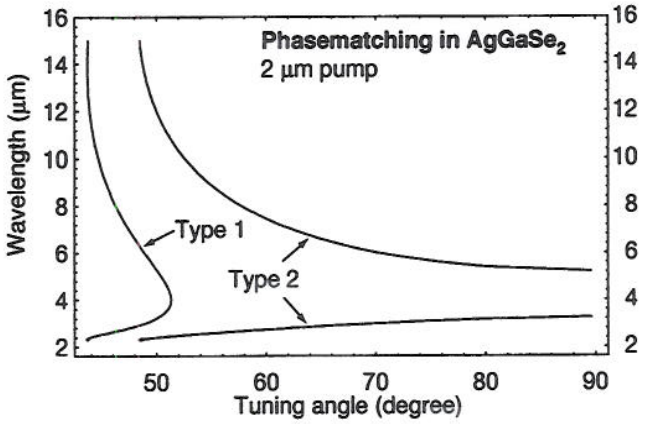

Figure 3.19 Calculated tuning curves for 2 μm pumped $AgGaSe_2$

We observe that Type 2 phase matching cannot be achieved in the 3-5 μm region with 2 μm pumping.

3.13.8 Noncritical phase matching

In Figure 3.20 calculated tuning curves for noncritical phase matching ($\theta = 90^\circ$) are shown. From section 3.13.5 it is clear that type 2/3 NCPM cannot be obtained for AGSe since the effective nonlinearlty is zero in this case.

From the figure it is clear that when the pump is tuned slightly around 1.5 μm, the output from the OPO is tuned from 3 μm to 5 μm.

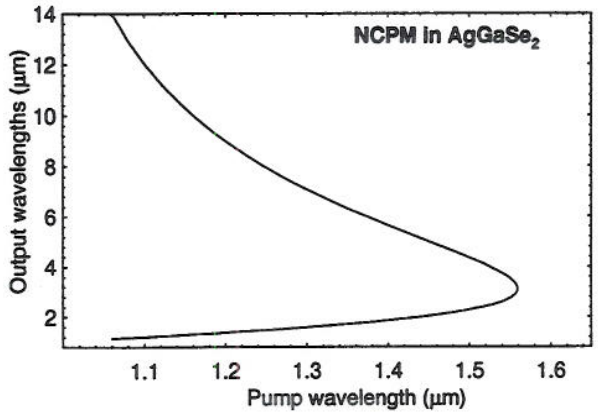

Figure 3.20 Calculated tuning curve for type 1 noncritical phase matching

3.13.9 Example: Calculations

Results from calculations with various OPO configurations with AGSe are listed below. In calculations of d_{eff}^2/n^3 we have assumed that $d_{36} = 33$ pm/V.

Pump	Signals (μm)	PM	θ	ϕ	d_{eff}/d_{36}	d_{eff}^2/n^3	Walkoff
2.0 μm	4.0 4.0	1	51.6°	45°	0.78	38 (pm/V)^2	0.7°
2.0 μm	4.0 4.0	2	-	-	-	-	-
2.0 μm	2.7 8.0	1	46.3°	45°	0.72	32 (pm/V)^2	0.7°
2.0 μm	2.7 8.0	2	57.9°	0°	0.90	50 (pm/V)^2	0.6°

3.13.10 Example: Experiments

Budni and coworkers at Lockheed Sanders have demonstrated a 2.05 μm pumped AGSe OPO that produced an average output of 600 mW when pumped with 3 W at 2.5 kHz pulse rate [13].

Komine and coworkers at Northrop Grumman demonstrated a NCPM AGSe OPO. They obtained 250 mW average power at 3.41 μm when pumped with 2 W 1.54 μm radiation from a NCPM KTP OPO with a pulse rate of 2.5 kHz [4].

3.13.11 Price and availability

AGSe crystals can be acquired from Cleveland Crystals (Cleveland, OH) and CASIX (Fujian, China). In Cleveland Crystals March 1996 price list, they charge USD 4368 for a 5 x 5 x 15 mm^3 sample and USD 12574 for a 10 x 10 x 20 mm^3 sample.

References

[1] R S Feigelson and R K Route. Recent development in the growth of chalcopyrite crystals for nonlinear infrared applications. In *SPIE Conference Proceedings*, vol. 567, SPIE, 1985, pp. 2-10.

[2] D A Roberts. Dispersion equations for nonlinear optical crystals: KDP, $AgGaSe_2$, and $AgGaS_2$. *Appl. Opt.*, 35: 4677-4688, 1996.

[3] G C Bhar. Refractive index interpolation in phase-matching. *Appl. Opt.*, 15: 305-307, 1976.

[4] H Komine, J M Fukumoto, A H J Long, and E A Stappaerts. Noncritically phase matched mid-infrared generation in $AgGaSe_2$. *IEEE J. Select Top. Quantum Electron.*, 1: 44-49, 1995.

[5] Datasheet, Cleveland Crystals, Cleveland, OH, 1996.

[6] N P Barnes, D J Gettemy, J R Hietanen, and R A Iannini. Parametric amplification in $AgGaSe_2$. *Appl. Opt.*, 28: 5162-5168, 1989.

[7] G D Boyd, H M Kasper, J H McFee, and F G Storz. Linear and nonlinear optical properties of some ternary selenides. *IEEE J. Quantum Electron.*, 8: 900-908, 1972.

[8] B F Levine and C G Bethea. Nonlinear susceptibility of GaP; relative measurement and use of measured values to determine a better absolute value. *Appl. Phys. Lett.*, 20: 272-257, 1972.

[9] H Kildal and J C Mikkelsen. The nonlinear optical coefficient, phasematching, and optical damage in the chalcopyrite $AgGaSe_2$. *Opt. Commun.*, 9: 315-318, 1973.

[10] M M Choy and R L Byer. Accurate second-order susceptibility measurements of visible and infrared nonlinear crystals. *Phys. Rev. B,* 14: 1693-1706, 1976.

[11] V G Dmitriev, G G Gurzadyan, and D N Nikogosyan. *Handbook of nonlinear optical crystals.* Springer series in optical sciences, Springer Verlag, Berlin, vol. 64, 1991.

[12] B C Ziegler and K L Schepler. Transmission and damage-threshold measurements in $AgGaSe_2$ at 2.1 μm. *Appl. Opt.*, 30: 5077-5080, 1991.

[13] P A Budni, M G Knights, E P Chicklis, and K L Schepler. Kilohertz $AgGaSe_2$ optical parametric oscillator pumped at 2 μm. *Opt. Lett.*, 18: 1068-1070, 1993.

[14] Y X Fan, R C Eckardt, R L Byer, R K Route, and R S Feigelson. Nonlinear infrared frequency conversion in $AgGaS_2$ and $AgGaSe_2$. In *Tunable Solid State Lasers II*, vol. A.B. Budgor, L. Esterowitz, and L.G. DeShazer, Eds, Springer Verlag, 1986, pp. 360-363.

3.14 $ZnGeP_2$

Zinc Germanium Phosphide (ZGP) is one of the most promising materials for both 3-5 μm and 8-10 μm generation, because of its high nonlinearity, its transparency range, and its thermal conductivity. It is a positive uniaxial crystal ($n_e > n_o$) with point group $\bar{4}2m$. The material has an absorption band at 0.53 μm, and has substantial absorption at 1 μm. Therefore, $ZnGeP_2$ is usually used with 2 μm laser pumping or in two-step conversion. Progress has been done in reducing the absorption at short wavelengths, and the material is practically loss-less at 2 μm today. Absorption above 10 μm (see Figure 3.21) limits the tunability in the 8-12 μm band.

3.14.1 Transmission range

In Figure 3.21 the measured transmission spectrum of ZGP is shown. Recent material development has further increased the transparency below 3 μm. ZGP has a bandgap at 0.53 μm [1].

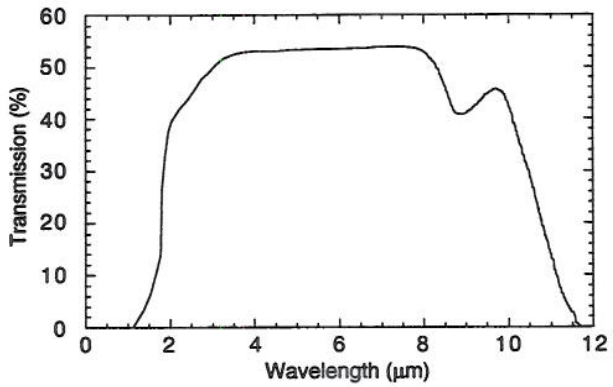

Figure 3.21 Measured transmission spectrum through an uncoated 10 mm thick $ZnGeP_2$ crystal [2]

3.14.2 Refractive index

The refractive indices are in the range 3.1-3.2 for wavelengths between 2 μm and 10 μm. The most recent publication of the dispersion relation in ZGP [3] use the formula:

$$n^2 = A + \frac{B}{\lambda^2 - C} - D\lambda^2$$

with the coefficients (valid for wavelengths in the range 1-12 μm)

	A	B	C	D
n_o	9.7465	0.7096	0.1169	0.00276
n_e	10.0039	0.7205	0.1531	0.00277

These will probably need modifications as the absorption between 1 μm and 2 μm is reduced. Other dispersion relations can be found in [4, 5]

3.14.3 Temperature coefficients

The temperature dependence of the refractive indicies of ZGP have been found to be [6]:

Wavelength	dn_o/dT (10^{-6} /K)	dn_e/dT (10^{-6} /K)
2.0 μm	141.9	152.9
5.0 μm	150.5	164.3
8.0 μm	161.0	174.3

3.14.4 Nonlinear second order coefficients

There are only three elements of the d-matrix that are nonzero, and when Kleinman symmetry is valid these are equal,

$$d_{14} = d_{25} = d_{36}$$

The value for these elements has been measured to be

Source	d_{36} (pm/V)	Method	Wavelength
[6]	111±33 (0.83 d_{14} GaAs)	SHG	10.6 μm
[6, 7]	75.4±13	(New value for GaAs)	
[8]	~50	SHG	9.6 μm
[9]	75±8	SHG	9.6 μm
[3]	70±7	SHG	2.6 μm

The value of d_{36} have traditionally been taken to be 75 pm/V. The most recent measurements supports this.

3.14.5 Effective nonlinearity

The expression for the effective nonlinearity for second order processes is given by the crystals point group.

Type 1 phase matching: $d_{eff} = d_{36}\sin(\theta)\sin(2\phi)$

Type 2/3 phase matching: $d_{eff} = d_{36}\sin(2\theta)\cos(2\phi)$

where θ is the angle between the direction of propagation and the crystal z-axis, and ϕ is the angle between the projection of the direction of propagation on the xy-plane and the crystal x-axis.

3.14.6 Optical damage

ZGP has had a reputation as a "cracky" material since the early 1970s. However, development of improved crystal growth techniques has substantially improved the material quality. Recent works report optical damage to the crystal surface when the fluence exceeds 10 J/cm² in 70-200 ns pulses [10]. For 150 ps pulses, a damage threshold of 30 GW/cm² (i.e. 4.5 J/cm²) has been reported [11].

3.14.7 Phase matching

Calculated phase matching curves for 2 μm pump wavelength are shown in Figure 3.22.

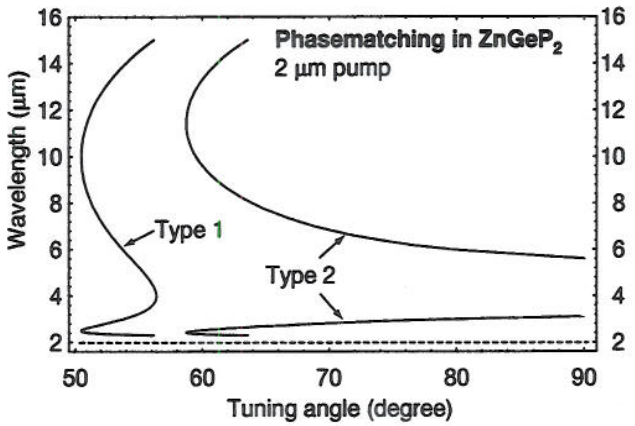

Figure 3.22 Calculated tuning curves for 2 μm pumped $ZnGeP_2$

We see that Type 2 phase matching cannot be achieved in the 3-5 μm region with 2 μm pumping.

3.14.8 Noncritical phase matching

Noncritical phase matching ($\theta = 90^\circ$) of type 1 is not possible in ZGP for pump wavelengths between 2 μm and 5 μm. For type 2 phase matching, $d_{eff} = 0$.

3.14.9 Example: Calculations

Results from calculations with various OPO configurations with ZGP are listed below. In calculations of d_{eff}^2/n^3 we have assumed that $d_{36} = 75.4$ pm/V.

Pump	Signals (μm)	PM	θ	ϕ	d_{eff}/d_{36}	d_{eff}^2/n^3	Walkoff
2.0 μm	4.0 4.0	1	56.4°	45°	0.83	126 (pm/V)²	0.7°
2.0 μm	4.0 4.0	2	-	-	-	-	-
2.0 μm	2.7 8.0	1	51.2°	45°	0.78	110 (pm/V)²	0.7°
2.0 μm	2.7 8.0	2	64.0°	0°	0.79	113 (pm/V)²	0.6°

3.14.10 Example: Experiments

The primary use of ZGP has been in frequency doubling of the output from CO_2 lasers. More recently, 2 micron pumped OPO operation has also been reported.

Ketteridge and coworkers at Lockheed Sanders recently reported on a ZGP OPO that produced an average power of 21 mW at 8.2 μm when pumped with an average power of 1 W from a 2.05 μm Ho:YLF laser [12]. The crystal was 6 x 6 x 12.5 mm and cut at 50.5 $^{\circ}$ for type 1 phase matching.

For 3-5 μm generation, a ZGP OPO with an output of over 2.5 W at a frequency of 4 kHz has been demonstrated. The OPO was pumped with 2.05 μm and had an overall efficiency close to 50% [13].

3.14.11 Price and availability

ZGP is a much studied material both in the USA and in the former Soviet Union. However, to the best of our knowledge only INRAD (Northvale, NJ) and Eksma, Inc. (Lithuania) grow the material on a commercial basis. Peter Schunemann at Lockheed Sanders (Nashua, NH) has developed significant improvements to the growth of ZGP over the past years, resulting in a significantly reduced absorption at 2 μm. Unfortunately, Sanders does not sell ZGP as most of their ZGP work is on contract with the US Air Force.

References

[1] G D Boyd, E Buehler, F G Storz, and J H Wernick. Linear and nonlinear optical properties of ternary $A^{II}B^{IV}C^{2V}$ chalcopyrite semiconductors. *IEEE J. Quantum Electron.*, 8: 419-426, 1972.

[2] K L Vodopyanov. Parametric generation of tunable infrared radiation in ZnGeP2 and GaSe pumped at 3 μm. *J. Opt. Soc. Am. B*, 10: 1723-1729, 1993.

[3] K Kato. Second-harmonic and sum-frequency generation in $ZnGeP_2$. *Appl. Opt.*, 36: 2506-2510, 1997.

[4] G C Bhar, L K Samanta, D K Ghosh, and S Das. Tunable parametric $ZnGeP_2$ crystal oscillator. *Sov. J. Quantum Electron.*, 17: 860-861, 1987.

[5] G C Bhar. Refractive index interpolation in phase-matching. *Appl. Opt.*, 15: 305-307, 1976.

[6] G D Boyd, E Buehler, and F G Storz. Linear and nonlinear optical properties of $ZnGeP_2$ and CdSe. *Appl. Phys. Lett.*, 18: 301-304, 1971.

[7] B F Levine and C G Bethea. Nonlinear susceptibility of GaP; relative measurement and use of measured values to determine a better absolute value. *Appl. Phys. Lett.*, 20: 272-257, 1972.

[8] H M Hobgood, T Henningsen, R N Thomas, R H Hopkins, M C Ohmer, W C Mitchel, D W Fischer, S M Hedge, and F K Hopkins. $ZnGeP_2$ grown by the liquid encapsulated Czochralski method. *J. Appl. Phys.*, 73: 4030-4037, 1993.

[9] P D Mason, D J Jackson, and E K Gorton. CO_2 laser frequency doubling in $ZnGeP_2$. *Opt. Commun.*, 110: 164-166, 1994.

[10] R D Peterson, K L Schepler, J L Brown, and P G Schunemann. Damage properties of $ZnGeP_2$ at 2 μm. *J. Opt. Soc. Am. B,* 12: 2142-2146, 1995.

[11] K L Vodopyanov, V G Voevodin, A I Gribenyukov, and L A Kulevski . High-efficiency picosecond parametric superradiance emitted by a $ZnGeP_2$ crystal in the 5-6.3 μ range. *Sov. J. Quantum Electron.*, 17: 1159-1161, 1987.

[12] P Ketteridge, P Budni, I Lee, P G Schunemann, and T Pollak. 8 micron ZGP OPO pumped at 2 microns. In *OSA Trends in Optics and Photonics on Advanced Solid State Lasers*, vol. 1, S.A. Payne and C.R. Pollock, Eds, Optical Society of America, Washington, DC, 1996, pp. 168-170.

[13] M G Knights. Multi-watt mid-IR optical parametric oscillator using $ZnGeP_2$. Presentation at OSA Meeting 7 February 1994 (According to F.K. Hopkins et al. in "Nonlinear materials research", NAECON 1995).

3.15 CdSe

Cadmium Selenide (CdSe) has a wide transparency range and several high nonlinearities. Its birefringence is relatively small so the of phase matchable wavelength ranges are small compared to the materials described in the previous sections. It is primarily used for long wavelength generation (8-20 μm) by the use of 2-3 μm pump wavelengths. It is a positive uniaxial crystal ($n_e > n_o$) with point group 6mm and has a bandgap at 0.5 μm.

3.15.1 Transmission range

There is a dicrepancy regarding the transmission properties of CdSe. Davydov et *al.* [1] reported the absorption coefficient in CdSe to be less than 0.01 cm^{-1} for wavelengths between 0.75 μm and 20 μm. Other reports indicate that there may be some absorption in both the high and low ends of this wavelength range. Isyanova et *al.* [2] states that absorption in the 1 μm band precludes direct pumping at this wavelength. In Figure 3.23 a measured transmission spectrum for CdSe is shown for wavelengths above 2 μm. This spectrum indicates that there is some absorption above 10 μm. However, this is an old measurement (from 1965) from a time when CdSe was a new material. Later material development may have improved the transparency features. Cleveland Crystals which grows CdSe states a better than 50% transmission through a 2 mm crystal in the range 0.8-18 μm [3].

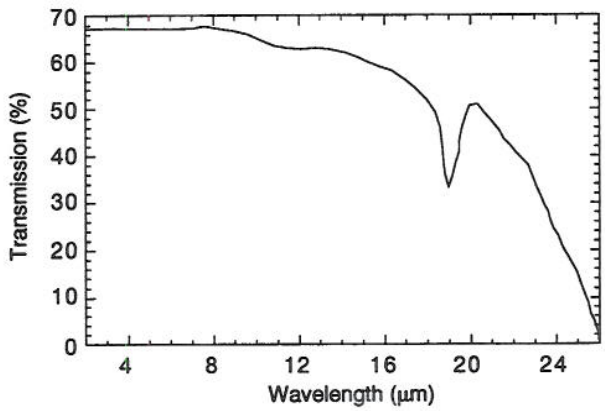

Figure 3.23 Measured transmission spectrum trough 1.7 mm uncoated CdSe [4]

3.15.2 Refractive index

The refractive indices for CdSe are in the range 2.4-2.5 for wavelengths 2-10 μm. The dispersion relation of CdSe has been found to follow the formula

$$n^2 = A + \frac{B\lambda^2}{\lambda^2 - C} + \frac{D\lambda^2}{\lambda^2 - E},$$

where the coefficients for wavelengths in the range 0.8-18 μm, have been calculated to be [5]:

	A	B	C	D	E
n_o	4.2243	1.768	0.227	3.12	3380
n_e	4.2009	1.8875	0.2171	3.6461	3629

3.15.3 Temperature dependence

The temperature dependence for both the refractive indices of CdSe is reported to be 120 $\cdot 10^{-6} K^{-1}$ at 1 μm [3].

3.15.4 Nonlinear second order coefficients

Five elements of the d-matrix are nonzero. When Kleinman symmetry is valid, four of these are equal:

$$d_{31} = d_{32} = d_{24} = d_{15}.$$

The fifth element is d_{33}. The magnitude of these elements (in pm/V) have been measured to be:

Source	d_{15}	d_{31}	d_{33}	Method	Wavelength
[6]	18 ± 1.8			SHG	10.6 μm
[7]			65.4	Wegde	2.12 μm
[7]			55.3	MD*	10.6 μm
[3]	31 ± 8	29 ± 6	44 ± 13	-	10.6 μm

*) MD: Used Miller's Δ to calculate d at other wavelength.

3.15.5 Effective nonlinearity

The only parametric interaction process possible in CdSe is type 2 phase matching [8]:

Type 2 phase matching: $d_{eff} = d_{15} \sin(\theta)$

where θ is the angle between the direction of propagation and the crystal z-axis. We note that the d_{33} element which has the largest value in CdSe cannot be used since it describes the interaction of three waves with polarization along the extraordinary axis (e = e+e) which cannot be phase matched.

3.15.6 Optical damage

The threshold for optical damage on the surfaces has been reported to be 30-60 MW/cm^2 in 10-300 ns pulses (i.e. 0.15-0.9 J/cm^2) [1, 3, 9, 10] for wavelengths between 1 μm and 10 μm.

3.15.7 Phase matching

Calculated type 2 phase matching curves for 2 μm and 3 μm pump wavelengths are shown in Figure 3.24.

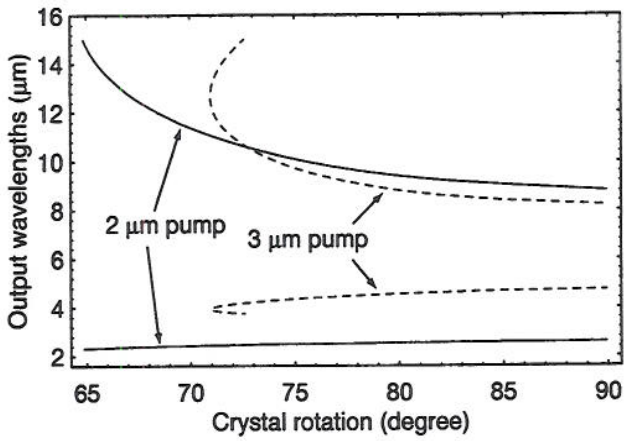

Figure 3.24 Calculated tuning curves for 2 μm and 3 μm pumped CdSe

We note that CdSe has a narrow phase matching range. In view of this it is not surprising that the most recent applications of CdSe have been with noncritical phase matching.

3.15.8 Noncritical phase matching

In Figure 3.25 calculated tuning curves for noncritical phase matching ($\theta = 90^\circ$) are shown.

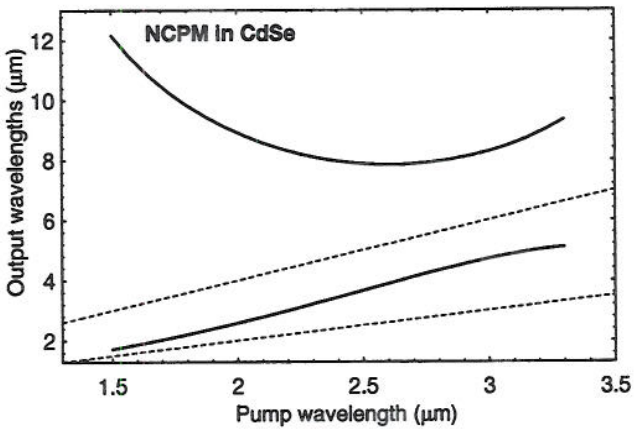

Figure 3.25 Calculated tuning curves for type 2 noncritical phase matching as function of pump wavelength. The dashed lines indicate the pumping wavelength and the double of the pumping wavelength

It should be noted that the OPO is tuned both in the 3-5 μm band and the 8-12 μm band when the pump is tuned from 2 μm to 3 μm.

3.15.9 Example

In a recent work, Isyanova and coworkers at Schwartz Electro-Optics have developed a Tandem OPO source generating 1.5-10 μm wavelengths [2]. In this work, a noncritically phase matched CdSe crystal with dimensions 10 x 10 x 35 mm^3 was pumped by the output of a tunable KTA OPO which in turn was pumped by a Nd:YLF laser. They obtained a total output energy (both signals) of approximately 4.5 mJ when pumped with 3.45 μm in 22 mJ 30 ns pulses. This was obtained with 210 mJ 1 μm pump pulses from the Nd:YLF-laser.

3.15.10 Price and availability

Cleveland Crystals (Cleveland, OH) manufactures CdSe crystals. In their March 1996 price list, they charge USD 1600 for a 5 x 15 x 15 mm^3 polished sample and USD 7400 for a 5 x 30 x 30 mm^3 polished sample.

References

[1] A A Davydov, L A Kulevskii, A M Prokhorov, A D Savel'ev, and V V Smirnov. Parametric generation with CdSe crystal pumped by CaF_2:Dy^{2+} laser. *JETP Lett.*, 15: 513-514, 1972.

[2] Y Isyanova, G A Rines, D Welford, and P F Moulton. Tandem OPO source generating 1.5-10 μm wavelengths. In *OSA Trends in Optics and Photonics on Advanced Solid State Lasers,* vol. 1, S.A. Payne and C.R. Pollock, Eds, Optical Society of America, Washington, DC, 1996, pp. 174-176.

[3] *Properties of the II-VI Crystals.* Information sheet, Cleveland Crystals, Cleveland, OH, 1984.

[4] D E McCarthy. The reflection and transmission of infrared materials: III, spectra from 2 μ to 50 μ. *Appl. Opt.*, 4: 317-320, 1965.

[5] G C Bhar. Refractive index interpolation in phase-matching. *Appl. Opt.*, 15: 305-307, 1976.

[6] G D Boyd, E Buehler, and F G Storz. Linear and nonlinear optical properties of $ZnGeP_2$ and CdSe. *Appl. Phys. Lett.*, 18: 301-304, 1971.

[7] M M Choy and R L Byer. Accurate second-order susceptibility measurements of visible and infrared nonlinear crystals. *Phys. Rev. B*, 14: 1693-1706, 1976.

[8] J E Midwinter and J Warner. The effects of phase matching method and of uniaxial crystal symmetry on the polar distribution of second-order non-linear optical polarization. *Brit. J. Appl. Phys.*, 16: 1135-1142, 1965.

[9] D Andreou. 16μm tunable source using parametric processes in non-linear crystals. *Opt. Commun.*, 23: 37-43, 1977.

[10] R L Herbst and R L Byer. Singly resonant CdSe infrared parametric oscillator. *Appl. Phys. Lett.*, 21: 189-191, 1972.

3.16 $CdGeAs_2$

In spite of poor transmission in the near- to mid-infrared, Cadmium Germanium Arsenide (CGA) is regarded as a very interesting material. This is because of its extremely high nonlinearity, 235 pm/V, the highest of any known birefringent compound and almost an order of magnitude larger than e.g. those of AGS and AGSe. The material also has a high thermal conductivity which is desirable in high power applications. It has a bandgap in the range of 2.0 μm [1], and there is substantial absorption below 3 μm. Therefore its primary use is conversion of a long (3-4 μm) wavelength pump to the 8-12 μm region. It is a positive uniaxial crystal ($n_e > n_o$) and has point group $\bar{4}2m$.

3.16.1 Transmission range

CGA has high absorption losses below 3 μm. Some of this stems from defects in the crystal, and it is expected that some of these absorption losses will be reduced with improved crystal growth. In Figure 3.26 a recent measurement of the absorption in CGA is shown.

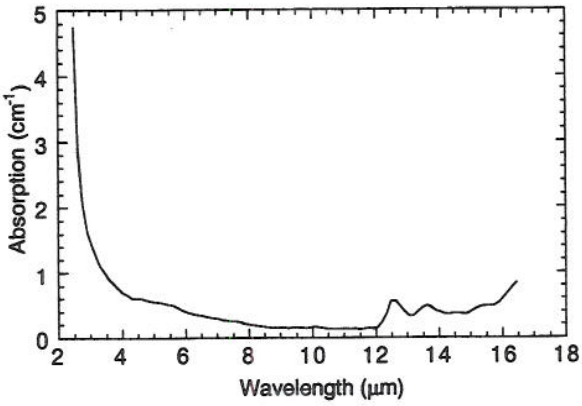

Figure 3.26 Measured absorption coefficient in CGA [2]

3.16.2 Refractive index

The refractive indices of CGA are in the range 3.5-3.65 for wavelengths in the range 4-10 μm. The dispersion relations for wavelengths in the range 2.4-11.5 μm have been found to follow the equation [3]

$$n^2 = A + \frac{B\lambda^2}{\lambda^2 - C} + \frac{D\lambda^2}{\lambda^2 - E}$$

where the coefficients are

	A	B	C	D	E
n_o	10.1064	2.2988	1.0872	1.6247	1370
n_e	11.8018	1.2152	2.6971	1.6922	1370

Other published measurements of the dispersion relations in CGA can be found in [4, 5].

3.16.3 Temperature dependence

The temperature dependence of the birefringence, d(Δn)/dT, in CGA was recently found to be 2.6 at 100K, 4.3 at 300K, and 5.1 at 400K, all in units of 10^{-5} K^{-1} [6].

3.16.4 Nonlinear second order coefficients

There are only three elements of the d-matrix that are nonzero, and when Kleinman symmetry is valid these are equal:

$$d_{14} = d_{25} = d_{36}$$

The magnitude of these elements has been measured to be:

$$d_{36} = 235 \pm 38 \text{ pm/V} \qquad [1]$$

with SHG at 10.6 μm.

3.16.5 Effective nonlinearity

The effective nonlinearity for second order processes in CGA is:

Type 1 phase matching: $d_{eff} = d_{36}\sin(\theta)\sin(2\phi)$

Type 2/3 phase matching: $d_{eff} = d_{36}\sin(2\theta)\cos(2\phi)$

where θ is the angle between the direction of propagation and the crystal z-axis, and ϕ is the angle between the projection of the direction of propagation on the xy-plane and the crystal x-axis.

3.16.6 Optical damage

The threshold for optical damage on the surfaces at 10.6 μm has been reported to be 40 MW/cm² in 160 ns pulses (i.e. 0.64 J/cm²) [4] and 1 kW/cm² for continuous radiation [5]. It seems reasonable to expect the threshold for damage to increase with the current improvements in the crystal growth technique [2].

3.16.7 Phase matching

Calculated phase matching curves for 4 μm pump wavelength are shown in Figure 3.27.

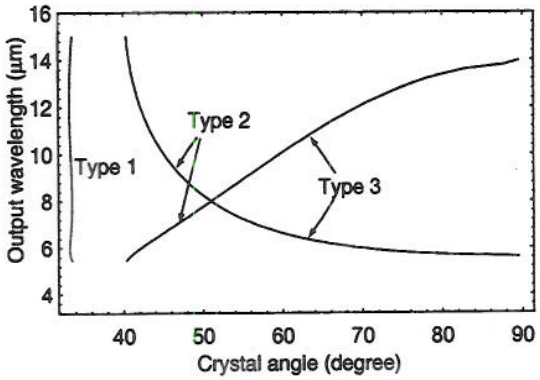

Figure 3.27 Calculated tuning curves for a 4 μm pumped $CdGeAs_2$ OPO

We observe that phase matching of type 1 is extremely sensitive to rotation angle. This indicates that the output from such an OPO will have a broad bandwidth.

3.16.8 Noncritical phase matching

Noncritical phase matching is not possible in CGA for pump wavelengths below 11μm.

3.16.9 Example: Calculations

Results from calculations with a CGA OPO are listed below. In calculations of d_{eff}^2/n^3 we have assumed that $d_{36} = 235$ pm/V.

Pump	Signals (μm)	PM	θ	ϕ	d_{eff}/d_{36}	d_{eff}^2/n^3	Walkoff
4.0μm	8.0 8.0	1	33.6°	45°	0.92	362 (pm/V)^2	1.3°
4.0μm	8.0 8.0	2	51.0°	0°	0.98	1132 (pm/V)^2	1.4°

3.16.10 Price and availability

We are not aware of any commercial growth of CGA. Peter Shunemann and coworkers at Lockheed Sanders (Nashua, NH) have recently published work on growth of CGA [2].

References

[1] G D Boyd, E Buehler, F G Storz, and J H Wernick. Linear and nonlinear optical properties of ternary $A^{II}B^{IV}C^{2V}$ chalcopyrite semiconductors. *IEEE J. Quantum Electron.*, 8: 419-426, 1972.

[2] P G Schunemann. Growth of $CdGeAs_2$ for far-IR OPO applications. In *Advanced Solid State Lasers 1996 Post Deadline Papers*, S.A. Payne and C.R. Pollock, Eds, Optical Society of America, Washington DC, 1996, paper PD8.

[3] G C Bhar. Refractive index interpolation in phase-matching. *Appl. Opt.*, 15: 305-307, 1976.

[4] H Kildal and J C Mikkelsen. Efficient doubling and cw difference frequency mixing in the infrared using the chalcopyrite $CdGeAs_2$. *Opt. Commun.*, 10: 306-309, 1974.

[5] R L Byer, H Kildal, and R S Feigelson. $CdGeAs_2$ - Anew nonlinear crystal phasematchable at 10.6 μm. *Appl. Phys. Lett.*, 19: 237-240, 1971.

[6] D W Fischer, M C Ohmer, and J E McCrae. Influences of temperature and transport properties on the birefringence of $CdGeAs_2$. *J. Appl. Phys.*, 81: 3579-3585, 1997.

3.17 GaSe

Gallium Selenide (GaSe) has a wide transparency range, a very strong birefringence and a high nonlinearity. It is a well researched material primarily in the former Soviet Union. However, the growth of high-quality crystals will be difficult because GaSe crystals are bonded very weakly in the c-direction, and it is at present not possible to polish GaSe at arbitrary angles - only z-cut crystals (i.e. $\theta = 0^\circ$) are possible. Due to its strong birefringence, the phase matching angles of the material are close to 0°. Therefore GaSe can still be used in OPOs. It is a negative uniaxial crystal ($n_o > n_e$) with point group $\bar{6}m2$ and has a bandgap at 0.62 μm. A comprehensive review of most of the work done on GaSe can be found in [1].

3.17.1 Transmission range

A measurement of the transmission spectrum of GaSe is shown in Figure 3.28. There is some absorption on wavelengths below 3 μm and above 13 μm.

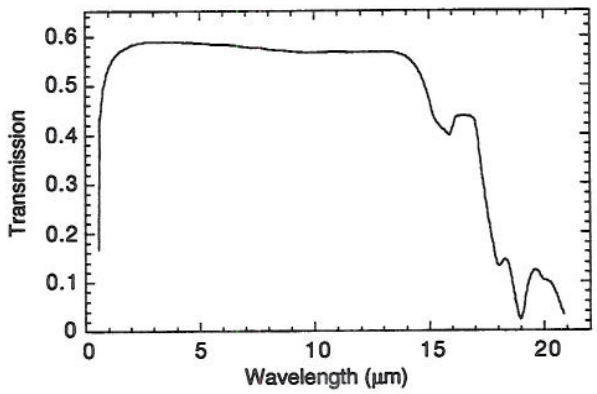

Figure 3.28 Measured transmission spectrum through 10 mm uncoated GaSe [2]

3.17.2 Refractive index

For wavelengths in the range 2-15 μm the refractive indices for GaSe are in the ranges 2.75-2.85 and 2.35-2.45 for the ordinary and extraordinary axes, respectively. Recently an improved dispersion relation for GaSe has been found. It uses the Sellmeier equations [3]

$$n^2 = A + \frac{B}{\lambda^2} + \frac{C}{\lambda^4} + \frac{D}{\lambda^6} + \frac{E\lambda^2}{\lambda^2 - F} \ .$$

where the coefficients are:

	A	B	C	D	E	F
n_o	7.443	0.4050	0.0186	0.0061	3.1485	2194
n_e	5.760	0.3879	-0.2288	0.1223	1.855	1780

These equations are valid for the wavelength range 0.65-18 μm. Other dispersion relations can be found in [4-7].

3.17.3 Nonlinear second order coefficients

Only three elements of the d-matrix are nonzero and when Kleinman symmetry is valid these have the same magnitude:

$$d_{22} = -d_{21} = -d_{16}.$$

The magnitude of d_{22} has been measured to be:

Source	d_{36} (pm/V)	Method	Wavelength
[6]	54.4±1	SHG	10.6 μm
[8]	75.4	SHG	10.6 μm

3.17.4 Effective nonlinearity

The expressions for the effective nonlinearities for second order processes are given by the crystals point group.

Type 1 phase matching: $d_{eff} = d_{22}\cos(\theta)\sin(3\phi)$

Type 2/3 phase matching: $d_{eff} = d_{22}\cos^2(\theta)\cos(3\phi)$

where θ is the angle between the direction of propagation and the crystal z-axis, and ϕ is the angle between the projection of the propagation vector on the xy-plane and the crystal x-axis.

3.17.5 Optical damage

The threshold for optical damage on the surfaces has been reported to be 20-35 MW/cm^2 in 10-25 ns pulses (i.e. 0.35-0.5 J/cm^2) [8, 9] for wavelengths around 1 μm.

3.17.6 Phase matching

Calculated phase matching curves for 2 μm and 3 μm pump wavelengths are shown in Figure 3.29. We note that GaSe has a wide phase matching range. The low value of the crystal rotation angle (θ) stems from the large birefringence in GaSe. It can further be noted that owing to the high sensitivity on rotation angle, PM of type 1 will lead to a high bandwidth. A 650 cm^{-1} bandwidth has been reported for near-degenerate type 1 PM compared to 20 cm^{-1} for type 2 PM [10].

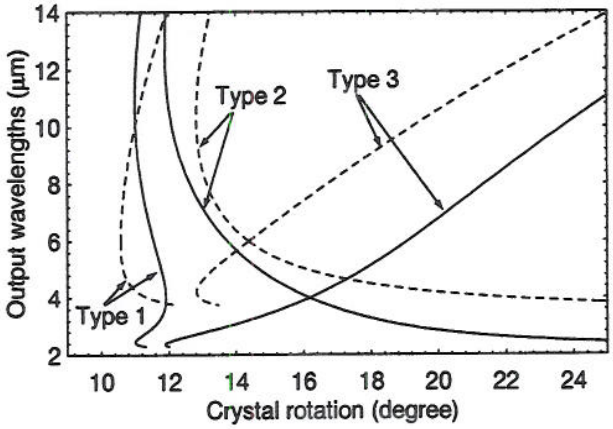

Figure 3.29 Calculated tuning curves for 2 μm (solid) and 3 μm (dashed) pumped GaSe OPO

3.17.7 Noncritical phase matching

Noncritical phase matching ($\theta = 90^\circ$) is not possible in GaSe since $d_{eff} = 0$ for both type 1 and type 2/3 phase matching.

3.17.8 Example: Calculations

Results from calculations with various OPO configurations with GaSe are listed below. In calculations of d_{eff}^2/n^3 we have assumed that $d_{36} = 54.4$ pm/V and n= 2.6.

Pump	Signals (μm)	PM	θ	ϕ	d_{eff}/d_{36}	d_{eff}^2/n^3	Walkoff
2.0μm	4.0 4.0	1	11.9°	30°	0.98	162 (pm/V)²	3.3°
2.0μm	4.0 4.0	2	16.2°	0°	0.92	143 (pm/V)²	4.4°
2.0μm	2.7 8.0	1	11.2°	30°	0.98	162 (pm/V)²	3.1°
2.0μm	2.7 8.0	2	12.6°	0°	0.95	153 (pm/V)²	3.5°
3.0μm	4.3 10.0	1	11.1°	30°	0.98	162 (pm/V)²	3.1°
3.0μm	4.3 10.0	2	12.9°	0°	0.95	152 (pm/V)²	3.6°

3.17.9 Example: Experiments

Recently Vodopyanov and Chazapis (Imperial College, UK) demonstrated a 2.8 μm pumped GaSe optical parametric generator that produced tunable output in the entire wavelength range 3.3-19 μm. The "threshold" for OPG in their 1.4 cm GaSe crystal was found to be 1.1 GW/cm², and the "quantum efficiency" was reported to be 3-5% at 5 GW/cm² pump intensity [11].

3.17.10 Price and availability

We are not aware of any commercial growth of GaSe, but crystals may possibly be bought from companies in the former Soviet Union. In a recent paper, V.G.

Voevodin of the Siberian Physical-Technical Institute (Tomsk, Russia) was acknowlegded for manufacturing the GaSe crystal [11].

References

[1] N C Fernelius. Properties of gallium selenide single crystal. *Prog. Crystal Growth and Charact.*, 28: 275-353, 1994.

[2] A Bianchi, A Ferrario, and M Musci. 4-12 μm tunable down-conversion in GaSe from a $LiNbO_3$ parametric oscillator. *Opt. Commun.*, 25: 256-258, 1978.

[3] K L Vodopyanov and L A Kulevskii. New dispersion relationships for GaSe in the 0.65-18 μm spectral region. *Opt. Commun.*, 118: 375-378, 1995.

[4] K L Vodopyanov. Wide tuning range OPG's pumped by short Er-laser pulses at λ=2.8 μm. In *OSA Proceedings on Advanced Solid State Lasers,* vol. 24, B.H.T. Chai and S.A. Payne, Eds, Optical Society of America, Washington, DC, 1995, pp. 194-197.

[5] G B Abdullaev, K R Allakhverdiev, L A Kulevskii, A M Prokhorov, E Y Salaev, A D Savelev, and V V Smirnov. Parametric conversion of infrared radiation in a GaSe crystal. *Sov. J. Quantum Electron.*, 5: 665-668, 1975.

[6] G B Abdullaev, L A Kulevskii, A M Prokhorov, A D Savelev, E Y Salaev, and V V Smirnov. GaSe, A new effective material for nonlinear optics. *JETP Lett.*, 16: 90-92, 1972.

[7] G B Abdullaev, K R Allakhverdiev, M E Karasev, V I Konov, L A Kulevskii, N B Mustafaev, P P Pashinin, A M Prokhorov, Y M Starodumov, and N I Chapliev. Efficient generation of the second harmonic of CO_2 laser radiation in GaSe crystal. *Sov. J. Quantum Electron.*, 19: 494-498, 1989.

[8] P Kupecek, E Batifol, and A Kuhn. Conversion de frequences optiques dans le seleniure de gallium (GaSe). *Opt. Commun.*, 11: 291-295, 1974.

[9] G B Abdullaev, L A Kulevsky, P V Nikles, A M Prokhorov, A D Savelev, E Y Salaev, and V V Smirnov. Difference frequency generation in a GaSe crystal with continuous tuning in the 560-1050 cm^{-1} range. *Sov. J. Quantum Electron.*, 6: 88-90, 1976.

[10] K L Vodopyanov and V G Voevodin. 2.8 μm laser pumped type I and type II travelling-wave optical parametric generator in GaSe. *Opt. Commun.*, 114: 333-335, 1995.

[11] K L Vodopyanov and V Chazapis. Extra-wide tuning range optical parametric generator. *Opt. Commun.*, 135: 98-102, 1997.

3.18 GaAs with domain inversion

Gallium arsenide (GaAs) has a high nonlinearity and a high thermal conductivity. It has a bandgap at ~860 nm and has good transmission in the infrared at wavelengths between 1 μm and 12 μm. Unfortunately, nonlinear processes cannot be phase matched in bulk GaAs since it is an isotropic material. However, quasi-phase-matched devices have been demonstrated where thin slices of GaAs cut in the {110} direction are rotated 180 degrees with respect to each other and stacked. A critical parameter for efficient operation of such a device is the loss per surface in the stack. One way to minimize this loss is to use Brewster angle stacks with small airgaps between each GaAs slice [1, 2].

Another and more robust way to make a QPM device is to diffusion bond the plates in the stack together. Such a stack will retain most of the material parameters of bulk GaAs, like a high optical damage threshold, but there have been problems related to reducing the loss per surface in the stack. Recent reports show that this problem is now about to be overcome [3-5]. There is also a considerable effort in developing QPM GaAs waveguide structures for low power applications. The current advances in the field of QPM GaAs give potential for the use of this material in future applications in nonlinear wavelength conversion.

3.18.1 Refractive index

GaAs has no natural birefringence. The refractive index is in the range 3.2-3.4 for wavelengths between 1.3 μm and 15 μm. For wavelengths in the range 1-10 μm the dispersion relation has been found to follow (λ in μm) [6]

$$n^2 = 7.10 + \frac{3.78l^2}{l^2 - 0.2767} + \frac{1.97l^2}{l^2 - 1391}$$

Other dispersion relations can be found in [7-10].

3.18.2 Nonlinear coefficient

GaAs has the cubic zincblende structure with space group $\bar{4}3m$. There are three nonzero elements in the d-matrix and these are equal when Kleinman symmetry is valid:

$$d_{14} = d_{25} = d_{36}$$

Measured values of these elements are listed below.

Source	d_{36} (pm/V)	Method	Wavelength
[11]	188±94	Wedge	10.6 μm
[12]	134±42	SHG	10.6 μm
[13]	90±5*	MF (GaP)	10.6 μm
[14]	173±28	Wedge	2.12 μm
[14]	151±24	SHG	10.6 μm

*) Levine and Bethea [13] measured the absolute value for GaP by the Maker fringes method and used this value and the relative value for GaAs published by Wynne and Bloembergen [11] to calculate a new absolute value for GaAs.

A value of ~150 pm/V at 10.6 μm seems to cover most of the published values. The corresponding nonlinear figure of merit for the QPM structure ($d_{eff} = 2d_{14}/\pi$) is d_{eff}^2/n^3 [a] 250 (pm/V)^2, which is approximately twice that of $ZnGeP_2$.

3.18.3 QPM period

So far, only frequency doubling of 10.6 μm radiation has been demonstrated with QPM GaAs. In this process, a 106 μm QPM period is required [15]. The QPM period for a given set of wavelengths can be found from the dispersion relation. If the QPM period is too short for reliable processing, odd multiples of this period can also be used. Examples of first order QPM periods are listed below. As can be seen, a 3. order QPM device for conversion of 2 μm pump will require a poling period of approximately 90 μm. This is in the same range as the 106 μm devices used for SHG of 10.6 μm, and should be feasible.

l_3	l_1	l_2	QPM
1 μm	1.5 μm	3 μm	3 μm
2 μm	4 μm	4 μm	29 μm
3 μm	4 μm	12 μm	76 μm

3.18.4 Current work

The critical parameter for QPM GaAs is the loss per surface in the stack. This loss determines the optimal number of plates in the stack; a lower loss gives more plates and then a higher wavelength conversion efficiency. Practical devices will require bonded stacks of 50 or more GaAs plates to achieve a 10% conversion efficiency with 10 MW/cm^2 input intensity [3]. The loss per surface should then be less than 0.1% for efficient energy conversion. At present, losses in this range has reportedly been achieved both at Thomson CSF (Paris, France) [4] and at Stanford University (Palo Alto, CA) [3, 16]. Research on QPM GaAs waveguides is currently being done at Bell Communications Research (Red Bank, NJ) and at Oki Electric Industry (Tokyo, Japan).

References

[1] D E Thompson, J D McMullen, and D B Anderson. Second-harmonic generation in GaAs "stack of plates" using high-power CO_2 laser radiation. *Appl. Phys. Lett.*, 29: 113-115, 1976.

[2] A Szilagyi, A Hordvik, and H Scholssberg. A quasi-phase-matching technique for efficient optical mixing and frequency doubling. *J. Appl. Phys.*, 47: 2025-2032, 1976.

[3] D Zheng, L A Gordon, Y S Wu, R K Route, M M Fejer, R L Byer, and R S Feigelson. Diffusion bonding of GaAs wafers for nonlinear optics applications. *J. Electrochem. Soc.*, 144: 1439-1441, 1997.

[4] P Schanne. Artificial nonlinear materials for optronics. Presentation at NATO Panel 4 RSG 13 Meeting, May 1996.

[5] L Gordon, G L Woods, R C Eckardt, R R Route, R S Feigelson, M M Fejer, and R L Byer. Diffusion-bonded stacked GaAs for quasi-phase-matched second-harmonic generation of a carbon dioxide laser. *Electr. Lett.*, 29: 1942-1944, 1993.

[6] J S Blakemore. Mid-infrared dispersion of the refractive index and reflectivity for GaAs. *J. Appl. Phys.*, 62: 4528-4532, 1987.

[7] S Adachi. Optical dispersion relations for GaP, GaAs, GaSb, InP, InAs, InSb, $Al_xGa_{1-x}As$ and $In_{1-x}Ga_xAs_yP_{1-y}$. *J. Appl. Phys.*, 66: 6030-6040, 1989.

[8] M Bertolotti, V Bogdanov, A Ferrari, A Jascow, N Nazorova, A Pikhtin, and L Schirone. Temperature dependence of the refractive index in semiconductors. *J. Opt. Soc. Am. B*, 7: 918-922, 1993.

[9] S A Geidur, A N Pikhtin, V T Prokopenko, and A D Yaskov. dispersion of the refractive index and induced birefringence in gallium arsenide. *Opt. Spectrosc.*, 46: 177-182, 1979.

[10] A N Pikhtin and A D Yaskov. Dispersion of the refractive index of semiconductors with diamond and zinc-blende structures. *Sov. Phys. Semicond.*, 12: 622-626, 1978.

[11] J J Wynne and N Bloembergen. Measurement of the lowest-order nonlinear susceptibility in III-V semiconductors by second-harmonic generation with a CO_2 laser. *Phys. Rev.*, 188: 1211-1220, 1969.

[12] J H McFee, G D Boyd, and P H Schmidt. Redetermination of the nonlinear optical coefficients of Te and GaAs by comparison with Ag_3SbS_3. *Appl. Phys. Lett.*, 17: 57, 1970.

[13] B F Levine and C G Bethea. Nonlinear susceptibility of GaP; relative measurement and use of measured values to determine a better absolute value. *Appl. Phys. Lett.*, 20: 272-257, 1972.

[14] M M Choy and R L Byer. Accurate second-order susceptibility measurements of visible and infrared nonlinear crystals. *Phys. Rev. B*, 14: 1693-1706, 1976.

[15] S K Wong. Effects of plate thickness and stack distribution of quasi-phase-matched materials on nonlinear frequency generation. *IEEE J. Quantum Electron.*, 32: 1560-1569, 1996.

[16] R L Byer, Stanford University, CA. Personal Communications, 1997.

3.19 Materials for 1–5 μm generation — Summary

Of the 8 materials reviewed in the preceeding sections, KTP and $LiNbO_3$ are the most easily available and well tried. $LiNbO_3$ is particularly attractive because the periodic poling process for this material is relatively well developed. The crystal thickness is limited to maximum 1 mm, but work is going on to improve this by diffusion bonding. Periodic poling has also been demonstrated in KTP, RTP, RTA, and CTA. In spite of the less developed poling process, these materials can be poled with crystal thicknesses and grating periods comparable to those of $LiNbO_3$. These results indicate that materials in the KTP family may be even more suitable for periodic poling than $LiNbO_3$. In both $LiNbO_3$ and the KTP family, the d_{33} element is much greater than any other element in the d-tensor. The 33-element can only be used with quasi phase matching.

$KNbO_3$ has high values of all the nonzero elements in the d-tensor. However, its large birefringence leads to large walk-off and small acceptance angles. $KNbO_3$ crystals are brittle and have a limited temperature range. We are not aware of any systems using $KNbO_3$ outside laboratories.

If operation in the entire 3–5 μm range is required, the choice of materials is restricted. KTP is not suitable for operation above 4 μm. The arsenates, KTA, RTA, and CTA, have better transmission at long wavelengths. DFG has generated 5.2 μm in KTA [1] and 4.16 μm in RTA [2]. CTA has been used in an OPO for 4.12 μm [3]. The absorption spectra for RTA and CTA are similar to that of KTA, so they can probably be used at equally long wavelengths. $LiNbO_3$ has generated 4.83 μm in an OPO [4]. $KNbO_3$ has been used in an OPO generating 5.2 μm with femto-second pulses [5]. The very high intensity in the short pulses allowed the use of a crystal only 1 mm long. For nano-second pulses the crystal would have to be longer and absorption at the longest wavelengths would be a much greater problem.

KTA, RTA, CTA, $LiNbO_3$, and $KNbO_3$ all have absorption above 4 μm, and the the generated power in the experiments cited above dropped as the wavelength approached 5 μm. The absorption would probably lead to thermal problems for high average power operation. The thermal conductivities are important parameters in this context, but we have not found data on this for all the materials. $LiIO_3$ is the only material in the group that has relatively high transmission at 5 μm. It has an absorption line at about 4.3 μm, but that may not be a problem in military applications because the atmosphere also absorbs at that wavelength. The main problems with $LiIO_3$ are that it is hygroscopic and has a low damage threshold.

Altogether, periodically poled $LiNbO_3$ is currently the most attractive material for 3–5 μm generation if the available crystal thickness is sufficient. The arsenates of the KTP family are also promising candidates for poling. RTA is commercially available and it has been poled. For use with birefringent phase matching, KTA is probably a good choice. It is easily available and it has high damage threshold and relatively good transmission in the long end of the wavelength range.

With any of these materials, absorption will reduce power in the wavelength range near 5 μm. If high power at 5 μm is required, it may be better to use one of the long wavelength materials discussed in the following sections.

Note that the choice of material may depend strongly on the details of the device to be built. For example, small walk-off may be essential if the pump beam is narrow, while it is much less important if the pump beam is wide.

References

[1] A.H. Kung, S. Fei, and H.L. Strauss. Mid-infrared sources using dye lasers in $KTiOAsO_4$ and $LiIO_3$. *Appl. Spect.*, 50:790–794, 1996.

[2] D.L. Fenimore, K.L. Schepler, D. Zelmon, S. Kück, U.B. Ramabadran, P. Von Richter, and D. Small. Rubidium titanyl arsenate difference-frequency generation and validation of new sellmeier coefficients. *J. Opt. Soc. Am. B*, 13:1935–1940, 1996.

[3] G.R. Holtom, R.A. Crowell, and L.K. Cheng. Femtosecond mid-infrared optical parametric oscillator based on $CsTiOAsO_4$. *Opt. Lett.*, 20:1880–1882, 1995.

[4] L.E. Myers, R.C. Eckardt, M.M. Fejer, R.L. Byer, and W.R. Bosenberg. Multigrating quasi-phase-matched optical parametric oscillator in periodically poled $LiNbO_3$. *Opt. Lett.*, 21:591–593, 1996.

[5] D.E. Spence, S. Wielandy, C.L. Tang, C. Bosshard, and P. Günter. High average power, high-repetition rate femtosecond pulse generation in the 1-5 μm region using an optical parametric oscillator. *Appl. Phys. Lett.*, 68:452–454, 1996.

3.20 Materials for 8–12 μm generation — Summary

Which material should be chosen for a tunable source in the 8–12 μm atmospheric window? This depends on application and the available pump source. Continued research and material development is expected to improve the performance of some of the materials listed in the previous sections. At present, the situation can be summarized:

The low thermal conductivity of $AgGaS_2$ and $AgGaSe_2$ limits the average conversion powers to a few watts. Although new OPO designs may improve the maximum output, this severely limits the use of these materials in high power operation. AGS can be used in direct conversion of 1 μm pump.

$ZnGeP_2$ has a significantly higher thermal conductivity ($\sim$ 35 times higher), but has some optical absorption from 2- and 3-phonon absorption. This absorption may be reduced by improved crystal growth (or cooling of the crystal), but today the average conversion power is limited to a few watts. It is expected that the available output powers from ZGP devices will increase significantly in the future.

CdSe has a low thermal conductivity, which will probably limit the use of the material in high power applications. It can be used in noncritical phase matching for conversion of a 1.5–2.5 μm pump to 8–12 μm.

Until recently, little work had been done on $CdGeAs_2$. Currently it is investigated as perhaps the most promising material owing to its extremely high nonlinearity and its wide transparency and phase matching ranges. Future crystal growth development is expected to reduce the absorption shoulder at shorter wavelengths (2–4 μm). The need for long wavelength pumping (above 2.5–3 μm) may limit the use of the material in some applications.

GaSe is a material well researched in the former Soviet Union. Its high nonlinearity and wide transparency and phase matching ranges are desirable material qualities. However, the crystal is bonded very weakly in the z-direction which makes growth of high quality crystals difficult. When used in OPO operation the material also suffers from a very large walk-off. Its rather low thermal conductivity may also limit the interest for this material in higher power operations.

Development of QPM GaAs devices is at its very early stages. However, recent improvements in the bonding techniques indicates that low loss stacks may be available in a not too distant future. If this is the case, then GaAs may become one of the more important materials in 8–12 μm generation. The large apertures attainable combined with the high thermal conductivity of GaAs (20% higher than ZGP) indicates that devices of this material can be well suited for high power operation.

At present, ZGP is the most promising material for high power tunable 8–12 μm generation. It is expected that future development will improve the transmission and the material quality of this material as well as of CGA and GaSe. GaSe and the other materials listed here (AGS, AGSe and CdSe) will probably primarily be used in lower power devices.

It should also be mentioned that most of the materials listed in this summary can also be used in generation of 3–5 μm radiation, and are often used in such applications.

This is especially the case when wavelengths in the 4.5–5 μm range is required, as the materials listed in the previous section tend to have significant absorption losses at wavelengths in this range.

4 OPO DESIGN

In this chapter, we discuss some aspects of OPO design that are not usually covered in detail in books. We also compare OPOs to other frequency conversion techniques and discuss the conditions where each technique is appropriate. Because optical damage is often the limiting mechanism in nonlinear conversion devices, the different configurations can be compared by keeping the fluence (or intensity in the CW case) in the cavity fixed and comparing the conversion efficiency of the configurations.

4.1 OPOs versus parametric generators

In bulk media with limited interaction lengths, nonlinear optical frequency conversion processes need very high intensities to operate efficiently. Practical devices operate close to the threshold for optical damage. There are several possible techniques for parametric frequency conversion, including different OPO configurations as well as other schemes. Difference frequency generators need two pump sources. In this section we only consider OPOs and parametric generators, which operate with a single pump source. The optimal scheme depends on the temporal character of the pump signal. The sources can be divided in three classes: CW (or quasi CW), nanosecond pulses (typical of Q-switched lasers), and picosecond or shorter pulses (typical of mode locked lasers). It is interesting to note how different techniques complement each other, each being suitable for one range of pulse lengths and unsuitable for other.

The conceptually simplest parametric conversion process is optical parametric generation (OPG) in a nonlinear crystal. This mechanism corresponds to amplified spontaneous emission (ASE) in a laser medium without a cavity. The signal starts from spontaneous parametric down conversion, and grows because of optical parametric amplification (OPA). To obtain good conversion efficiency in a crystal of practical length, the intensity has to be very high. To avoid damage, the pulses must be correspondingly short. This consideration limits the OPG/OPA technique to pulses shorter than a few picoseconds. With pump intensity of the order of 10 GW/cm^2, reasonable efficiency can be achieved in a crystal of a few cm [1].

For longer pulses, the intensity must be reduced to avoid damage. The required interaction length increases, and the only practical solution is to put the nonlinear crystal in a cavity, i.e. to build an OPO. In the OPG/OPA, the pump and signals copropagate for the whole duration of the conversion process. In the OPO however, the signals typically make hundreds of round trips in the resonator while the pump makes one or two passes through it. The pump energy is not converted efficiently until the signal has reached a sufficiently high level, therefore the buildup time of the signal becomes important. If it is too long compared to the pump pulse, most of the pump energy may pass before efficient conversion starts. This explains why OPOs are not suitable for very short pump pulses.

To achieve rapid growth of the signal in a pulsed OPO, the amplifying interaction should fill a large part of the signal's path in the resonator. This implies that a linear resonator should be only slightly longer than the nonlinear crystal, and bidirectional pumping should be used so that the signal is amplified in both directions. In a ring

resonator, nonlinear crystals can be inserted in more than one leg.

In CW OPOs, the startup time is not critical, so the cavity length is not so important. Synchronously pumped OPOs deserve special mention. They are used with mode locked pump lasers, and the cavity length of the OPO is matched to the cavity length of the laser. Although the pump pulses are short, the OPO scheme can be used because it does not operate on single independent pulses.

4.2 Resonant signals in OPOs

An OPO with a cavity in which a single signal is resonant is called a singly resonant OPO (SRO). SROs tend to have relatively high thresholds. When a Q-switched pump source is used, the intensity is usually high enough to allow efficient operation of an SRO, but it has been difficult to pump SROs with CW sources. With the recent progress in materials for quasi phase matching, SROs have become feasible even for CW systems [2].

In the simplest OPOs, the pump beam makes a single pass through the nonlinear crystal. By reflecting the pump back through the crystal, efficiency can be improved for three reasons:

- In the initial part of the pump pulse, the signal grows more rapidly because it is amplified in both passes through the crystal. The signal pulse starts earlier and a greater part of the pump pulse can be converted.
- If the intensities are not large enough to deplete the pump in a single pass, more energy may be converted in the return pass.
- The two-pass pump can reduce the problem of back-conversion (see Section 2.3.4). Both mirrors can be fully transparent for the nonresonant signal, so each pass starts with only one signal of nonzero amplitude. Because sum frequency generation requires photons in both signals, this reduces the possible back conversion. Even if there is back conversion in the first pass, the generated pump light may be converted to signal light in the second pass.

The main drawback with the linear, two-pass OPO is that the reflected pump may disturb or damage the pump laser, so an optical isolator is required.

To reduce threshold and increase conversion efficiency for weak pump sources, one can make a double resonant OPO (DRO) in which both signals are resonant. The cavity length must be controlled to maintain this condition. There has been problems with bad stability because the output power is sensitive to sub-wavelength variation of the cavity length. Tuning has also been difficult. Stable DRO operation and tuning has been demonstrated in a monolithic cavity made from a $LiNbO_3$ crystal [3]. Note that type 1 phase matched OPOs near degeneracy are necessarily double resonant.

An alternative for low power operation is a pump resonant OPO (PRO) in which the pump and one of the signals are resonant. This avoids the stability problems of the DRO, but the cavity length has to be locked to the frequency of the pump source.

An interesting variation of the PRO is obtained by making the OPO cavity a part of the pump laser cavity. This is called intracavity OPO (ICOPO). It avoids the difficulty of locking the OPO cavity to the pump frequency. In external OPOs pumped by pulsed lasers, the energy in the first part of the pump pulse is not converted because the OPO signal needs time to build up to a level that can deplete the pump. In an ICOPO, this waste of pump energy can be avoided because the cavity has a high finesse at the pump wavelength. In principle, energy can only escape by being converted to a signal wavelength that has output coupling, and all pump energy is stored until it is converted. In practice, this ideal situation is precluded by losses, but nevertheless the ICOPO may be an efficient solution. Cavity length, signal output coupling and pump intensity must be adjusted for optimal operation. If the OPO pulse starts too early, it may quench laser operation before the energy in the laser medium has been efficiently extracted.

Even triple resonant OPOs have been reported [4]. Another interesting possibility is the nonresonant OPO (NRO) [5]. It utilizes a two-pass pump beam so there is amplification in both directions. One mirror is fully transparent for one signal and highly reflective for the other. The other mirror is opposite. No signal is resonant, but the feedback necessary for oscillation is provided by the nonlinear process itself. It has been claimed that this configuration is particularly suitable for injection seeding, because it avoids the requirement of locking the resonator length to the seed wavelength [6]. We think this claim is incorrect. If the OPO contains a modulated signal, it is easy to see that this signal will repeat periodically, implying that the OPO has a longitudinal mode structure. At the seeded end of the OPO, both signals incident on the crystal are nonzero. For efficient conversion, they must satisfy a phase relation, and this is equivalent to the resonance condition in a normal cavity. Closer inspection of the equations for the growth of the signals in presence of a seed source reveal that seed frequency mismatch has exactly the same effect as in an SRO with the same net round trip gain.

In an SRO, one has the choice of which signal to make resonant. The parametric process creates the same number of photons at each signal wavelength, so the total fluence in the cavity is minimized by making the lowest frequency signal resonant. In practice, the damage threshold of the optical components may depend on the wavelength, so the optimal design with respect to damage risk depends on the wavelengths and coatings in question. If the output coupling is small, cavity losses can be important for the resonant signal. If only one signal is going to be used, efficiency is maximized by making the unused signal resonant and making the output mirror fully transparent for the desired wavelength. In this way, the unused signal suffers most of the losses. In some situations, the signals may have significantly different losses. This will be the case if the nonlinear crystal has absorption at one of the signal wavelengths. If the average power is high, the signal with least absorption should be made resonant to minimize power dissipation in the crystal. In the two-pass pump OPO, the nonresonant signal is emitted in both ends of the resonator. Therefore only the resonant signal can be coupled efficiently to a single beam. Table 4.1 gives a summary of the mirror reflectivities in linear single resonant and nonresonant OPOs.

	M_1, λ_1	M_1, λ_2	M_1, λ_3	M_2, λ_1	M_2, λ_2	M_2, λ_3
1-pass, λ_1 resonant	HR	-	HT	OC	HT	HT
1-pass, λ_2 resonant	-	HR	HT	HT	OC	HT
2-pass, $\lambda_1$resonant	HR	HT	HT	OC	HT	HR
Nonresonant	HR	HT	HT	HT	HR	HR

Table 4.1 Mirror reflectivities for linear OPOs. HT - high transmission, HR - high reflection, OC - output coupling.

4.3 Resonators and mode matching

It is common to make OPOs with plane-plane resonators. The signal mode is then determined by the gain guiding due to the transverse pump distribution. This works fine provided the beams are wide enough that diffraction losses are small. The pump power must be high enough to give sufficient intensity with this width. If the pump power is smaller, the beam must be made narrower and diffraction losses become important. Since the signal makes tens or hundreds of round trips, while the pump makes only one or two passes through the crystal, diffraction losses become a problem for the signal first. Diffraction loss for the signal can be reduced by using a stable resonator. Apart from damage considerations, there is another limit to how much the beams can be focused: If the spot size is too small the short Rayleigh length z_0 will limit the effective interaction distance. A crude estimate of the minimum pump power required for an OPO of length L can be made as follows: Suppose that the OPO needs $gL > K$, and that g for $\Delta k = 0$ is $g = \eta\sqrt{N_3} = \eta\sqrt{I_3/\hbar\omega_3}$ as defined in Equation (2.53). Thus we need $I_3 > \hbar\omega_3 K^2/(L^2\eta^2)$. For the effective interaction length to equal L, we need $z_0 > L/2$, or $w_0^2 > L\lambda/(2\pi n)$, where w_0 is the beam spot radius. The minimum pump power is then

$$P = I_3\pi w_0^2 = \frac{hcK^2}{2nL\eta^2} \tag{4.1}$$

See [7] for modelling and experimental work on a low-threshold SRO. The minimum power is lower for DROs than for SROs, because the DRO can operate with lower pump intensity. For very small pump powers, wave guide OPOs can be used. They combine small beam area with long interaction length and small diffraction losses. Some common nonlinear materials, like $LiNbO_3$ and KTP, can be used for wave guides.

Unstable resonators with magnification greater than 1 were found to give the best results in a comparison of stable, plane-plane, and unstable resonators [8]. Simulation results indicate that variable reflectivity mirrors (VRM) may lead to good beam quality [9], but we are not aware of any experimental demonstrations of this. Making a VRM with specified reflectivities at 3 different wavelengths is probably very difficult.

In an SRO, the resonator determines the phase profile only of the resonant signal. The nonresonant signal is free to take the phase profile that leads to maximum gain. This makes the SRO relatively tolerant to the phase profile of the pump. In the DRO, on the other hand, the phase profiles of both signals are determined by the resonator. For efficient conversion, the correct phase relation must be satisfied all over the transverse beam profile. This implies that the pump wave front must be mode matched to the resonant signal modes.

A disadvantage with all linear OPOs is that the gain is determined by the intensity in a single direction, while the beams in both directions add towards the damage threshold. Ring resonators avoid this problem, and they have the additional advantages of being less sensitive to feedback and easier to seed. Note that ring OPOs are automatically unidirectional because only the signals travelling in the same direction as the pump are amplified. A ring with a single crystal corresponds to a single pass linear OPO. As with the linear cavity, one can make either signal resonant. The round trip time is longer in a ring cavity than in a linear cavity. This tends to reduce the initial growth rate of the signal, but it is usually compensated by the increased intensity that can be used. A ring OPO equivalent to the two-pass pump configuration can be made by inserting nonlinear crystals in two legs of the ring. This has the same advantages as the two-pass linear OPO, and in addition it avoids the problem with pump reflection to the laser. Like the two-pass linear OPO, the ring OPO with two crystals can be made nonresonant.

4.4 Coatings and mirrors

Fabricating dielectric coatings with high damage resistance is a major problem in mid-IR generation. In lasers, anti-reflection coatings can often be replaced by Brewster cut faces. In OPOs, this is usually not possible because the interacting waves have different polarizations. However, when quasi phase matching is used, the waves can have the same polarization, so Brewster faces could be used.

4.5 Walk-off compensation

We mentioned in Section 2.4.3 that walk-off can be reduced by using two nonlinear crystals. By rotating one crystal with respect to the other, it is possible to reverse the direction of walk-off. Such rotation can also change the sign of the effective nonlinearity χ_{eff}, but in most cases it is possible to find a rotation that reverses walk-off and preserves χ_{eff} [10]. The two-crystal configuration has the additional advantage of increasing pump acceptance angle [11]. The reason is that the phase mismatch induced by the divergence has opposite signs in the two crystals.

4.6 Pump beam quality

Critically phase matched OPOs can be sensitive to phase-front variations of the pump beam [12]. The effects of different types of phase aberrations were studied numerically in [13]. Noncritically phase matched OPOs, however, may operate efficiently in spite of multimode pump beams [14].

4.7 OPO threshold

For a CW OPO, the threshold pump power is well defined: It is the power that makes the signal gain per round trip equal the resonator loss. The threshold power depends on the spatial profile of the pump beam. In pulsed OPOs, there must be many round trips

with net gain before the signal reaches an appreciable level. The pump power must exceed the CW threshold power before efficient conversion takes place. The threshold energy for a pulsed OPO is somewhat loosely defined as the pump energy that leads to a certain minimum signal energy [12]. The threshold energy and power depend on the length and the temporal shape of the pump pulse.

4.8 Composite OPO systems

Many systems combining OPOs and other frequency conversion devices have been reported. One reason to use a composite conversion system is that very few nonlinear materials are transparent at both 1.06 μm and in the 8–12 μm range. A Nd:YAG pumped KTP OPO pumping an $AgGaSe_2$ OPO generated radiation tunable from 6.9–13 μm [15]. A similar system with intra-cavity KTP or KTA OPO was tunable in the 2.5–5 μm range [16]. Radiation in the same wavelength bands have been generated by OPOs followed by difference frequency generation of the two signal waves [17, 18]. An advantage of the latter scheme is that the mid-IR wave is generated in a single pass through an uncouted crystal, requiring no mirrors.

OPOs with intra-cavity SFG and SHG have also been reported. An OPO pumping another OPO in the same resonator has been studied theoretically [19], but fabricating mirrors with specified reflectivities at 5 different wavelengths is probably beyond the present state of the art.

References

[1] S. Lin and T. Suzuki. Tunable picosecond mid-IR pulses generated by OPG / OPA in MgO:$LiNbO_3$ crystals. *Opt. Lett.*, 21:579–581, 1996.

[2] R.G. Batchko, D.R. Weise, T. Plettner, G.D. Miller, M.M. Fejer, and R.L. Byer. 532nm-pumped continuous wave singly resonant optical parametric oscillator based on periodically poled lithium niobate. In C.R. Pollock and W.R. Bosenberg, editors, *Advanced solid-state lasers*, volume 10 of *OSA Trends in Optics and Photonics*, pages 182–184, 1997.

[3] R.C. Eckardt, C.D. Nabors, W.J. Kozlovsky, and R.L. Byer. Optical parametric oscillator frequency tuning and control. *J. Opt. Soc. Am. B*, 8:646–667, 1991.

[4] C. Richy, E. Giacobino, and C. Fabre. Observation of bistability and delayed bifurcation in a triply resonant optical parametric oscillator. *J. Opt. Soc. Am. B*, 12:456, 1995.

[5] D.R. Guyer and D.D. Lowenthal. Novel cavity design for a high efficiency, high energy near infrared β-$Ba_2B_2O_4$ parametric iscillator. In R.A. Fisher and J.F. Reintjes, editors, *Nonlinear optics*, volume 1220 of *Proc. SPIE*, pages 41–44, 1990.

[6] W.R. Bosenberg and D.R. Guyer. Broadly tunable, single-frequency optical parametric frequency-conversion system. *J. Opt. Soc. Am. B*, 10:1716–1722, 1993.

[7] J.A.C. Terry, Y. Cui, Y. Yang, W. Sibbett, and M.H. Dunn. Low-threshold operation of an all-solid-state KTP optical parametric oscillator. *J. Opt. Soc. Am. B*, 11:758–769, 1994.

[8] W.A. Neuman and S.P. Velsko. Effect of cavity design on optical parametric oscillator performance. In S.A. Payne and C.R. Pollock, editors, *Advanced Solid-*

State Lasers, volume 1 of *OSA Trends in Optics and Photonics*, pages 179–181, 1996.

[9] A. Dubois, T. Lepine, P. Georges, and A. Brun. OPO radiance optimization using a numerical model. In C.R. Pollock and W.R. Bosenberg, editors, *Advanced solid-state lasers*, volume 10 of *OSA Trends in Optics and Photonics*, pages 394–396, 1997.

[10] G.T. Moore and K. Koch. Phasing of tandem crystals for nonlinear optical frequency conversion. *Opt. Lett.*, 124:292–294, 1996.

[11] D.J. Armstrong, W.J. Alford, T.D. Raymond, A.V. Smith, and M.S. Bowers. Parametric amplification and oscillation with walkoff-compensating crystals. *J. Opt. Soc. Am. B*, 14:460–474, 1997.

[12] S.J. Brosnan and R.L. Byer. Optical parametric oscillator threshold and linewidth studies. *IEEE J. Quantum Electron.*, 15:415–431, 1979.

[13] W.A. Neuman. OPO performance with an aberreated input pump beam. In M.C. Gupta, W.J. Kozlovsky, and D.C. MacPherson, editors, *Nonlinear frequency generation and conversion*, volume 2700 of *Proc. SPIE*, pages 250–261, 1996.

[14] L.R. Marshall, A. Kaz, and O. Aytur. Multimode pumping of optical parametric oscillators. *IEEE J. Quantum. Electron.*, 32:177–182, 1996.

[15] S. Chandra, T.H. Allik, J.A. Hutchinson, R. Utano, and G. Catella. Opo performance in the 7-13 μm band from 1.5 μm pumped $AgGaSe_2$. In C.R. Pollock and W.R. Bosenberg, editors, *Advanced solid-state lasers*, volume 10 of *OSA Trends in Optics and Photonics*, pages 270–273, 1997.

[16] T. Chuang, R. Burnham, and R.B. Jones. All solid-state mid infrared laser source. In C.R. Pollock and W.R. Bosenberg, editors, *Advanced solid-state lasers*, volume 10 of *OSA Trends in Optics and Photonics*, pages 262–264, 1997.

[17] D.L. Fenimore, K.L. Schepler, D. Zelmon, S. Kück, U.B. Ramabadran, P. Von Richter, and D. Small. Rubidium titanyl arsenate difference-frequency generation and validation of new sellmeier coefficients. *J. Opt. Soc. Am. B*, 13:1935–1940, 1996.

[18] R. Utano and M.J. Ferry. 8-12 μm generation using difference frequency generation in $AgGaSe_2$ of a Nd:YAG pumped KTP OPO. In C.R. Pollock and W.R. Bosenberg, editors, *Advanced solid-state lasers*, volume 10 of *OSA Trends in Optics and Photonics*, pages 267–269, 1997.

[19] G.T. Moore and K. Koch. The tandem optical parametric oscillator. *IEEE J. Quantum Electron.*, 32:2085–2094, 1996.

APPENDIX

A NONLINEAR INTERACTION IN A BIREFRINGENT MEDIUM

From Maxwell's equations we have

$$\nabla^2\tilde{\mathbf{E}} - \nabla(\nabla\cdot\tilde{\mathbf{E}}) = \mu_0\ddot{\tilde{\mathbf{D}}} + \mu_0\ddot{\tilde{\mathbf{P}}} \tag{A.1}$$

where $\tilde{\mathbf{D}} = \epsilon_0\epsilon\tilde{\mathbf{E}}$ is the linear part of the displacement, $\epsilon = 1 + \chi^{(1)}$ is the dielectric tensor, and $\tilde{\mathbf{P}}$ is the nonlinear polarization.

We first consider only the linear part of the equation and find the corresponding plane wave eigenmodes. Suppose that an eigenmode has wave vector $\mathbf{k} = k\mathbf{u}$, elecric field $\tilde{\mathbf{E}} = \mathbf{e}\exp(-i(\omega t - \mathbf{k}\cdot\mathbf{r}))$, and displacement $\tilde{\mathbf{D}} = \epsilon_0\epsilon\tilde{\mathbf{E}} = \epsilon_0\alpha\mathbf{d}\exp(-i(\omega t - \mathbf{k}\cdot\mathbf{r}))$ where $\mathbf{u}$, $\mathbf{e}$, and $\mathbf{d}$ are unit vectors and α is defined by $\epsilon\mathbf{e} = \alpha\mathbf{d}$. The Maxwell equation $\nabla\cdot\mathbf{D} = 0$ requires that $\mathbf{d}$ is normal to $\mathbf{u}$. Since the medium is birefringent, $\mathbf{e}$ need not be parallel to $\mathbf{d}$. Inserting this trial solution in the equation, we find

$$\nabla^2\tilde{\mathbf{E}} = -k^2\mathbf{e}\exp(-i(\omega t - \mathbf{k}\cdot\mathbf{r})) \tag{A.2}$$

$$\nabla\cdot\tilde{\mathbf{E}} = i(\mathbf{k}\cdot\mathbf{e})\exp(-i(\omega t - \mathbf{k}\cdot\mathbf{r})) = ik\sin\rho\exp(-i(\omega t - \mathbf{k}\cdot\mathbf{r})) \tag{A.3}$$

$$\nabla(\nabla\cdot\tilde{\mathbf{E}}) = -k^2\mathbf{u}\sin\rho\exp(-i(\omega t - \mathbf{k}\cdot\mathbf{r})) \tag{A.4}$$

$$\mu_0\ddot{\tilde{\mathbf{D}}} = -\omega^2c^{-2}\alpha\mathbf{d}\exp(-i(\omega t - \mathbf{k}\cdot\mathbf{r})) \tag{A.5}$$

where $\pi/2 - \rho$ is the angle between $\mathbf{u}$ and $\mathbf{e}$ (or equivalently, ρ is the angle between $\mathbf{e}$ and $\mathbf{d}$). These equations imply that $\mathbf{e}$ lies in the plane of $\mathbf{d}$ and $\mathbf{u}$. Since the Poynting vector is $\mathbf{S} = \langle\tilde{\mathbf{E}}\times\tilde{\mathbf{H}}\rangle$, and $\tilde{\mathbf{H}}$ is normal to $\tilde{\mathbf{D}}$ and $\mathbf{k}$, ρ is also the angle between $\mathbf{S}$ and $\mathbf{k}$, i.e. the walk-off angle. Equating the components along $\mathbf{d}$ and $\mathbf{u}$ we find

$$-k^2(\mathbf{e}\cdot\mathbf{d}) = -\omega^2c^{-2}\alpha \tag{A.6}$$

$$-k^2(\mathbf{e}\cdot\mathbf{u}) + k^2\sin\rho = 0 \tag{A.7}$$

The second equation is satisfied by the definition of ρ, while the first equation becomes $k^2\cos\rho = \omega^2c^{-2}\alpha$. The refractive index is defined by $k^2 = \omega^2n^2c^{-2}$, so $n^2 = \alpha/\cos\rho$. Given $\mathbf{d}$, we can find $\mathbf{e}$ and α by

$$n^2 = \frac{\alpha}{\cos\rho} = \frac{\alpha}{\mathbf{d}\cdot\mathbf{e}} = \frac{1}{\mathbf{d}\cdot(\alpha^{-1}\mathbf{e})} = \frac{1}{\mathbf{d}\cdot(\epsilon^{-1}\mathbf{d})} \tag{A.8}$$

Note that n cannot be found directly from $\mathbf{e}\cdot(\epsilon\mathbf{e})$ because this equals $\mathbf{e}\cdot(\alpha\mathbf{d}) = \alpha\cos\rho = n^2\cos^2\rho$.

It is clear that the index of refraction depends on the propagation direction. Rotate $\mathbf{k}$ a small angle θ in the plane of $\mathbf{k}$ and $\mathbf{d}$. To first order, the new unit vector in the propagation direction is $\mathbf{u}' = \mathbf{u} + \theta\mathbf{d}$ and the new unit vector in the direction of the displacement is $\mathbf{d}' = \mathbf{d} - \theta\mathbf{u}$. We know that $\epsilon^{-1}\mathbf{d} = \alpha^{-1}\mathbf{e} = \alpha^{-1}(\mathbf{d}\cos\rho + \mathbf{u}\sin\rho)$. Because ϵ is symmetric, it follows that $\epsilon^{-1}\mathbf{u} = \alpha^{-1}(\mathbf{d}\sin\rho + \mathbf{u}x)$ where x is a constant.

We find the refractive index of the wave in direction $\mathbf{u}'$ by

$$\begin{aligned}(n+\Delta n)^2 =& \frac{1}{\mathbf{d}'\cdot(\epsilon^{-1}\mathbf{d}')} = \frac{1}{(\mathbf{d}-\theta\mathbf{u})\cdot\epsilon^{-1}(\mathbf{d}-\theta\mathbf{u})} = \\ & \frac{\alpha}{(\mathbf{d}-\theta\mathbf{u})\cdot(\mathbf{d}\cos\rho+\mathbf{u}\sin\rho-\theta(\mathbf{d}\sin\rho+\mathbf{u}x))} = \\ & \frac{\alpha}{\cos\rho-\theta\sin\rho-\theta\sin\rho+\theta^2 x} \approx \text{(To first order in } \theta) \\ & \frac{\alpha}{\cos\rho-2\theta\sin\rho} = \frac{\alpha}{\cos\rho(1-2\theta\tan\rho)} \approx n^2(1+2\theta\tan\rho)\end{aligned} \tag{A.9}$$

This implies $2n\,\Delta n = 2n^2\theta\tan\rho$ and hence

$$\frac{dn}{d\theta} = n\tan\rho \tag{A.10}$$

Now that we have found the eigenmodes, we consider the evolution of a beam propagating in the presence of a driving nonlinear polarization. For simplicity we choose the z-axis along the direction of propagation and the x-axis along the displacement. Let the polarization be

$$\tilde{\mathbf{P}} = \mathbf{x}p(x,y,z)\exp(-i(\omega t - k_p z)) \tag{A.11}$$

where $\mathbf{x}$ is a unit vector in the x-direction. We assume that the electric field can be expressed in terms of a linear combination of eigenmodes with slowly varying amplitudes $\bar{e}$:

$$\tilde{\mathbf{E}}(x,y,z) = \iint dk_x dk_y \mathbf{e}(k_x,k_y)\bar{e}(k_x,k_y,z)\exp(-i(\omega t - k_x x - k_y y - k_z z)) \tag{A.12}$$

$$\text{where } k_z(k_x,k_y) = k_0\left(1+\tan\rho\frac{k_x}{k_0} - \frac{k_x^2+k_y^2}{2k_0^2}\right) \tag{A.13}$$

Here $k_0 = \omega n_0/c$, and n_0 is the refractive index of the mode with $k_x = k_y = 0$. This expansion is an exact representation, it includes the small longitudinal field components that must be present in a field with transverse variation. Consider first the evolution of the amplitude $\bar{e} = \bar{e}(k_x,k_y,z)$ of one of the modes. We use the same notation as before with the unit vectors $\mathbf{u}$, $\mathbf{d}$, and $\mathbf{e}$. In addition we use $\mathbf{x}$ and $\mathbf{z}$ for the unit vectors in these directions. We insert the field corresponding to this mode in Equation (A.1) and ignore second derivatives of the slowly varying amplitude $\bar{e}$. For compactness, we suppress the arguments of $\mathbf{e}$ and $\bar{e}$.

$$\nabla^2\tilde{\mathbf{E}} = \mathbf{e}(-k^2\bar{e} + 2ik_z\bar{e}')\exp(-i(\omega t - \mathbf{k}\cdot\mathbf{r})) \tag{A.14}$$

$$\begin{aligned}\nabla\cdot\tilde{\mathbf{E}} =& \mathbf{e}\cdot(i\mathbf{k}\bar{e} + \bar{e}'\mathbf{z})\exp(-i(\omega t - \mathbf{k}\cdot\mathbf{r})) = \\ & (ik\sin\rho\bar{e} + (\mathbf{e}\cdot\mathbf{z})\bar{e}')\exp(-i(\omega t - \mathbf{k}\cdot\mathbf{r}))\end{aligned} \tag{A.15}$$

$$\nabla(\nabla\cdot\tilde{\mathbf{E}}) = (-k^2\sin\rho\bar{e}\mathbf{u} + ik(\mathbf{e}\cdot\mathbf{z})\bar{e}'\mathbf{u} + ik\sin\rho\bar{e}'\mathbf{z})\exp(-i(\omega t - \mathbf{k}\cdot\mathbf{r})) \tag{A.16}$$

$$\mu_0\ddot{\tilde{\mathbf{D}}} = -\omega^2 c^{-2}\alpha\mathbf{d}\exp(-i(\omega t - \mathbf{k}\cdot\mathbf{r})) \tag{A.17}$$

$$\mu_0\ddot{\tilde{\mathbf{P}}} = -\mu_0\omega^2 p\mathbf{x}\exp(-i(\omega t - k_p z)) \tag{A.18}$$

where $\bar{e}' = d\bar{e}/dz$. We multiply both sides with $\mathbf{d}$ and $\mathbf{u}$. All the terms corresponding to the linear equation cancel, so we are left with

$$(2ik_z(\mathbf{e}\cdot\mathbf{d}) - ik(\mathbf{z}\cdot\mathbf{d}))\bar{e}'\exp(i\mathbf{k}\cdot\mathbf{r}) = -\mu_0\omega^2 p(\mathbf{x}\cdot\mathbf{d})\exp(ik_p z) \tag{A.19}$$

$$(2ik_z\sin\rho - ik(\mathbf{e}\cdot\mathbf{z}) - ik\sin\rho(\mathbf{z}\cdot\mathbf{u})\bar{e}'\exp(i\mathbf{k}\cdot\mathbf{r}) = -\mu_0\omega^2 p(\mathbf{x}\cdot\mathbf{u})\exp(ik_p z) \tag{A.20}$$

The small changes in polarization directions are essential to derive walk-off and the direction dependent refractive index. But now, when we are interested in the perturbations caused by the nonlinear polarization, we can make approximations. If we assume $\mathbf{e}\cdot\mathbf{z} \approx \sin\rho$, $\mathbf{z}\cdot\mathbf{u} \approx 1$, $\mathbf{x}\cdot\mathbf{u} \approx 0$, and $k \approx k_z$, Equation (A.20) is satisfied. And if we assume $\mathbf{e}\cdot\mathbf{d} \approx 1$, $\mathbf{z}\cdot\mathbf{d} \approx 0$, and $\mathbf{x}\cdot\mathbf{d} \approx 1$, Equation (A.20) becomes

$$2ik_z\bar{e}'\exp(i\mathbf{k}\cdot\mathbf{r}) = -\mu_0\omega^2 p\exp(ik_p z) \tag{A.21}$$

Multiplying with $\exp(-i(k_x x + k_y y))$ and integrating over x and y

$$\bar{e}' = \frac{i\mu_0\omega^2}{2k_z}\bar{p}(k_x,k_y)\exp(iz(k_p - k_z)) \tag{A.22}$$

where

$$\bar{p}(k_x,k_y) = \frac{1}{(2\pi)^2}\iint dxdyp(x,y)\exp(-i(k_x x + k_y y)) \tag{A.23}$$

Using this result, we can find the evolution of the complete field:

$$\frac{\partial\tilde{\mathbf{E}}}{\partial z} = \iint dk_x dk_y(i(k_0 + k_x\tan\rho - \frac{k_x^2+k_y^2}{2k_0})e + e')\mathbf{e}(k_x,k_y)\exp(-i(\omega t - \mathbf{k}\cdot\mathbf{r})) \tag{A.24}$$

We simplify by approximating $\tilde{\mathbf{E}} \approx \tilde{E}\mathbf{e}_0$ and $\mathbf{e}(k_x,k_y) \approx \mathbf{e}_0$ for all the modes. When we insert (A.22) for $\bar{e}'$ and carry out the integration, the second term becomes

$$i\beta p(x,y)\exp(-i(\omega t - k_p z)) \text{ where } \beta = \frac{\mu_0\omega^2}{2k_z} \approx \frac{\mu_0\omega c}{2n_0} \tag{A.25}$$

When the first term is integrated, it becomes

$$ik_0\tilde{E} + \tan\rho\frac{\partial\tilde{E}}{\partial x} - \frac{i}{2k_0}\nabla_T^2\tilde{E} \text{ where } \nabla_T^2 = \frac{\partial^2}{\partial x^2} + \frac{\partial^2}{\partial y^2} \tag{A.26}$$

so the result is

$$\frac{\partial\tilde{E}}{\partial z} = ik_0\tilde{E} + \tan\rho\frac{\partial\tilde{E}}{\partial x} - \frac{i}{2k_0}\nabla_T^2\tilde{E} + i\beta p(x,y)\exp(-i(\omega t - k_p z)) \tag{A.27}$$

Now let $\tilde{E}(x,y,z) = e(x,y,z)\exp(-i(\omega t - k_0 z))$, where e is a slowly varying amplitude. The equation for e is

$$\frac{\partial e}{\partial z} = \tan\rho\frac{\partial e}{\partial x} - \frac{i}{2k_0}\nabla^2 e + i\beta p(x,y)\exp(iz(k_p - k_0)) \tag{A.28}$$

The first term on the right hand side describes walk-off, the second describes diffraction, and the last term is the nonlinear driving polarizaton. If we assume that the nonlinear

polarization $\tilde{P}$ is created by two other waves, $\tilde{P} = 2\epsilon_0\chi_{\text{eff}}e_3e_2^*\exp(i(k_3 - k_2)z - i\omega t)$, the driving term becomes

$$2i\frac{\mu_0\omega_1 c}{2n_1}\epsilon_0\chi e_3 e_2^*\exp(i(k_3 - k_2)z) = i\omega_1\frac{\chi}{cn_1}e_3e_2^*\exp(i(k_3 - k_2 - k_1)z) \qquad \text{(A.29)}$$

which is equal to the corresponding term in the plane wave equations. In a nonlinear device, the waves usually have different polarizations and hence walk-off in different directions. Thus $\partial/\partial x$ in the walk-off term may be replaced with $\partial/\partial y$ for other waves.